

ISSN 2074-272X

науково-практичний  
журнал

2019/1



# **EIE** електротехніка і **EIE** електромеханіка

**Electrical Engineering**

**& Electromechanics**

**Електротехніка. Визначні події. Славетні імена**

**Електричні машини та апарати**

**Електротехнічні комплекси та системи.**

**Силова електроніка**

**Теоретична електротехніка та електрофізика**

**Техніка сильних електричних та магнітних полів.**

**Кабельна техніка**

**Електричні станції, мережі і системи**

**Ювілеї**

**З 2015 р. журнал індексується у міжнародній**

**наукометричній базі Web of Science**

**Core Collection: Emerging Sources**

**Citation Index**



# «ELECTRICAL ENGINEERING & ELECTROMECHANICS»

SCIENTIFIC & PRACTICAL JOURNAL

Journal was founded in 2002

## Founders:

National Technical University «Kharkiv Polytechnic Institute» (Kharkiv, Ukraine)

State Institution «Institute of Technical Problems of Magnetism of the NAS of Ukraine» (Kharkiv, Ukraine)

## INTERNATIONAL EDITORIAL BOARD

<b>Klymenko B.V.</b>	<b>Editor-in-Chief</b> , Professor, National Technical University "Kharkiv Polytechnic Institute" (NTU "KhPI"), Ukraine
<b>Sokol Ye.I.</b>	<b>Deputy Editor</b> , Professor, Corresponding member of NAS of Ukraine, Rector of NTU "KhPI", Ukraine
<b>Rozov V.Yu.</b>	<b>Deputy Editor</b> , Professor, Corresponding member of NAS of Ukraine, Director of State Institution "Institute of Technical Problems of Magnetism of the NAS of Ukraine"(SI "ITPM NASU"), Kharkiv, Ukraine
<b>Batygin Yu.V.</b>	Professor, Kharkiv National Automobile and Highway University, Ukraine
<b>Biró O.</b>	Professor, Institute for Fundamentals and Theory in Electrical Engineering, Graz, Austria
<b>Bolyukh V.F.</b>	Professor, NTU "KhPI", Ukraine
<b>Colak I.</b>	Professor, Nisantasi University, Istanbul, Turkey
<b>Doležel I.</b>	Professor, University of West Bohemia, Pilsen, Czech Republic
<b>Féliachi M.</b>	Professor, Technological Institute of Saint-Nazaire, University of Nantes, France
<b>Gurevich V.I.</b>	Ph.D., Honorable Professor, Central Electrical Laboratory of Israel Electric Corporation, Haifa, Israel
<b>Ida N.</b>	Professor, The University of Akron, Ohio, USA
<b>Kildishev A.V.</b>	Associate Research Professor, Purdue University, USA
<b>Kuznetsov B.I.</b>	Professor, SI "ITPM NASU", Ukraine
<b>Kyrylenko O.V.</b>	Professor, Member of NAS of Ukraine, Institute of Electrodynamics of NAS of Ukraine (IED of NASU), Kyiv, Ukraine
<b>Nacke B.</b>	Professor, Gottfried Wilhelm Leibniz Universität, Institute of Electrotechnology, Hannover, Germany
<b>Podoltsev A.D.</b>	Professor, IED of NASU, Kyiv, Ukraine
<b>Rainin V.E.</b>	Professor, Moscow Power Engineering Institute, Russia
<b>Rezynkina M.M.</b>	Professor, NTU "KhPI", Ukraine
<b>Shkolnik A.A.</b>	Ph.D., Central Electrical Laboratory of Israel Electric Corporation, member of CIGRE (SC A2 - Transformers), Haifa, Israel
<b>Trichet D.</b>	Professor, Institut de Recherche en Energie Electrique de Nantes Atlantique, Nantes, France
<b>Yatchev I.</b>	Professor, Technical University of Sofia, Sofia, Bulgaria
<b>Yuferov V.B.</b>	Professor, National Science Center "Kharkiv Institute of Physics and Technology", Ukraine
<b>Zagirnyak M.V.</b>	Professor, Member of NAES of Ukraine, rector of Kremenchuk M.Ostrohradskyi National University, Ukraine
<b>Zgraja J.</b>	Professor, Institute of Applied Computer Science, Lodz University of Technology, Poland

## ISSUE 1/2019

### TABLE OF CONTENTS

#### *Electrical Engineering. Great Events. Famous Names*

<b>Baranov M.I.</b> An anthology of the distinguished achievements in science and technique. Part 47: Aircraft designer Igor Sikorsky and his accomplishments in design of airplanes and helicopters.....	3
---	---

#### *Electrical Machines and Apparatus*

<b>Bondar R.P.</b> Research of the magnetoelectric linear oscillatory motor characteristics during operation on elastoviscous loading .....	9
<b>Halchenko V.Ya., Bondarenko Yu.Yu., Filimonov S.A., Filimonova N.V.</b> Determination of influence of geometric parameters of piezoce-ramic plate on amplitude characteristics of linear piezomotor .....	17
<b>Pliuhin V., Sukhonos M., Pan M., Petrenko O., Petrenko M.</b> Implementing of Microsoft Azure machine learning technology for electric machines optimization .....	23

#### *Electrotechnical Complexes and Systems. Power Electronics*

<b>Volontsevich D.O., Veretennikov E.A., Kostianik I.V., Iaremchenko A.S., Efremova A.I., Karpov V.O.</b> Determination of the electric drive power for lightly armored caterpillar and wheeled vehicles using single- or two-stage mechanical gearboxes .....	29
--	----

#### *Theoretical Electrical Engineering and Electrophysics*

<b>Bialobrzheskyi O.V., Rodkin D.I.</b> Alternative indicators of power of electric energy in a single-phase circuit with polyharmonic current and voltage .....	35
<b>Makarchuk O., Calus D., Moroz V., Galuszkiewicz Z., Galuszkiewicz P.</b> Two-dimensional fem-analysis of eddy currents loss in laminated magnetic circuits .....	41

#### *High Electric and Magnetic Field Engineering. Cable Engineering*

<b>Guryn A.G., Golik O.V., Zolotaryov V.V., Antonets S.Yu., Shchebeniuk L.A., Grechko O.M.</b> A statistical model of monitoring of insulation breakdown voltage stability in the process of enameled wires production .....	46
<b>Samokhvalova Zh.V., Samokhvalov V.N.</b> Magnetic-pulse pressing of electrical connections for stranded wires.....	51
<b>Shutenko O.V., Zagaynova A.A., Serdyukova G.N.</b> Analysis of operating conditions and modes influence on technical state of main insulation of high-voltage bushings of different design.....	57

#### *Power Stations, Grids and Systems*

<b>Koliushko D.G., Rudenko S.S.</b> Analysis of methods for monitoring of existing energy objects grounding devices state at the present stage.....	67
---	----

**Editorial office address:** Dept. of Electrical Apparatus, NTU «KhPI», Kyrpychova Str., 2, Kharkiv, 61002, Ukraine  
**phones:** +380 57 7076281, +380 67 3594696, **e-mail:** a.m.grechko@gmail.com (**Grechko O.M.**)

**ISSN (print) 2074-272X**  
**ISSN (online) 2309-3404**

© National Technical University «Kharkiv Polytechnic Institute», 2019

© State Institution «Institute of Technical Problems of Magnetism of the NAS of Ukraine», 2019

Printed 20 February 2019. Format 60 x 90 1/8. Paper – offset. Laser printing. Edition 200 copies.  
Printed by Printing house «Madrid Ltd» (11, Maksymilianivska Str., Kharkiv, 61024, Ukraine)

M.I. Baranov

## AN ANTHOLOGY OF THE DISTINGUISHED ACHIEVEMENTS IN SCIENCE AND TECHNIQUE. PART 47: AIRCRAFT DESIGNER IGOR SIKORSKY AND HIS ACCOMPLISHMENTS IN DESIGN OF AIRPLANES AND HELICOPTERS

*Purpose. Preparation of short scientifically-historical essay about one of founders of world aviation, prominent Ukrainian and American aircraft designer I.I. Sikorsky. Methodology. Known scientific methods of collection, analysis and analytical treatment of scientific and technical information, touching becoming and development of world aviation and resulted in scientific monographs, journals and internet-reports. Results. A short scientifically-historical essay about a prominent Ukrainian and American aircraft designer Igor Ivanovich Sikorsky, becoming one of founders of world aviation. Basic scientific and technical achievements of I.I. Sikorsky in an area of design of airplanes and helicopters, emigrating because of overcame civil war from Russia to the USA (1919). It is shown that I.I. Sikorsky is the founder of not only American but also domestic aviation industry. I.I. Sikorsky became the first on our planet incarnating in reality the dream of the genius Italian inventor Leonardo da Vinci on creation of helicopter. He became the «father» of world design of helicopters. By him in Russia and the USA 17 base types of airplanes and 18 base types of helicopters were developed and built, operating on piston and gas-turbine engines. Helicopters development by I.I. Sikorsky firstly the world accomplished flying (with refuelling in mid air) over Atlantic (S-61, 1967) and Pacific (S-65, 1970) oceans. It is marked that one of reliability indexes of the designs of aircrafts created by him is that until now the Presidents of the USA fly on helicopters with inscription of «Sikorsky» onboard. Originality. Certain systematization is executed known from scientific publications and other mass of scientific and technical materials media, touching becoming and development of world aviation and contribution to world design of airplanes and helicopters of prominent Ukrainian and American aircraft designer I.I. Sikorsky. Practical value. Scientific popularization and deepening for University students, engineering, technical and scientific workers of scientific and technical knowledge in the field of history of becoming and development of world design of airplanes and helicopters, extending their scientific and technical range of interests and further development of scientific and technical progress in society. References 12, figures 12.*

*Key words:* aviation, prominent Ukrainian and American aircraft designer Igor Sikorsky, basic achievements in construction of airplanes and helicopters, scientifically-historical essay.

*Наведено короткий науково-історичний нарис про видатного українсько-американського авіаконструктора Ігоря Івановича Сікорського, який став одним з основоположників світової авіації. Описані основні досягнення І.І. Сікорського в галузі літако- і вертолітобудування, що емігрував із охопленою громадянською війною Росії в США (1919 р.). Показано, що І.І. Сікорський є засновником не тільки американської, але і вітчизняної авіаційної промисловості. І.І. Сікорський став першою на нашій планеті людиною, яка утілила в реальність мрію геніального італійського винахідника Леонардо да Вінчі по створенню вертольота. Бібл. 12, рис. 12.*

*Ключові слова:* авіація, видатний українсько-американський авіаконструктор Ігор Сікорський, основні досягнення в літако- і вертолітобудуванні, науково-історичний нарис.

*Приведен краткий научно-исторический очерк о выдающемся украинско-американском авиаконструкторе Игоре Ивановиче Сикорском, ставшем одним из основоположников мировой авиации. Описаны основные достижения И.И. Сикорского в области самолето- и вертолетостроения, эмигрировавшего из охваченной гражданской войной России в США (1919 г.). Показано, что И.И. Сикорский является основателем не только американской, но и отечественной авиационной промышленности. И.И. Сикорский стал первым на нашей планете человеком, воплотившим в реальность мечту гениального итальянского изобретателя Леонардо да Винчи по созданию вертолета. Библ. 12, рис. 12.*

*Ключевые слова:* авиация, выдающийся украинско-американский авиаконструктор Игорь Сикорский, основные достижения в самолето- и вертолетостроении, научно-исторический очерк.

**Introduction.** In the history of mankind there are many talented personalities who brought one or another area of scientific and technical knowledge to a new higher level of their development. One of these personalities was our compatriot Igor Ivanovich Sikorsky (Fig. 1), who became the largest aircraft designer of the 20th century [1]. Many outstanding achievements of design thought in world aviation are connected with his name. It should be noted that the beginning of the development of aircraft industry in the Russian Empire is closely related to the talent of this person. A significant part of that in aviation, which made by a Ukrainian by origin I.I. Sikorsky, associated with the development of design of aircrafts and helicopters in the USA [1, 2]. Paying tribute to this outstanding Ukrainian-American aircraft designer, we

will try in the form of a brief scientific and historical essay to trace his life and career in aviation.

**The goal of the paper** is preparation of a brief scientific and historical essay on one of the founders of world aviation, an outstanding Ukrainian-American aircraft designer I.I. Sikorsky.

**1. The beginning of the life and career.** The hero of our essay was born on May 25, 1889 in the family of a Doctor of Medicine, Professor at Saint-Vladimir Kyiv University Ivan Alekseevich Sikorsky, known in the Russian Empire and abroad for his many publications on psychiatry [1]. The father raised his younger son (Igor was the fifth child in the family) according to his own methodology in devotion to the Church, the Throne and

© M.I. Baranov



Fig. 1. Outstanding aircraft designer of the 20th century Igor Ivanovich Sikorsky (25.05.1889 – 26.10.1972) [2]

the Fatherland. He managed to develop in him an unshakable will and instill in him a unique perseverance in achieving his noble goal [1]. The mother of the future aircraft designer, Maria Stefanovna (nee Temryuk-Cherkasova), who was a medical doctor by training (by profession due to domestic chores and raising children she did not work), instilled in Igor a love of music, literature and art. He began studying at the 1st Kyiv Gymnasium, and in 1903 he wished to continue his education at the Naval Cadet Corps (Saint Petersburg). At the end of general education classes, he leaves this Corps in order to obtain higher technical education. Young I.I. Sikorsky, in order to realize his true vocation, in 1906 moves to Paris and entered the Duvigne de Lannoy Technical School [1]. After studying at this school for just one year, in 1907, due to the death of his mother, he returned to Kyiv and entered the Mechanical Department of the Emperor Alexander II Kyiv Polytechnic Institute (KPI). Successfully completing the first academic year at the KPI, I.I. Sikorsky decided to do practical work in his own workshop for the development and creation of aircrafts [1]. It should be noted that the KPI, founded in 1898, was a higher technical school of Russia of a new type, where students received deep natural-science fundamental training in mathematics, physics, chemistry and other disciplines on which general engineering courses were built [4]. Training of students at the KPI was combined with professional and practical work in industry and in scientific laboratories. The KPI strongly encouraged research and practical work of teachers and students in specialized research groups at the Institute. The idea of building an aircraft of his own design fully captured the young and promising young man in the field of domestic aircraft industry I.I. Sikorsky, who forgot about his studies at the KPI for the time being (the period of his studies at the KPI is considered to be the period of 1907-1911 [3]). His first experiments on the creation of a helicopter ended in failure. Soberly assessing the situation, he decided to postpone work on creating his own helicopter until better times and start developing airplanes with a fixed wing. For the period 1910-1911, he created with his own money five types of biplanes of the

S-1 – S-5 series with an internal combustion engine of power from 15 to 50 hp. (Fig. 2). Having reached the height of a flight of 450 meters on an S-5 type biplane and time in the air of about 1 hour, the aircraft designer I.I. Sikorsky gained world fame [4].



Fig. 2. Young aircraft designer I.I. Sikorsky on his one of the first airplanes of type S-2 (1910, Kyiv) [2]

**2. Major achievements of the aircraft designer I.I. Sikorsky in airplane industry.** In December 1911, on a biplane of his own design of the type S-6 with an engine of 100 hp, I.I. Sikorsky set the world record for aircraft speed in airspace – 111 km/h [5]. From 1912 to 1917 a student Igor Sikorsky, who did not finish his study at the KPI, held a high position as chief designer of the Aviation Department of the Russian Baltic plant in Saint Petersburg (later renamed by the forces of the Russian revolutionary movement in Petrograd), which supplied the airplanes for the Russian army [1]. It is interesting to note that in 1914, for his outstanding achievements in the field of Russian military aircraft manufacturing, I.I. Sikorsky received an Engineering Diploma from the Saint Petersburg Polytechnic Institute, which became under Soviet rule known throughout the world as the Leningrad Polytechnic Institute (now this educational institution is called Saint Petersburg Technical University). It is at this Russian plant I.I. Sikorsky creates the first in the world multi-engine heavy airplanes «Russian Knight» and «Ilya Muromets» (Fig. 3). His biplanes and monoplanes brought Russia fame as one of the world's leading aviation powers.



Fig. 3. Four-engine bomber «Ilya Muromets» (S-22) of military transport purpose developed by I.I. Sikorsky (1913, Saint Petersburg, Russia) [2]

However, in 1918, the talented aircraft designer who had done so much for the development of Russian aviation, a former senior student of the KPI Igor Sikorsky, who had escaped from the Red Terror, was forced to leave Russia and sail by the English ship from Murmansk to France [19]. Having worked in Paris for about a year at one of the aircraft building factories, our young aircraft designer came to the fateful conclusion for him that there are more prospects for the development of heavy aircraft building across the ocean in America. Note that the aircraft designer I.I. Sikorsky, even before the start of World War I in 1914, firmly concluded that aviation would have a future for large aircrafts with two or more engines. In his opinion, such aircrafts over single-engine airplanes had clear advantages both in flight range and in transport capabilities. In addition, this type of aircrafts was safer than single-engine «brothers». In March 1919, he arrives (or rather sails) from Europe to North America to the seaport of New York – a large entrance «gate» for numerous immigrants from around the world. From now until the end of his long life, his unique intelligence and creative forces were largely entirely focused on the development of the American aviation industry, the protection and prosperity of his beloved family. After the usual initial hard ordeals and several years of severe survival in a foreign land, in 1923 the purposeful aircraft designer I.I. Sikorsky founded his first aircraft manufacturing Company, Sikorsky Aero Engineering Corporation, in the United States, developing and producing aircrafts [2]. The first aircraft produced by this American company was the passenger twin-engine biplane S-29 (Fig. 4) [2].



Fig. 4. One of the first twin-engine civilian type S-29 biplane designed and developed by I.I. Sikorsky in the USA (1924) [2]

Life of I.I. Sikorsky in 1924 began to improve: from the former USSR two sisters and a grown daughter Tatiana from his first marriage came to him for permanent residence (his first wife refused to move to the United States). Soon, Igor Ivanovich entered into a second marriage with the Russian émigré Elizaveta Alekseevna Semenova. This marriage turned out to be happy for the Sikorsky couple: one after another, the sons Sergey, Nikolay, Igor and Georgy were born in their family [1]. At that time, their father stubbornly continued to promote his aircrafts on the American vehicle market. I.I. Sikorsky «discovers» for himself a

niche in the aircraft industry unused in the United States – the production of amphibious aircrafts capable of taking off from the surface of the water and landing on it. In 1928, I.I. Sikorsky received US passport, and in 1929 his company became a branch of the larger American company United Aero Craft. At it, he holds the position of a design engineering manager for aircrafts [7]. This US aircraft manufacturing Company produces twin-engine ten-seat amphibious aircrafts of the S-38 type (Fig. 5) [1, 7].

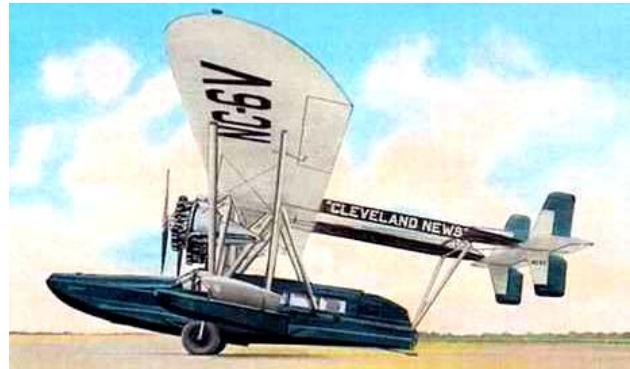


Fig. 5. Two-engine ten-seat amphibious aircraft of type S-38 developed by I.I. Sikorsky (1929, USA) [1]

In 1931 this flying «boat» by I.I. Sikorsky opened the post-passenger service in the zone of the Caribbean islands and to South America. By the summer of 1937, the «Pan American» Company on his four-engine amphibious aircraft of the S-42 type began to successfully serve the transpacific and transatlantic routes [7]. Later, these mainline aircrafts were replaced with his more comfortable and reliable flying «boats» of the S-44 type (Fig. 6).



Fig. 6. Four-engine long-range fifty-passenger amphibious aircraft of type S-44 developed by aircraft designer I.I. Sikorsky (1937, USA) [2]

By 1939, I.I. Sikorsky developed and created 17 types of aircrafts in the «metal» [7]. In the late 1930s, due to a change in aviation commercial conjuncture for amphibious aircrafts, I.I. Sikorsky returns to the idea of building his own helicopter.

**3. Major achievements of the aircraft designer I.I. Sikorsky in helicopter industry.** At the end of 1938, I.I. Sikorsky, together with his assistants, began to develop a fundamentally new and at that time still unknown aircraft – a helicopter. So the great aircraft

designer for the third time (for the first time – in Russia since 1910, and the second time – in the USA since 1924) practically from scratch begins his creative career in the aircraft industry. His first experimental helicopter of the VS-300 (S-46) type with an open tubular frame took off on September 14, 1939 under the control of the aircraft designer himself [1]. This helicopter had an original single-screw design scheme with an automatic blade skew and, accordingly, one lifting screw. To counteract the torque, resulting in a circular movement of the cockpit of the aircraft, on its tail a small screw with a mechanical drive from the engine of the main lifting screw was installed [1, 2]. At present, this single-rotor helicopter design scheme is considered to be classic. Since then, at least 90% of all helicopters in the world have been built on this base. Then, in 1939, many aircraft designers of the world considered this scheme unpromising. In 1942, I.I. Sikorsky created a double-seat helicopter of the «Sikorsky XR-4» or S-47 type (Fig. 7), which soon entered the USA serial production [2].



Fig. 7. Aircraft designer I.I. Sikorsky in the cockpit of his new technical «brainchild» – the world's first serial US helicopter type «Sikorsky XR-4» (1942, USA) [2]

This type of helicopter turned out to be the only helicopter of the countries of the anti-Hitler coalition during World War II. The aircraft manufacturer Sikorsky Aero Craft, which has become the leader in US helicopter manufacturing and was part of the large American company United Aero Craft, is once again gaining autonomy and a new production base in Bridgeport. Shares of this Company grew. Due to the large growth in production orders for helicopters, a new factory was built for their production in Stratford, where I.I. Sikorsky and moved his residence. As the main purpose of the helicopter, he considered the saving of human lives. In this regard, we quote the phrase he expressed [2]: «... *I am sure that the helicopter will become a unique vehicle for saving lives*». The S-52 light helicopter was the first helicopter in the world to perform aerobatics. In 1953, I.I. Sikorsky, using his single-rotor scheme, created a heavy helicopter with a lifting weight of 14 tons [2]. Successful use of combat helicopters designed by I.I. Sikorsky in the Korean War forced the leadership of the former USSR to pay close attention to the rotorcraft technique. So he indirectly influenced the development of the Soviet helicopter industry. The best helicopter created by

I.I. Sikorsky in 1954, is considered a passenger helicopter type S-58 (Fig. 8). In terms of its technical and economic characteristics, it surpassed all the helicopters of the world of its time [2].



Fig. 8. Passenger helicopter type S-58 – the best design of the great aircraft designer I.I. Sikorsky, which became for him a «swan song» (1954, USA) [2]

Fig. 9 shows a general view of a helicopter crane, designed and created by I.I. Sikorsky [1, 2].



Fig. 9. General view of the helicopter crane development by aircraft designer I.I. Sikorsky, in operation (1950s, USA) [2]

Aircraft designer I.I. Sikorsky (Fig. 10), as the founder of the world helicopter industry, for many years remained at the unattainable scientific and technical «height». In addition to 17 types of airplanes developed and built in Russia and the United States, he created 18 basic types of helicopters in the United States [2]. During his life, I.I. Sikorsky received over 80 various honorary awards, prizes and diplomas. Among them are the Russian Order of Saint Vladimir of the 4th degree, gold medals of Daniel Guggenheim, James Watt and a Diploma from the National Gallery of Fame of Inventors. In 1948, he was awarded a rare award – the Wright Brothers Memorial Prize, and in 1967 he was awarded the John Fritz Medal of Honor for scientific and technical achievements in the field of basic and applied sciences [2]. Note that in world aviation only Orville Wright was awarded this medal before him as the founder of world aircraft design. Aircraft designer I.I. Sikorsky was elected an honorary Doctor of many leading Universities in the world [2, 7].

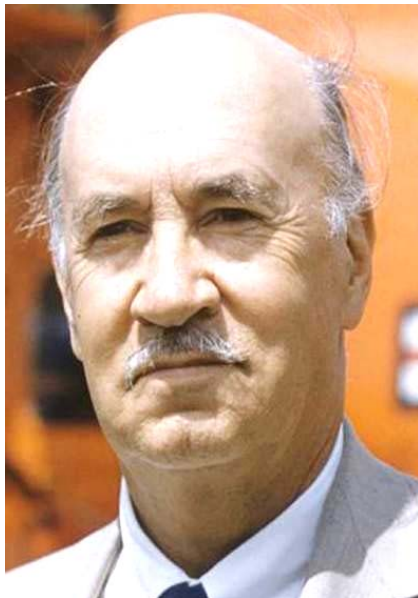


Fig. 10. The world-recognized master of world aviation, aircraft designer I.I. Sikorsky during the heyday of his inventive and engineering activities on American soil (1950s, Easton, Connecticut, USA) [10]

**4. Universal human qualities of the aircraft designer I.I. Sikorsky.** What kind of person was this outstanding aircraft designer? Medium height, with a soft and even shy manner of speaking and behavior among people [2]. Judging by the data from literary sources [7, 8], he possessed remarkable physical and moral strength. He was fond of mountaineering: he conquered a number of mountain peaks of the USA and Canada. He was particularly interested in terrestrial volcanoes. He considered them as *«mighty and majestic phenomena of the earthly nature»* [2]. He was quite a closed man. Human communication he preferred privacy. Often he went by car to the nature far from the city bustle. He was a caring father. His daughter Tatiana became Professor of sociology at Bridgeport University. His eldest son, Sergey, became design engineer and worked with him at an aircraft manufacturing Company (he went up to the position of Vice-President, that is, deputy for his father). Other sons of I.I. Sikorsky chosen other professions: Nikolay became a violinist, Igor became a lawyer, and George became a mathematician [2]. I.I. Sikorsky considering the patriarchal upbringing in the family of his parents was a deeply religious man. He financially supported the Russian Orthodox Church in America [2]. He was the author of a number of theological works. His head was usually crowned with a favorite «Fedora» hat (see Fig. 1). He and his associates believed that this hat usually brings him good luck both at work and at home.

According to people who knew the outstanding aircraft designer closely, he was exclusively a peace-loving person, and considered the main mission of aviation to be the relief of people's everyday life and work [5]. According to the son of the pioneer of the helicopter industry of the USA Sergey Sikorsky, his father I.I. Sikorsky was a versatile person: a highly qualified engineer, first-class pilot and philosopher [9]. In addition to aviation, he was interested in many things – literature, classical music, history, theology. According to the words

of the eldest son Sergey [9]: *«... the father did not become a millionaire in the USA. But our family lived comfortably and without material problems».*

**5. Return of the great aircraft designer I.I. Sikorsky to his alma mater.** In 1998, a memorial plaque was opened at the KPI in honor of the famous aircraft designer and its former student [4]. It decorated the brick wall of the building of the former research workshops, in which the young purposeful Igor Sikorsky worked on the creation of his first airplanes. On May 14, 2008 a monument to I.I. Sikorsky was opened (Fig. 11) [11].



Fig. 11. Monument to the outstanding Ukrainian-American aircraft designer I.I. Sikorsky on the campus of the National Technical University of Ukraine «Kyiv Polytechnic Institute» (2008, Kyiv, Ukraine) [11]

On the marble slab of the pedestal of this world's first monument to an outstanding aircraft designer of the 20th century, the honored artist of Ukraine, sculptor Nikolai Oleinik carved the following words of I.I. Sikorsky, told him in his declining years [4]: *«... I take off my hat to the alma mater prepared me for the conquest of the sky».* Rector of the KPI, Academician of the National Academy of Sciences of Ukraine M.Z. Zgurovsky at the opening of the monument to the former talented student of the KPI, who has become a world-famous aircraft designer, noted that *«... I.I. Sikorsky will inspire young polytechnics to fulfill their dreams with his image, example and his fate»* [11]. On August 26, 2016 the NTUU «KPI» (Fig. 12) became known as the Igor Sikorsky National Technical University of Ukraine «Kyiv Polytechnic Institute» [12]. The corresponding order No. 992 of August 17, 2016 was signed by the Minister of Education and Science of Ukraine L.M. Hrynevych [12].



Fig. 12. General view of the main academic building of the Igor Sikorsky NTUU «KPI» (2016, Kyiv, Ukraine) [12]

So the great compatriot and aircraft designer of modernity, after his death, returned to his native city of Kyiv and to his unforgettable alma mater.

**Conclusions.** Many scientific and technical achievements in the field of world aircraft and helicopter design are connected with the name of our famous compatriot Igor Ivanovich Sikorsky, who became one of the largest aircraft designers of the 20th century. He developed and built 17 basic types of airplanes and 18 basic types of helicopters working on piston and gas turbine engines in Russia and the USA. He became the «father» of the world helicopter industry. Helicopters developed by him for the first time in the world flew (with air refueling) through the Atlantic (S-61, 1967) and Pacific (S-65, 1970) oceans. One of the indicators of the reliability of the aircraft designs created by him is that until now the US Presidents fly helicopters with the words «Sikorsky» on board. Outstanding Ukrainian-American aircraft designer I.I. Sikorsky played a crucial role in the formation and development of world aviation. For his aircrafts, he was awarded many honorary titles and awards. The main reward to him, nevertheless, remains the gratitude of people from all continents of our planet for peaceful purposes using the flying machines created by him and the principles of their design and construction developed by him.

How to cite this article:

Baranov M.I. An anthology of the distinguished achievements in science and technique. Part 47: Aircraft designer Igor Sikorsky and his accomplishments in design of airplanes and helicopters. *Electrical engineering & electromechanics*, 2019, no.1, pp. 3-8. doi: 10.20998/2074-272X.2019.1.01.

REFERENCES

1. Available at: <https://www.pravmir.ru/igor-ivanovich-sikorskij-geroj-izgnannik-otec-aviacii> (accessed 11 May 2017). (Rus).
2. Available at: <https://www.maximonline.ru/longreads/photogallery/article/chelovek-s-vintom> (accessed 9 May 2017). (Rus).
3. Available at: <http://kpi.ua/ru/sikorsky> (accessed 19 October 2017). (Rus).
4. Available at: <http://kpi.ua/ru/node/7895> (accessed 29 July 2017). (Rus).
5. Available at: <https://history.vn.ua/book/person/80.html> (accessed 29 January 2018). (Rus).
6. Available at: <http://www.tvc.ru/news/show/id/69580> (accessed 22 February 2018). (Rus).
7. Available at: <http://to-name.ru/biography/igor-sikorskij.htm> (accessed 10 March 2018). (Rus).
8. Katyshhev G.I., Mikheev M.R. *Aviakonstruktor Igor Ivanovich Sikorskiy. 1889-1972* [Aircraft Designer Igor Ivanovich Sikorsky. 1889-1972]. Moscow, Nauka Publ., 1989. 176 p. (Rus).
9. Available at: <https://fakty.ua/149040-syn-legendarnogo-aviakonstruktora-igor-ya-sikorskogo> (accessed 8 May 2018). (Rus).
10. Available at: <http://www.tvc.ru/news/show/id/69580> (accessed 18 April 2018). (Rus).
11. Available at: <http://kpi.ua/ru/node/950> (accessed 23 May 2018). (Rus).
12. Available at: <https://gordonua.com/news/society/kiievskiy-politeh-nicheskij-institut-poluchil-imya-sikorskogo-147197.html> (accessed 10 June 2018). (Rus).

Received 01.10.2018

M.I. Baranov, Doctor of Technical Science, Professor, Scientific-&-Research Planning-&-Design Institute «Molniya», National Technical University «Kharkiv Polytechnic Institute», 47, Shevchenko Str., Kharkiv, 61013, Ukraine, phone +380 57 7076841, e-mail: baranovmi@kpi.kharkov.ua

R.P. Bondar

**RESEARCH OF THE MAGNETOELECTRIC LINEAR OSCILLATORY MOTOR CHARACTERISTICS DURING OPERATION ON ELASTOVISCOUS LOADING**

*Purpose.* To development of mathematical model for calculation of the magnetolectric linear vibration motor performance with elastoviscous loading and research of machine characteristics in the different operational modes depending on loading parameters. *Methodology.* Experimental results by means of the developed test setup according to the specified methods are obtained. Moreover we have correlated the experimental data obtained by means of the development experimental setup with the simulated results using analytical model of the linear oscillatory motor with elastoviscous loading. In the analytical model of the linear vibration motor a one-mass vibration system with equivalent parameters of stiffness and viscous friction is considered. *Results.* Calculations of performance data for three operating modes of the oscillatory motor – for constant value of current, constant amplitude and acceleration of vibrations are carried out. Results of calculation by means of analytical model are coordinated with the experimental data obtained with help of a prototype of the linear motor and the load machine. *Originality.* Analytical expressions for performance data of the linear vibration motor which are based on the analytical model and an equivalent circuit with the lumped parameters are obtained. It is shown that for calculation of performance data depending on parameters of loading it is possible to use analytical model which is based on an equivalent circuit with constant inertial parameters of the linear motor. *Practical value.* Results of the work can be used for designing new and improvements of the existing vibration devices on the basis of linear motors with the specified performance data. References 7, tables 1, figures 7.

*Key words:* magnetolectric linear motor, elastoviscous loading, performance data.

*Розглянуто магнітоелектричний лінійний двигун вібраційної дії циліндричної топології. Шляхом лінеаризації рівнянь динаміки, отримано вирази для розрахунку робочих характеристик двигуна в залежності від параметрів пружно-в'язкого навантаження. Характеристики визначаються для трьох режимів роботи – для сталого значення струму двигуна та для сталих амплітуди коливань і прискорення. Проведено дослідження в лінійній постановці, де розглядається одномасова коливальна система, в якій параметри навантаження враховуються як еквівалентні коефіцієнти жорсткості та в'язкого тертя. Для побудови розрахункової схеми заміщення використовується метод електромеханічних аналогій. Проведено експериментальні дослідження робочих характеристик магнітоелектричного двигуна вібраційної дії та виконано порівняльний розрахунок характеристик за допомогою представленої лінійної моделі. Бібл. 7, табл. 1, рис. 7.*

*Ключові слова:* магнітоелектричний лінійний двигун, пружно-в'язке навантаження, робочі характеристики.

*Рассмотрен магнитоэлектрический двигатель вибрационного действия цилиндрической топологии. Путем линеаризации уравнений динамики, получены выражения для расчета рабочих характеристик двигателя в зависимости от параметров упруго-вязкой нагрузки. Характеристики определяются для трёх режимов работы – для постоянного значения тока двигателя и для постоянных амплитуды колебаний и ускорения. Выполнено исследование в линейной постановке, где рассматривается одномассовая колебательная система, в которой параметры нагрузки учитываются как эквивалентные коэффициенты жесткости и вязкого трения. Для построения расчетной схемы замещения используется метод электромеханических аналогий. Выполнены экспериментальные исследования рабочих характеристик магнитоэлектрического двигателя вибрационного действия, а также сравнительный расчет характеристик с помощью представленной линейной модели. Библ. 7, табл. 1, рис. 7.*

*Ключевые слова:* магнитоэлектрический линейный двигатель, упруго-вязкая нагрузка, рабочие характеристики.

**Introduction.** Vibration technology is the basis of many modern technological processes associated with the movement and processing of materials, sealing, sorting, granulation, etc. Typically, rotary motors with appropriate mechanical transmissions are used to implement reciprocating propulsion motion. Low efficiency of rotary actuators is caused by significant mechanical losses in transmission devices, and insufficient reliability by dynamic overloads and non-durability of the typical series of induction motors used in them.

Linear motors (LMs) are an alternative to traditional drives based on rotational motors with transmissions that convert the rotational motion into straightforward one. Their advantages include the lack of mechanical gears, low noise, high reliability and improved handling.

The use of vibration devices with a drive from linear motors has its own peculiarities, which are determined by the nature of the operation process. In order for the vibrator to perform a certain technological operation (sealing, mixing, etc.), it is necessary to ensure the conformity of the electromechanical characteristics of the LM to the requirements of the operation process.

A series of works is devoted to the research and calculation of the characteristics of the LM of vibrational action. Considerable attention during the study of such systems was given to the analysis of the dynamic behavior of the drive, depending on the parameters of the LM and the operating frequency [1-3], that is, the frequency characteristics. In this case, the electromechanical system is considered as single-mass, on the basis of a linear substitution circuit with constant lumped parameters. The influence of the parameters of the elastoviscous loading on the frequency characteristics of the LM (in particular the power factor) was investigated in [4]. In [5], limitations were found for using a linear model by comparison with the results of calculations with the help of a refined nonlinear model based on the finite element method. The use of frequency dependent parameters of the substitution circuit [6] allowed expanding the frequency range of the linear model to determine the characteristics of the LM of vibration action.

The above work solves the problem of calculating the characteristics of a vibrator with a drive from LM

© R.P. Bondar

depending on the frequency. In this case, LM parameters are defined, for example, on the basis of finite element analysis. However, the parameters and the nature of the loading, especially when it is variable, have a significant effect on the characteristics. Such a change may result in the emergence of emergency modes, or the inefficient use of the machine and low efficiency. Therefore, the question of researching the performance characteristics of the LM of vibration action depending on the load parameters and the creation of mathematical models for calculating the parameters of the LM with the given performance characteristics is relevant.

**The goal of the work** is development of a mathematical model for calculating the performance characteristics of the LM of vibration action with elastoviscous loading and the study of the influence of load parameters on the characteristics of the machine in different operating modes.

The results of the work can be used to design new and improve the existing vibration devices on the basis of LM with the given performance.

**Influence of load parameters on the characteristics of LM of vibration action. Linear problem definition.** To determine the influence of the load parameters on the performance characteristics, we conduct a study using the linear model of the LM of vibration action, characterized by the following assumptions.

The voltage of the power supply and the current of the LM are sinusoidal. The parameters of the machine are constant and do not depend on the mode of operation. An equivalent mechanical circuit (Fig. 1,a) is represented by a concentrated mass  $m_a$ , which performs harmonic vibrations relative to the position of the mechanical equilibrium with the coordinate  $x_a = 0$  under the action of the sinusoidal electromagnetic force of the LM  $F_{ev}(i_v)$ . The restorative and dissipative forces are represented by the corresponding coefficients of rigidity of elastic suspension  $k_v$  and viscous friction  $b_v$ .

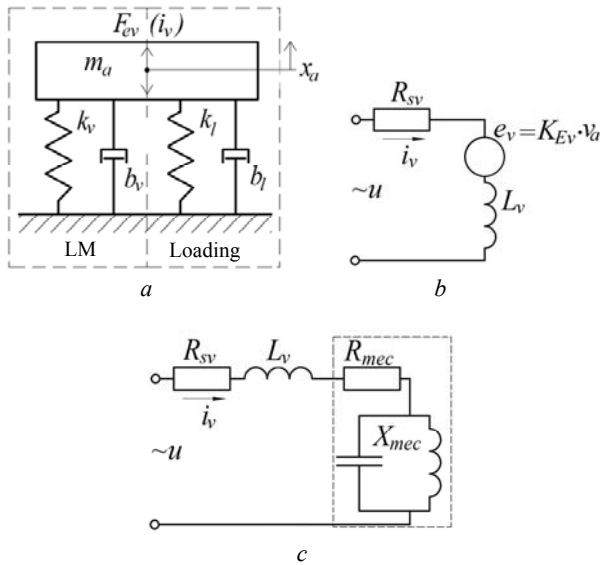


Fig. 1. Equivalent mechanical (a) and electrical circuits (b, c)

The force rating of the load is represented by the sum of the elastic component, proportional to the

movement of the armature of the LM  $x_a$ , and the viscous friction force proportional to the velocity  $v_a$ , i.e.

$$F_l(x_a, v_a) = k_l x_a + b_l v_a, \quad (1)$$

where  $k_l$ ,  $b_l$  are the respectively, coefficients of rigidity and viscous friction of the loading. A similar nature of the loading is typical, in particular, for compressors drives [4].

It is also considered that the electric circuit of the substitution of the LM (Fig. 1,b) is represented by a series of connected resistance  $R_{sv}$ , inductance  $L_v$  (constant averaged value) and source  $e_v$ , which respectively simulate the active resistance of the stator winding, the inductance of the stator winding and the EMF induced by the movement of the armature. The nonlinear properties of the magnetic cores of the machine are neglected.

The following system of differential equations corresponds to the presented substitution circuits:

$$\left. \begin{aligned} u_v &= i_v R_{sv} + L_v \frac{di_v}{dt} + K_{E_v} v_a; \\ m_a \frac{d^2 x_a}{dt^2} &= F_{ev}(i_v) - F_l(x_a, v_a) - k_v x_a - b_v \frac{dx_a}{dt}; \\ \frac{dx_a}{dt} &= v_a, \end{aligned} \right\} \quad (2)$$

where  $u_v = U_m \sin(2\pi ft)$  is the supply voltage of the LM winding;  $U_m$  is the supply voltage amplitude;  $i_v$  is the LM stator current;  $K_{E_v}$  is the coefficient of the EMF of the LM;  $F_{ev}(i_v) = K_{F_v} i_v$  is the LM electromagnetic force;  $K_{F_v}$  is the coefficient of the electromagnetic force.

In the frequency domain, the system (2) is written as

$$\left. \begin{aligned} \underline{U}_v &= \underline{I}_v (R_{sv} + j\omega L_v) + K_{E_v} \underline{V}_a; \\ -m_a \omega^2 \underline{X}_a &= K_{F_v} \underline{I}_v - (k_l + k_v) \underline{X}_a - j\omega (b_l + b_v) \underline{X}_a; \\ j\omega \underline{X}_a &= \underline{V}_a, \end{aligned} \right\} \quad (3)$$

where  $\omega$  is the angular frequency of supply voltage and mechanical vibrations.

From the second equation of system (3) we define the displacement

$$\underline{X}_a = \frac{K_{F_v} \underline{I}_v}{k_l + k_v - m_a \omega^2 + j\omega (b_l + b_v)}. \quad (4)$$

Having selected the real and imaginary parts of equation (4) and taking the initial phase of current of the LM equal to zero, it is possible to determine the amplitude of vibrations through the corresponding components of the complex displacement

$$X_{am} = \frac{K_{F_v} I_{vm}}{\sqrt{(k_l + k_v - m_a \omega^2)^2 + \omega^2 (b_l + b_v)^2}}, \quad (5)$$

where  $I_{vm}$  is the amplitude value of the LM winding current.

To determine the resonant frequency, we find the derivative of (5) by frequency and equate it to zero, from where

$$\omega_r = \sqrt{\frac{k_l + k_v}{m_a} - \frac{(b_l + b_v)^2}{2m_a^2}}. \quad (6)$$

Consider how the properties of a vibration system change depending on the load parameters.

From equation (5) it follows that when  $k_l + k_v < m_a \omega^2$ , the growth of the coefficient  $k_l$  leads to an

increase in the amplitude of vibrations, and if  $k_l + k_v > m_a \omega^2$  to decrease. An increase in the damping factor  $b_l$  leads to a decrease in the amplitude of vibrations and vice versa.

We consider other characteristics of the LM of vibration action, using the method of electromechanical analogies. For this it is convenient to introduce a mechanical link of the system with appropriate supports, the values of which can be obtained from the following.

From equation (4) it follows that

$$j\omega \underline{X}_a = \underline{V}_a = \frac{j\omega K_{Fv} \underline{I}_v}{k_l + k_v - m_a \omega^2 + j\omega(b_l + b_v)}.$$

Substituting this expression in the first equation of system (3), we obtain

$$\underline{U}_v = \underline{I}_v \left( R_{sv} + j\omega L_v + \frac{j\omega K_{Fv} K_{Ev}}{k_l + k_v - m_a \omega^2 + j\omega(b_l + b_v)} \right),$$

where it can be seen that the complete resistance of the system has electrical  $\underline{Z}_e = R_{sv} + j\omega L_v$  and mechanical

$$\underline{Z}_{mec} = \frac{j\omega K_{Fv} K_{Ev}}{k_l + k_v - m_a \omega^2 + j\omega(b_l + b_v)}$$
 components.

By analogy with electric circuits, active and reactive mechanical resistances are defined respectively as real and imaginary parts of the complex full mechanical resistance, that is,

$$\underline{Z}_{mec} = \frac{K_{Fv} K_{Ev} (b_l + b_v) \omega^2}{(k_l + k_v - m_a \omega^2)^2 + (b_l + b_v)^2 \omega^2} + j \frac{\omega K_{Fv} K_{Ev} (k_l + k_v - m_a \omega^2)}{(k_l + k_v - m_a \omega^2)^2 + (b_l + b_v)^2 \omega^2}. \quad (7)$$

The real part of expression (7) is the active mechanical resistance

$$R_{mec} = \frac{K_{Fv} K_{Ev} (b_l + b_v) \omega^2}{(k_l + k_v - m_a \omega^2)^2 + (b_l + b_v)^2 \omega^2},$$

and the imaginary one is the reactive mechanical resistance

$$X_{mec} = \frac{\omega K_{Fv} K_{Ev} (k_l + k_v - m_a \omega^2)}{(k_l + k_v - m_a \omega^2)^2 + (b_l + b_v)^2 \omega^2}.$$

The appropriate substitution circuit is presented in Fig. 1,c.

After determining the resistance, the LM power factor can be determined according to the expression

$$PF_v = \frac{R_{sv} + R_{mec}}{\sqrt{(R_{sv} + R_{mec})^2 + (X_{sv} + X_{mec})^2}}, \quad (8)$$

where  $X_{sv} = \omega L_v$  is the reactance of the LM winding.

According to the substitution circuit shown in Fig. 1,c, the current value of the supply voltage of the LM is determined from the expression

$$U_v = I_v \sqrt{(R_{sv} + R_{mec})^2 + (X_{sv} + X_{mec})^2}. \quad (9)$$

Then the power consumption will be equal

$$P_v = U_v I_v PF_v. \quad (10)$$

One of the possible operating modes of the LM of vibration action is the mode when the constant value of current  $I_v = \text{const}$  is supported in the winding. The

amplitude of vibrations, the power factor, the voltage and the power of the LM, for this mode, can be determined by the expressions (5, 8-10) respectively. Such a mode of operation is favorable in order to avoid electrical overloads, but it does not exclude mechanical overloads. In addition, this mode is not always optimal for providing the necessary mechanical characteristics of the drive (amplitude, speed, driving force or acceleration of the working body). Therefore, it is also advisable to consider the problem when it is necessary to determine the current of the LM, the properties of the elastic system and the coefficient of electromagnetic force for the given mechanical characteristics. As the latter, we consider the modes when the steady amplitude of vibrations  $X_{am} = \text{const}$  and the steady acceleration  $A_{am} = \text{const}$  should be ensured.

From expression (5), the current value of the current, which provides the required amplitude of vibrations, will be equal to

$$I_v|_{X_{am}=\text{const}} = \frac{X_{am} \sqrt{(k_l + k_v - m_a \omega^2)^2 + \omega^2 (b_l + b_v)^2}}{\sqrt{2} K_{Fv}}, \quad (11)$$

where it is seen that when  $k_l + k_v < m_a \omega^2$ , the growth of the coefficient  $k_l$  leads to a decrease in the current required to maintain a constant amplitude of vibrations, and if  $k_l + k_v > m_a \omega^2$  to increase. The increase in the damping factor  $b_l$  leads to an increase in the current of the LM and vice versa.

The steady acceleration mode  $A_{am} = X_{am} \omega^2 = \text{const}$ , provided that the vibration mass is constant, also ensures the constancy of the inertia force, since the latter equals  $F_0 = m_a X_{am} \omega^2$ .

Taking into account the above, the current value of the LM current, for a constant acceleration mode, is determined from the expression

$$A_{am} = \frac{K_{Fv} I_{vm} \omega^2}{\sqrt{(k_l + k_v - m_a \omega^2)^2 + \omega^2 (b_l + b_v)^2}},$$

where

$$I_v|_{A_{am}=\text{const}} = \frac{A_{am} \sqrt{(k_l + k_v - m_a \omega^2)^2 + \omega^2 (b_l + b_v)^2}}{\sqrt{2} K_{Fv} \omega^2}. \quad (12)$$

Voltage, power factor and power for the last two modes can be calculated by the expressions (8-10) taking into account (11, 12).

The connection of the above characteristics with the main dimensions and parameters of the LM is determined by the coefficient of electromagnetic force [7]  $K_{Fv} = \Psi_m \pi / \tau$ , where  $\Psi_m$  is the amplitude of the flux linkage of the winding;  $\tau$  is the pole division.

**Design of experimental LM of vibration action and loading machine.** Both experimental and load-bearing machines have cylindrical configuration. The stator of the experimental machine (Fig. 2,a) has a laminated core 1 of electrical steel and a winding of two coils 2. An armature of the machine contains a permanent magnet magnetized in axial direction 3 and two poles 4, which are made of structural steel and have radial incisions for reduction of eddy currents.

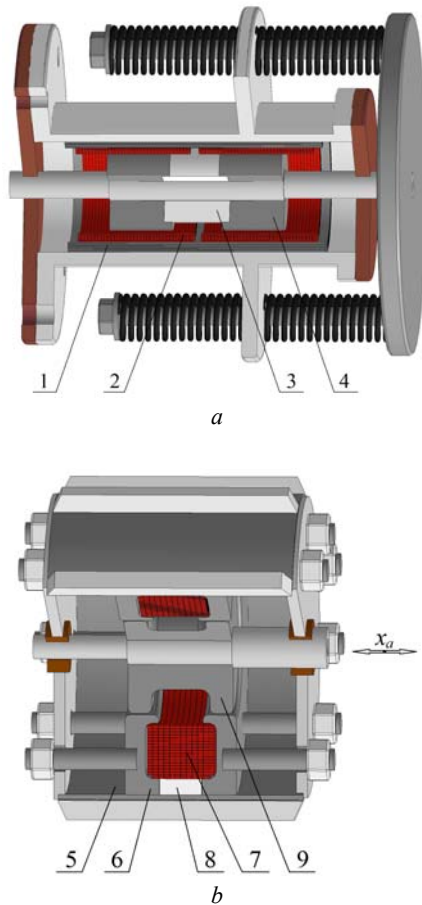


Fig. 2. Design of experimental (a) and loading (b) machines

The loading of the experimental motor is carried out using the loading machine shown in Fig. 2,b. The stator of the machine contains a body 5, a core with two ferromagnetic poles 6, between which there is a winding 7. In order to improve the specific power indicators, in a stator core a permanent magnet 8 of toroidal shape with an axial direction of magnetization is used. The electromagnetic force of the machine is determined by the force and direction of the current in the winding, as well as the position of the ferromagnetic armature 9 relative to the stator. Stator poles and armature are solid and have radial incisions to reduce eddy currents.

The main design parameters of experimental and loading machines are given in Table 1.

In accordance with the above mechanical and electrical substitution circuits (see Fig. 1), the parameters for the calculation of performance characteristics are as follows.

The mass of the oscillating part (the total mass of the armatures of the experimental and loading machinery, as well as the attached weight of the elastic suspension) is  $m_a = 6.72$  kg. Elastic suspension of the LM has rigidity  $k_v = 153291$  N/m, coefficient of viscous friction  $b_v = 44.9$  kg/s.

Parameters if the electrical substituting circuit of the LM (see Fig. 1,b) are:  $K_{Fv} = K_{Ev} = 13.1$ ;  $R_{sv} = 3.1 \Omega$ ;  $L_{sv} = 0.02$  H.

The parameters of the loading machine vary depending on the supply current and are within range  $b_l = (17 \div 31)$  kg/s,  $k_l = (3600 \div 26100)$  N/m.

Table 1

Design parameters of experimental and drive machines

Amplitude of vibrations (operating)		mm	10
Armature			
Permanent magnet	material	NdFeB(N42)	
	residual magnetic flux density	T	1.3
Stator			
Magnetic core	outer diameter	mm	89
	length	mm	165
Stator windings	wire section	mm <sup>2</sup>	1.06
	number of turns	–	300
Pole division		mm	79
Operation vibration amplitude		mm	10
Physical parameters			
Permanent magnet	material	NdFeB(N42)	
	residual magnetic flux density	T	1.3
Armature	material	Steel 3	
Winding	number of turns	380	
	wire	ПВД, Ø1.12	
Main dimensions			
Pole division		mm	36
Overall dimensions	diameter	mm	160
	length	mm	120

**Experimental study of the performance characteristics of the LM of vibration action.** Investigation of LM characteristics, depending on the load parameters, was carried out on the experimental stand presented in Fig. 3.

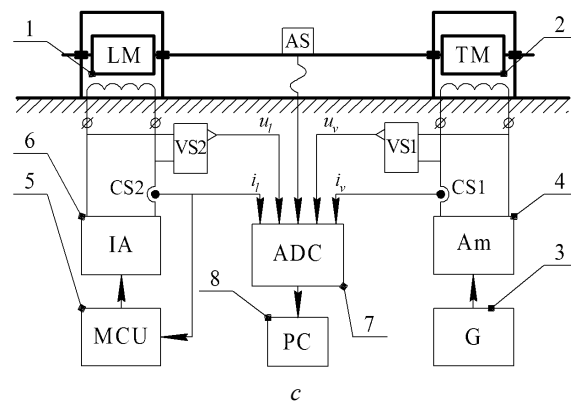


Fig. 3. Stand for the study of the characteristics of the LM of vibration action: a, b – external view; c – circuit

The armature of the experimental LD of vibration action 1 (LM) is rigidly connected to the armature of the loading machine 2 (TM). The power supply of the experimental machine is carried out from a sinusoidal source, which is realized with the help of generator 3 (G) and amplifier 4 (Am).

During experiments, a constant current value is maintained in the winding of the loading machine. To do this, a hysteresis current controller, made on microcontroller 5 (MCU), which controls the inverter 6 (IA), is used.

Measurement of voltages, currents of the LM and loading machine is performed using sensors VS1, VS2, CS1, CS2. The installation is equipped with an accelerometer AS, which is attached to the armature of the experimental machine. Measured values signals are fed to the multichannel measuring unit ADC 7 (ADC) and transmitted to the computer 8 (PC), which acts as a recorder.

Fig. 4 shows the dependencies of controlled quantities as time functions for the case when:  $I_v = 4.75$  A;  $I_l = -2$  A;  $X_{am} = 0.0048$  m;  $f = 23.5$  Hz.

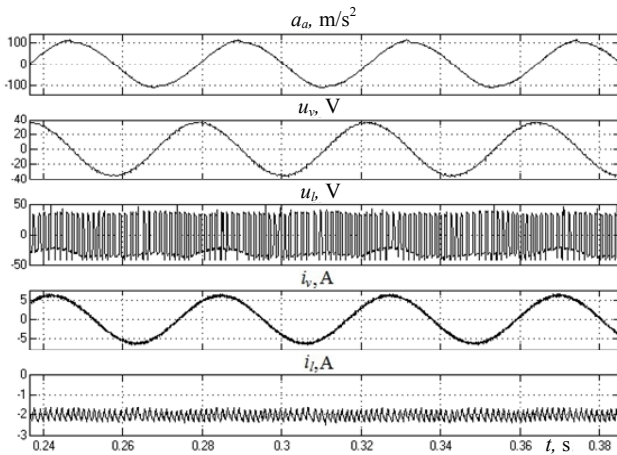


Fig. 4. Voltages and currents of the LM ( $u_v$ ,  $i_v$ ) and loading machine ( $u_l$ ,  $i_l$ ),  $a_a$  – accelerations

The presented below experimental operational characteristics are obtained as a result of appropriate processing and recalculation of the time charts of the measured values, namely:

- determining effective values of the voltage  $U_v$  and current  $I_v$  of the motor

$$U_v = \sqrt{\frac{1}{T} \int_{t-T}^t u_v^2 dt}; \quad I_v = \sqrt{\frac{1}{T} \int_{t-T}^t i_v^2 dt};$$

- determined average value of the loading machine current  $I_l$

$$I_l = \frac{1}{T} \int_{t-T}^t i_l dt;$$

- determining vibration amplitude

$$|X_{am}| = \frac{\sqrt{a_n^2 + b_n^2}}{\omega^2},$$

$$\text{where } a_n = \frac{2}{T} \int_{t-T}^t a_a \cos(n\omega t) dt; \quad b_n = \frac{2}{T} \int_{t-T}^t a_a \sin(n\omega t) dt$$

are the coefficients of the Fourier series;  $n$  is the order of the harmonic (and  $n = 1$ , that is, the calculation was carried out according to the basic harmonic frequency of the mechanical oscillations  $\omega$ );  $T = 1/f$  is the period;

- calculating active power  $P_v$  and power factor  $PF_v$  of the motor

$$P_v = \frac{1}{T} \int_{t-T}^t u_v i_v dt; \quad PF_v = \frac{P_v}{U_v I_v}.$$

In Fig. 5 marker shows the experimental characteristics of the LM of vibration action for the operating mode when it's current is constant –  $I_v = 4.75$  A. Characteristics are presented for three values of the frequency: 24.2; 24.9; 25.6 Hz. In this frequency range, with given LM and load parameters, the system is near the frequency of mechanical resonance  $\omega_r$ .

The lines show the calculation results using the above linear model. The corresponding dependencies were determined by the equations (5, 8-10).

Amplitude of vibrations (Fig. 5,a), for the mode  $I_v = \text{const}$ , has clearly expressed maxima corresponding to the parameters of the mechanical resonance at the corresponding frequencies. The maximum value of the amplitude decreases with increasing damping coefficient of loading  $b_l$ , which also follows from equation (5). As a result of the decrease in the amplitude of vibrations (and hence the velocity), the voltage  $K_{Ev} v_a$ , which is included in the equation of the balance of the system voltage (2), decreases. Therefore, with the increase of damping, the value of the voltage required to provide a constant current decreases (Fig. 5,b).

Several factors influence on the form of dependencies of the power factor  $PF_v$  on the load parameters (Fig. 5,c). Depending on the frequency and parameters, the mechanical resistance can be active-inductive or active-capacitive. In the latter case, electrical resonance is possible if the value of the capacitive mechanical resistance is balanced by the inductive resistance of the LM. During the passage through the frequency  $\omega = \sqrt{(k_l + k_v)/m_a}$ , reactive mechanical resistance changes its character from inductive to capacitive or vice versa [5]. The change in the power factor from the coefficient of rigidity of the loading  $k_l$  depends on how the latter differs from the value corresponding to the change in the sign of the reactive resistance, i.e.  $k_l = \omega^2 m_a - k_v$ . Changing the mechanical resistances (active and reactive) will determine the nature of the change (increase or decrease) of the power factor.

In Fig. 6 marker shows the experimental characteristics of the LM of vibration action for the mode of the steady-state vibration amplitude  $X_{am} = 0.007$  m.

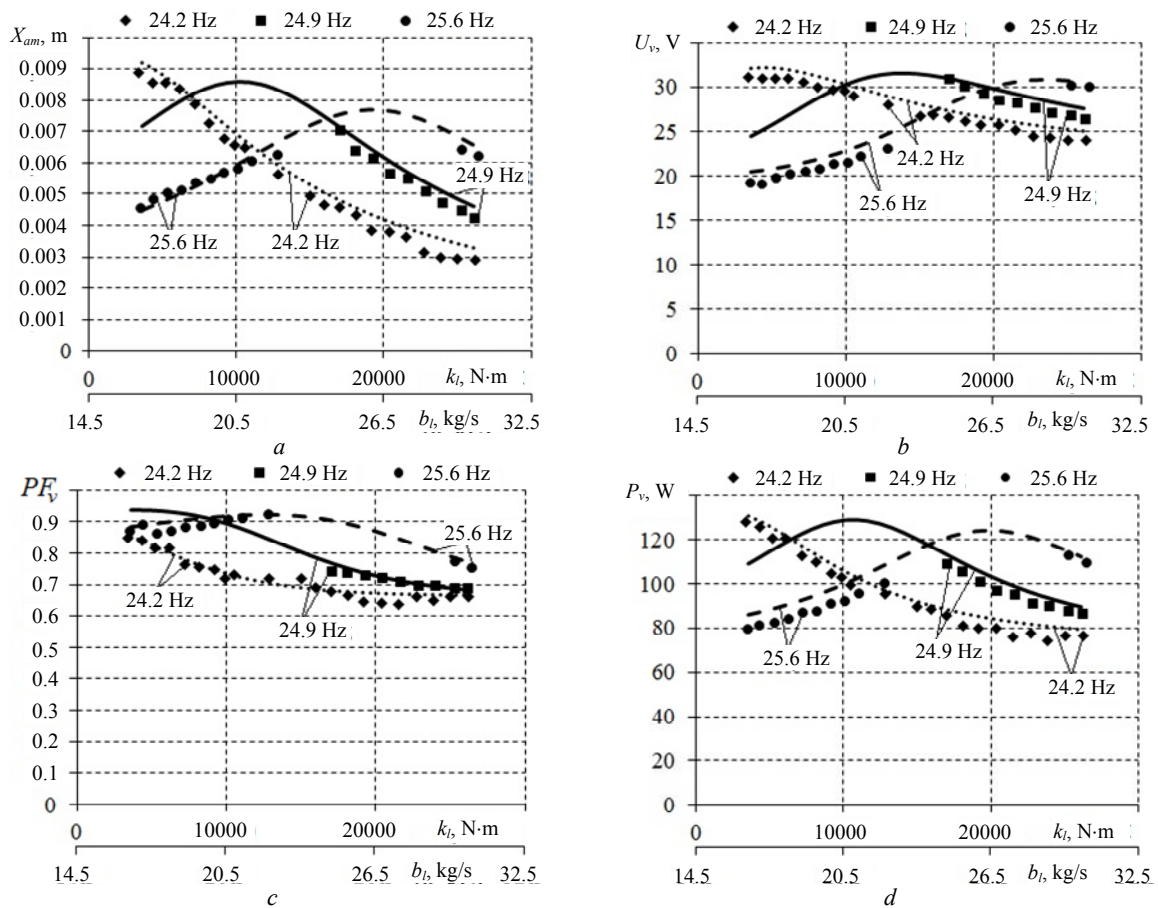


Fig. 5. Characteristics of the LM of vibration action for the mode  $I_v = \text{const}$

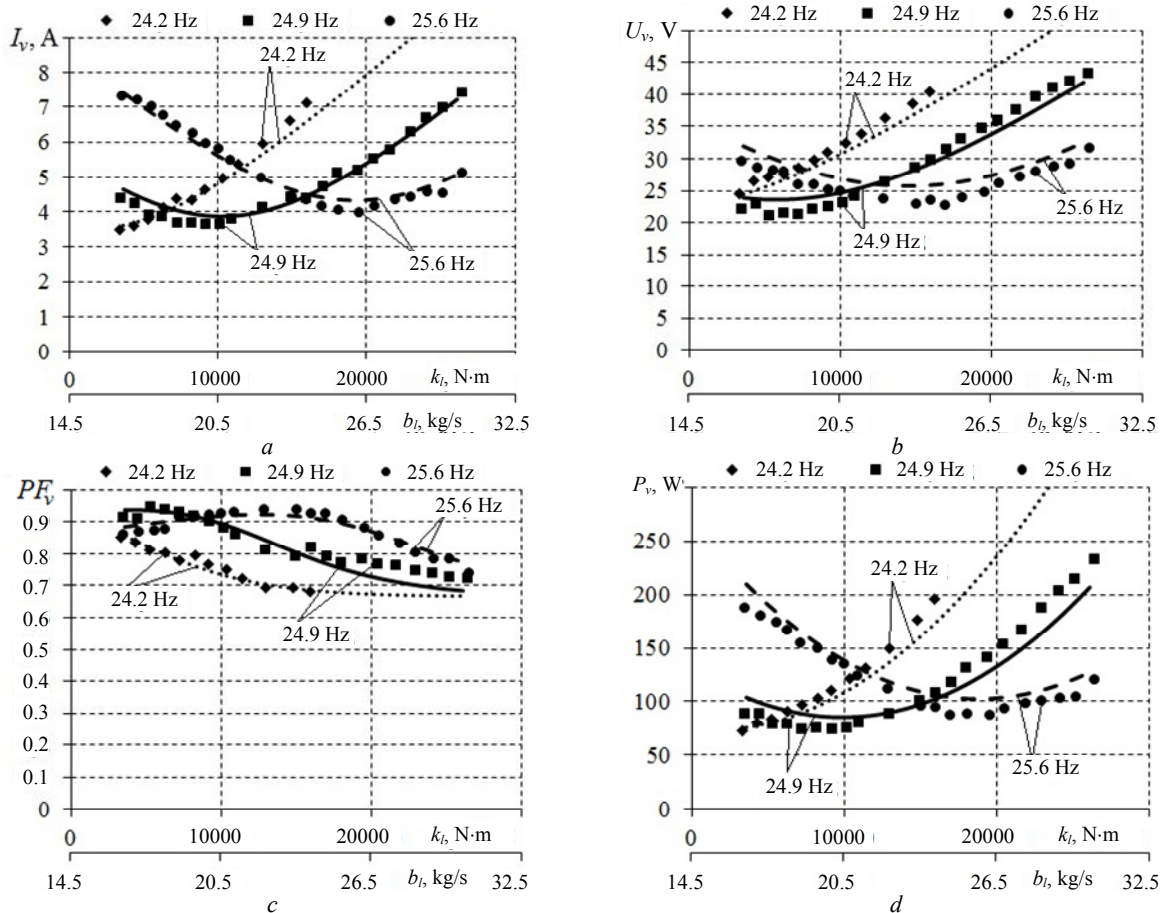


Fig. 6. Characteristics of the LM of vibration action for the mode  $X_{am} = \text{const}$

The lines show the calculation results using a linear model. The corresponding dependencies were determined according to the equations (8-11).

In this mode there is a significant change in the current and voltage of the LM. The minimum value of current (Fig. 6,a) approximates to the parameters of mechanical resonance, which in particular follows from equation (11). From this equation, it is also seen that with the increase of the coefficient  $b_l$ , increased current values are needed to provide given amplitude of vibrations.

In Fig. 7 marker shows the experimental dependencies of the LM characteristics on load parameters for the case of steady acceleration  $A_{am} = 192 \text{ m/s}^2$  (in amplitude).

The lines show the results of the calculation of characteristics using a linear model. The corresponding dependencies were determined by the equations (8-10, 12).

The characteristics for a stable acceleration case are similar to those for stable amplitude of vibrations, since the quantities are proportional. The difference lies in the fact that in this mode, with increasing frequency, the amplitude of vibrations decreases, and the form of the characteristics varies less depending on the frequency. Therefore, the minimum values of current, voltage and power corresponding to the near-resonance parameters are close and slightly increase with increasing frequency.

As can be seen from Fig. 5-7, the results of calculations according to the linear model are satisfactorily consistent with the experimental data. Since the operating frequency range is relatively small ( $\Delta f = 1.4 \text{ Hz}$ ), the machine parameters change practically does not appear depending on the frequency, which makes it possible to use the steady values of LM parameters for the calculation of the operating characteristics.

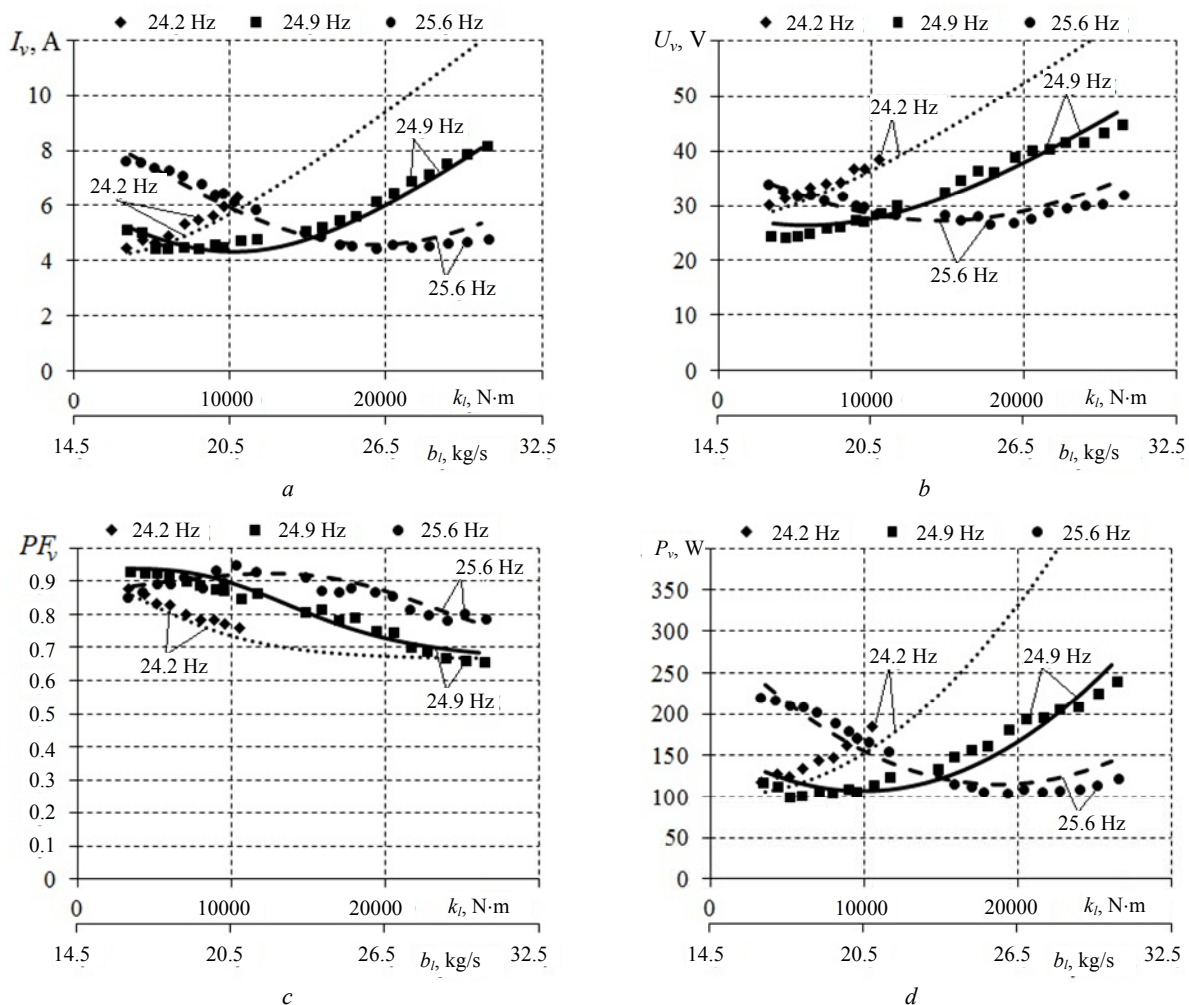


Fig. 7. Characteristics of the LM of vibration action for the mode  $A_{am} = \text{const}$

### Conclusions.

1. In the paper analytical expressions for the performance characteristics of a linear motor of vibration action based on a linear model and a substitution circuit with lumped parameters are obtained.

2. The calculation of performance characteristics for three modes of operation – for the constant value of current, constant amplitude and acceleration of

oscillations is carried out. The results of the calculations according to the linear model are satisfactorily consistent with the experimental data obtained using the prototype of the LM and loading linear machine.

3. In the mode of constant current, the operating amplitude of oscillations has clearly expressed maxima that correspond to the parameters of mechanical resonance. The maximum value of the amplitude

decreases with increasing damping coefficient of the loading.

4. In the mode of steady-state oscillation amplitude there is a significant change in the current and voltage of the LM. The minimum value of the current approximates to the parameters of mechanical resonance. Also, with increasing damping coefficient, increased current value is needed to provide given amplitude of oscillations.

5. The form of the characteristics for the case of steady acceleration changes little depending on frequency. Therefore, the minimum values of current, voltage and power corresponding to the near-resonance parameters are close and slightly increase with increasing frequency.

6. It is shown that in order to calculate the performance characteristics, depending on the load parameters, a linear model based on the substitution circuit with steady, inertial values of LM parameters can be used.

#### REFERENCES

1. Jang-Young Choi, Han-Bit Kan. Comparison and dynamic behavior of moving-coil linear oscillatory actuator with/without mechanical spring driven by rectangular voltage source. *Journal of International Conference on Electrical Machines and Systems*, 2014, vol.3, no.4, pp. 394-397. doi: **10.11142/jicems.2014.3.4.394**.
2. Kyu-Hwan Hwang, Yun-Hyun Cho. Design and dynamic characteristics analysis of moving magnet linear actuator for human. *Proceedings of the IEEE International Conference on*

*Mechatronics*, 2004, pp. 251-254. doi: **10.1109/ICMECH.2004.1364447**.

3. Watada M. Kinetic characteristics of cylindrical moving coil linear DC motor for vibrator. *7th International Conference on Electrical Machines and Drives*, 11-13 September 1995, pp. 359-362. doi: **10.1049/cp:19950894**.

4. Yu M., Ye Y., Lu Q., Xia Y. A study on power factor of linear oscillatory motor with two separated stators. *2009 International Conference on Electrical Machines and Systems (ICEMS 2009)*, Nov. 2009, pp. 1-5. doi: **10.1109/icems.2009.5382915**.

5. Bondar R.P., Golenkov G.M., Lytvun A. Yu., Podoltsev A.D. Modelling of power characteristics of the vibrator with a linear electric drive. *Electromechanical and energy saving systems*, 2013, no.2, pp. 66-74. (Ukr).

6. Bondar R.P., Podoltsev A.D. Complex model with frequency dependent parameters for electrodynamic shaker characteristics. *Technical electrodynamics*, 2017, no.1, pp. 44-51. (Ukr). doi: **10.15407/techned2017.01.044**.

7. Bondar R.P. Definition of parameters of an equivalent circuit of the linear electrodynamic vibrator. Part 1. *Mining, construction, road and melioration machines*, 2015, no.85, pp. 109-118. (Ukr).

Received 24.09.2018

R.P. Bondar, Candidate of Technical Science, Associate Professor,  
Kyiv National University of Construction and Architecture,  
31, Povitroflotsky Ave., Kyiv, 03037, Ukraine,  
phone +380 44 2415510, e-mail: rpbondar@gmail.com

#### How to cite this article:

Bondar R.P. Research of the magnetoelectric linear oscillatory motor characteristics during operation on elastoviscous loading. *Electrical engineering & electromechanics*, 2019, no.1, pp. 9-16. doi: **10.20998/2074-272X.2019.1.02**.

V.Ya. Halchenko, Yu.Yu. Bondarenko, S.A. Filimonov, N.V. Filimonova

## DETERMINATION OF INFLUENCE OF GEOMETRIC PARAMETERS OF PIEZOCERAMIC PLATE ON AMPLITUDE CHARACTERISTICS OF LINEAR PIEZOMOTOR

*Purpose. The purpose of the paper is to determine the influence of the geometric parameters of the stator of a linear piezoceramic motor in the form of a piezoceramic plate on the characteristics of its amplitude oscillations. Methodology. For the research, mathematical modeling in the COMSOL Multiphysics software package was used, taking into account the interrelation of electrostatic and mechanical phenomena. Results. By numerical simulation of the process of operating of a linear piezoceramic motor, a rational ratio of the width to the length of the piezoceramic plate is determined. Originality. The rational value of the thickness  $h$  of the piezoceramic plate of the motor is also established. Approximate dependencies are proposed for determining the parameters of the relationship between the geometric dimensions of the piezoceramic plate of a linear piezomotor, which makes it possible to predict its characteristics. The adequacy of calculation models is confirmed by experimental studies. Practical value. The results obtained can be used in the design of piezoceramic motors. References 15, figures 8.*

*Key words:* piezoceramics, piezoceramic motor, piezoceramic plate.

*Метою статті є визначення впливу геометричних параметрів статора лінійного п'єзокерамічного двигуна у вигляді п'єзокерамічної пластини на характеристики її амплітудних коливань. Для проведення досліджень використовувалося математичне моделювання в середовищі пакета програм COMSOL Multiphysics з урахуванням взаємозв'язку електростатичних і механічних явищ. Шляхом чисельного моделювання процесу функціонування лінійного п'єзокерамічного двигуна визначено раціональне відношення ширини до довжини п'єзокерамічної пластини. Встановлено також раціональне значення товщини  $h$  п'єзокерамічної пластини двигуна. Запропоновані апроксимаційні залежності для визначення параметрів зв'язку між геометричними розмірами п'єзокерамічної пластини лінійного п'єзодвигуна, що дозволяє прогнозувати його характеристики. Адекватність модельних розрахунків підтверджена експериментальними дослідженнями. Отримані результати можуть використовуватися при проектуванні п'єзокерамічних двигунів. Бібл. 15, рис. 8.*

*Ключові слова:* п'єзокераміка, п'єзокерамічний двигун, п'єзокерамічна пластина.

*Целью статьи является определение влияния геометрических параметров статора линейного пьезокерамического двигателя в виде пьезокерамической пластины на характеристики ее амплитудных колебаний. Для проведения исследований использовалось математическое моделирование в среде пакета программ COMSOL Multiphysics с учетом взаимосвязи электростатических и механических явлений. Путем численного моделирования процесса функционирования линейного пьезокерамического двигателя определено рациональное отношение ширины к длине пьезокерамической пластины. Предложены аппроксимационные зависимости для определения параметров связи между геометрическими размерами пьезокерамической пластины линейного пьезодвигателя, что позволяет прогнозировать его характеристики. Адекватность модельных расчетов подтверждена экспериментальными исследованиями. Полученные результаты могут использоваться при проектировании пьезокерамических двигателей. Библ. 15, рис. 8.*

*Ключевые слова:* пьезокерамика, пьезокерамический двигатель, пьезокерамическая пластина.

**Introduction.** Piezoelectric motors are used in microscopy, robotics, photographic equipment, nanometrology, nanolithography, nanoprint, microdosing, etc. They can be used for vacuum and cryogenic equipment, as well as ultra-precise positioning of objects and systems, in particular, for radar systems [1-3].

Piezomotors are devices in which mechanical movement is achieved due to the inverse piezoelectric effect. The materials that form the basis of such drives are called piezoelectrics. The inverse piezoelectric effect consists in changing the linear dimensions of a piezoelectric when an electric field is applied to it.

The relevance of the use of piezoelectric motors in various precision measuring and tracking systems, the adjustable values of which are angular and linear displacements, is explained by several factors. This is, first of all, their high resolution (up to 0.1 nm), the possibility of self-stopping of the drive link, the maximum duration of trouble-free operation, as well as their high reliability [3]. A demonstration application based on piezomotors is a theodolite [4], which is an

exact instrument on which a movable telescope is mounted for measuring angles in the horizontal and vertical planes.

Piezoelectric motors have a number of advantages over electromagnetic ones, namely [2]: the absence of radiated magnetic fields and their resistance to their influence; the possibility of miniaturization; wide range of rotational speeds and torques on the shaft; fire resistance; absence of windings; simple manufacturing technology and, consequently, higher efficiency.

At the same time, behind the external design simplicity of a piezoelectric motor, there is a whole series of physical phenomena that are interconnected in a complex way [5, 6]. The difficulties of their joint accounting significantly restrain the development and improvement of this type of motors.

**The object of the research** is the interaction processes of transverse bending and longitudinal mechanical oscillations of the stator of a linear piezoceramic motor. **The subject of the research** is

© V.Ya. Halchenko, Yu.Yu. Bondarenko, S.A. Filimonov, N.V. Filimonova

the piezoelectric element of a linear piezoceramic motor, i.e. stator.

**The goal of the work** is determination of the influence of the geometric parameters of a piezoceramic plate of a linear piezoceramic motor on the characteristics of its amplitude oscillations.

**Problem definition.** To achieve this goal, it is necessary to consistently solve a number of problems: determine the resonance frequency at which the piezoceramic element, namely, the stator pusher, becomes elliptical oscillations; determine the maximum amplitude of oscillations of the pusher when changing the geometry (width and length) of the piezoceramic plate; determine the rational ratio of the width to the length of the piezoceramic plate and the rational thickness of the piezoceramic plate with the selected effective ratio of its width to length.

**Literature review.** Piezoelectric motors according to the principle of the final movement of the rotor (carriage) can be classified into linear and rotational types. This paper discusses a linear piezoelectric motor. One of the most common types of linear piezoelectric motors is the design shown in Fig. 1 [4, 7-9]. The main elements of this piezoelectric motor are: rectangular monolithic piezoceramic plate (stator) 1 with electrodes 2, 3; friction tip (pusher) 4, as well as a carriage (rotor, which is not shown in the Figure). Electrode 2 is divided into two sections – 5, 6. The pusher and the plate are a one-piece construction made of a piezoceramic material. Piezoceramic plate from side 7 under the action of an external force  $F$  is pressed against the carriage (rotor).

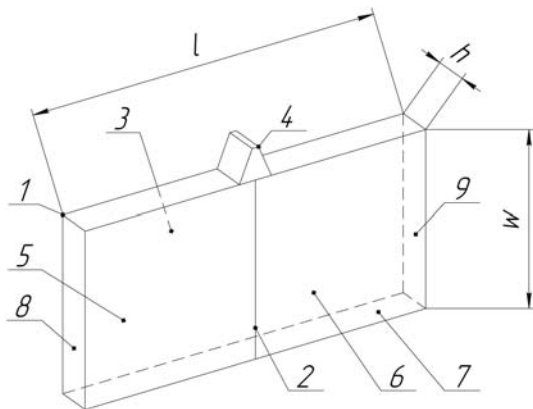


Fig. 1. Piezoceramic plate of a linear piezoceramic motor of the Company Physik Instrumente

The piezoelectric motor operates as follows (Fig. 1). The control voltage is applied to one of the sections 5 or 6 of the electrode 2, which depends on the chosen direction of movement of the carriage, and to the opposite electrode 3, which is common («ground»). In this design of a piezoelectric motor, in order to obtain a linear movement of the carriage, in the pusher oscillations are excited in two mutually perpendicular directions. In this case, the longitudinal vibrations in the pusher are excited by the longitudinal oscillations of the piezoplate (stator), and the transverse bending vibrations – by mechanical way, due to the interaction of the pusher with the surface of the carriage. Thus, the pusher begins to perform oscillations in the shape of an ellipse and push the carriage.

One of the main criteria for designing such a linear piezoelectric motor is the complex matching of the geometric parameters of a piezoceramic plate, namely, length, width and thickness, for maximum energy transfer to its carriage [10]. Incorrect selection of these parameters significantly affects the technical characteristics of the linear piezoceramic motors.

In the works [11, 12] the description of this design of a piezoceramic motor is given, and they say about «a certain ratio of length to width of the selected element».

In the works [5, 7-9], only one of the possible ratios of width to plate length is given, at which acceptable results can be obtained is presented. In this case, the dependence on the change in its thickness is not given. At the same time, it is not known whether such a choice is close to optimal.

Theoretically, there are other ratios of width to length of the piezoelectric element, at which the maximum oscillations or close to them are reached.

Analysis of technical literature, research papers, and patents showed that in the existing works the choice of parameters is not considered, and also the dependencies for the geometry of the piezoceramic plate of a linear piezoceramic motor, providing an effective mode of operation, are not presented.

Thus, the determination of rational parameters of a piezoceramic plate of a linear piezoceramic motor is an important and urgent task.

**Materials and methods.** Mathematical dependencies are known for calculating piezoceramic elements of standard shapes (plate, disk, ring, bar and rod) without small structural details on them [13].

The parameters of the piezoceramic plate (static shift along the length  $\Delta l$ , width  $\Delta w$  and thickness  $\Delta h$ ) can be determined using the empirical formulas below [13]:

$$\begin{aligned} \Delta l &= \frac{d_{31} \cdot V_l}{h}; \\ \Delta w &= \frac{d_{31} \cdot V_w}{h}; \\ \Delta h &= d_{33} \cdot V; \end{aligned} \quad (1)$$

where  $\Delta l$  is the static shift in length,  $\Delta w$  is the static shift in width,  $\Delta h$  is the static shift in thickness,  $d_{31}$  and  $d_{33}$  are the piezoelectric modules,  $h$  is the thickness of the piezoceramic plate,  $V_l$ ,  $V_w$  and  $V$  is the applied voltage to the corresponding side of the plate (length, width and thickness).

At the same time, the use of elementary methods of calculation does not allow visualizing the shape of oscillation of the entire piezoceramic element, and therefore does not make it possible to determine the acceptable shape of its oscillations.

Considering the technical features of piezoelectric motors, which make it difficult to experimentally determine and select the correct oscillation shape of the piezoelectric element, it is optimal to use for this purpose numerical calculation methods implemented by specialized CAD systems.

To study the influence of the design parameters of the piezoceramic plate of a linear piezoelectric motor, numerical simulation of the operation of the piezoelectric element was carried out using the COMSOL Multiphysics 3.5 software package.

The COMSOL piezoelectric device interface combines the functionality of modeling of solid mechanics modules and electrostatics COMSOL's Solid Mechanics and Electrostatics into one tool for modeling piezoelectric materials. Piezoelectric devices in COMSOL Multiphysics 3.5 are simulated using the Piezoelectric Effects module. Since the operation of piezoelectric motors is based on the reverse piezoelectric effect, therefore, the Stress-Charge Form mode is selected in the Piezoelectric Effects module.

The piezoelectric element is characterized by the connection between the deformation and the electric field, which is determined by the material or constitutive relations [13]:

$$T = c_E S - e^T E; \quad D = eS - \epsilon_S E; \quad (2)$$

where  $S$  is the deformation,  $T$  is the mechanical stress,  $E$  is the electric field strength,  $D$  is the electric displacement.

The material parameters  $c_E$ ,  $e$  and  $\epsilon_S$  in (2) correspond to the stiffness of the material, the coefficient of electromechanical coupling and the dielectric permeability. These values are of the 4th, the 3rd and the 2nd rank tensors, respectively, but since tensors are symmetric for physical reasons, they can be represented as matrices in an reduced notation, which is usually more convenient [14].

For modeling, Lagrangian finite elements with elementary second order basis functions, Lagrange-Quadratic, were used.

The linear piezoceramic motor was analyzed in the Frequency response mode. The calculated finite element mesh in the «Mesh» section is selected as orthogonalized – Normal. The investigated 3D model is represented by a set of elements obtained as a result of meshing with a tetragonal dividing. Direct is used as a solver, in which the SPOLES numerical method is chosen to solve systems of linear equations with sparse matrices.

The material used for modeling a piezoceramic plate was a brand of piezoceramic PZT-5H. Variants of the geometry of the piezoceramic plate are represented by the parameters  $K = w/l$  in dimensionless form, obtained by the ratios of width  $w$  to its length  $l$ .

At the first stage of modeling, the parameter  $K$  changed from 0.125 to 1.25 with a step of 0.125, while the thickness remained constant at 3 mm. At this stage, a rational relationship was determined between the length and width of the piezoceramic plate. At the second stage of the simulation, with the chosen ratio of the parameter  $K$ , the thickness of the piezoceramic plate was changed from 1 to 6 mm with a step of 1 mm. The geometrical dimensions of the pusher did not change (Fig. 2).

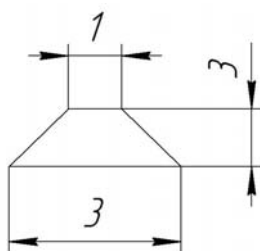


Fig. 2. Linear piezoelectric motor pusher dimensions

The boundary conditions for the model of a piezoelectric motor are as follows: piezoceramic plate 1 in width on both sides 8, 9 (Fig. 1) has the type of boundary conditions Roller; electrical voltage (Electric potential) of 100 V is applied to the partitioned electrode 5, and the ground (Ground) to the entire electrode 3 on the opposite side.

When conducting numerical simulations in the COMSOL Multiphysics software package, the resonance frequency was first determined at which the piezoceramic element, namely the plunger, acquires elliptical oscillations. The dynamics of elliptical movements of the piezoelectric motor pusher is quite complex and is provided by resonant phenomena, which is described in detail in [3]. Important for their implementation is the provision of the resonance mode, which is fixed at stepwise variation of the control voltage frequency and manifests itself in a sharp increase in amplitude periodic oscillations of the piezoelectric element sizes at one of the model frequencies. Approximate resonant frequency approximately without taking into account the influence of the pusher can be determined using the recommendations [15]. In the vicinity of this frequency with a step of 100 Hz, numerical experiments were conducted using the COMSOL software package to determine its exact value. Then, when the geometrical dimensions of the piezoceramic plate were changed, the maximum amplitude of the oscillation of the pusher was determined, and the rational ratio of the width to the length of the piezoceramic plate was selected. Finally, studies were conducted on the choice of a rational thickness of a piezoceramic plate.

**Experimental studies** were conducted to verify the adequacy of the results obtained by numerical simulation. Fig. 3 shows a schematic representation of an experimental linear piezoelectric motor.

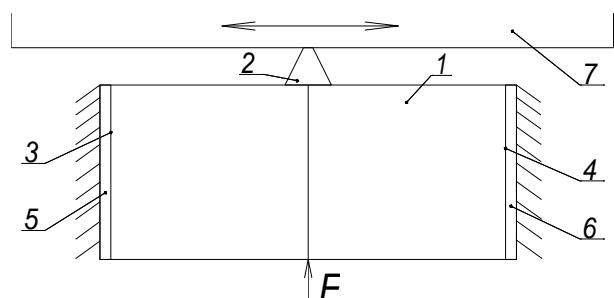


Fig. 3. Schematic representation of an experimental linear piezoelectric motor

The methodology of the experiments is as follows. The piezoelectric plate 1 with the hub 2 is fixed so that it is fixed from opposite sides by width 3, 4 across damping rubber gaskets 5, 6. The hub 2 of the piezoelectric plate 1 is firmly pressed against the rolling guide (carriage) 7 by the pressing force  $F$  acting from the opposite side and created by a leaf spring. The pressing force can be changed using adjustment screws.

**Results of investigations.** Some of the results of numerical simulation of oscillations of a piezoceramic plate of a linear motor are presented in Fig. 4, which

illustrates the oscillations of a piezoceramic plate of the motor. In Fig. 4, 6, on the right, on the vertical axis, the color scale of the gradation of the amplitude of oscillations of the geometric dimensions of a piezoplate is shown. The values of the resonant frequency of oscillations are taken based on the graphical images of the conducted numerical studies in the COMSOL Multiphysics environment in the pusher region. The numerical values of the frequency are displayed in the

postprocessor window of the package automatically and correspond to the maximum amplitude of the piezoplate oscillations. Thus, we obtain a set of frequencies taken for various ratios of the geometric parameters of the piezoceramic plate. For example, the frequency  $f_{theor} = 74.9$  kHz is obtained with the following plate sizes:  $l = 40$  mm;  $w = 20$  mm;  $h = 3$  mm. When modeling the size of the piezoceramic plate was changed in the range  $w = 10\div 60$  mm,  $l = 10\div 60$  mm.

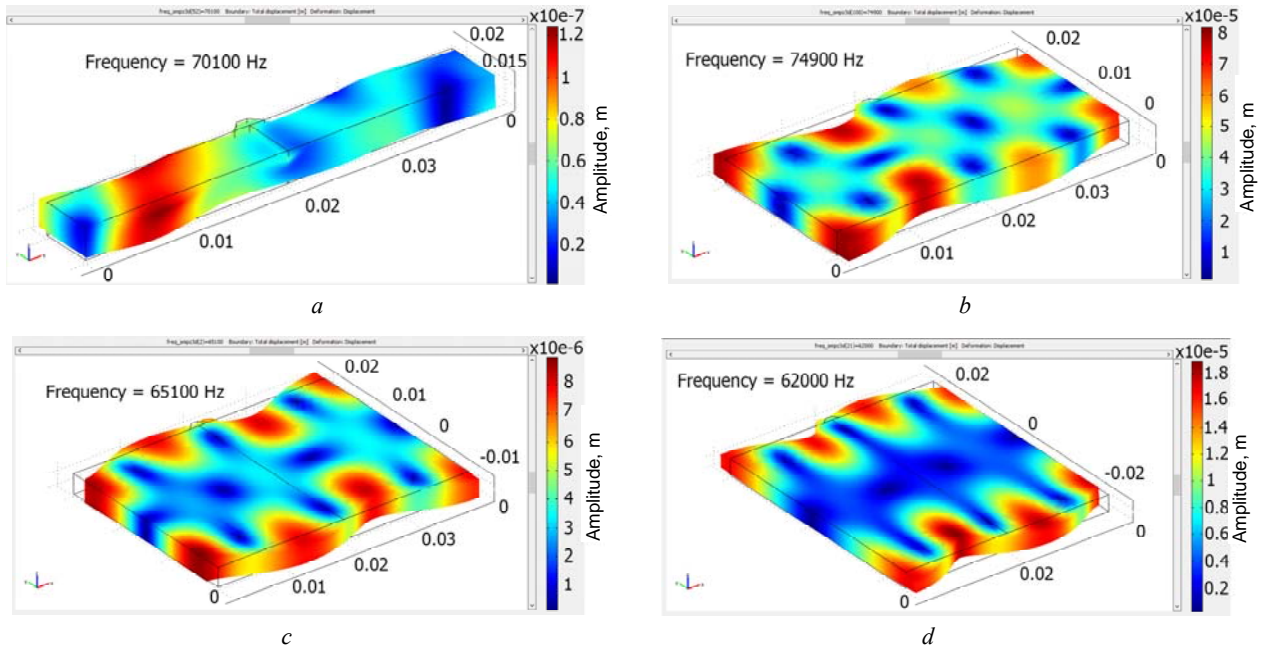


Fig. 4. Some of the results of simulation of amplitude oscillations of a piezoelectric element of a linear motor with different ratios of width to plate length:  $a - K = 0.125$ ;  $b - K = 0.5$ ;  $c - K = 0.875$ ;  $d - K = 1.125$

As a result of the simulation, resonant frequencies were determined that correspond to the elliptical shape of the pusher oscillation are determined.

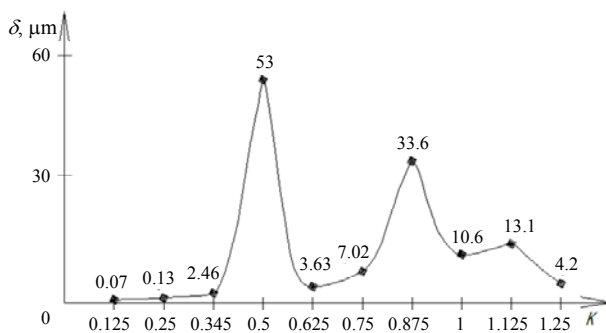


Fig. 5. The dependence of the amplitude of oscillations of the pusher on parameter  $K$  of a piezoceramic plate

The obtained results of numerical simulation are presented in graphical form by the dependence of the amplitude of oscillations of the pusher on the parameter  $K$  of the piezoceramic plate and are shown in Fig. 5.

As can be seen from the graphs, two ratios can be selected at which the maximum amplitude of the pusher is reached, namely,  $53 \mu\text{m}$  for  $K = 0.5$ , and also  $33.6 \mu\text{m}$  for  $K = 0.875$ .

The graphical dependence for the amplitude of oscillations of the pusher obtained as a result of numerical simulation was approximated using the least-squares method by a second-order polynomial function

$$\delta = \frac{1}{a + bx + cx^2}, \quad (3)$$

where  $\delta$  is the pusher oscillation amplitude,  $x$  is the parameter  $K$  of the piezoelectric plate,  $a = 4.074768$ ,  $b = -16.243571$ ,  $c = 16.263542$ ,  $d = 1206.5824$  are the coefficients.

This model is adequate in the range of variation of parameter  $K$  of a piezoelectric plate from 0.345 to 0.625.

After choosing the geometry of the piezoceramic plate, its rational thickness was determined. To do this, during modeling this parameter varied in the range from 1 to 6 mm with a step of 1 mm.

Some of the results of numerical simulation of oscillations of a piezoceramic plate of a linear motor are presented in Fig. 6.

The results obtained are graphically shown in Fig. 7.

It is obvious that the rational thickness of the piezoceramic plate is 3 mm, while the amplitude of oscillations of the pusher was  $53 \mu\text{m}$ , which follows from the analysis of the graphical dependencies shown in Fig. 5, 7.

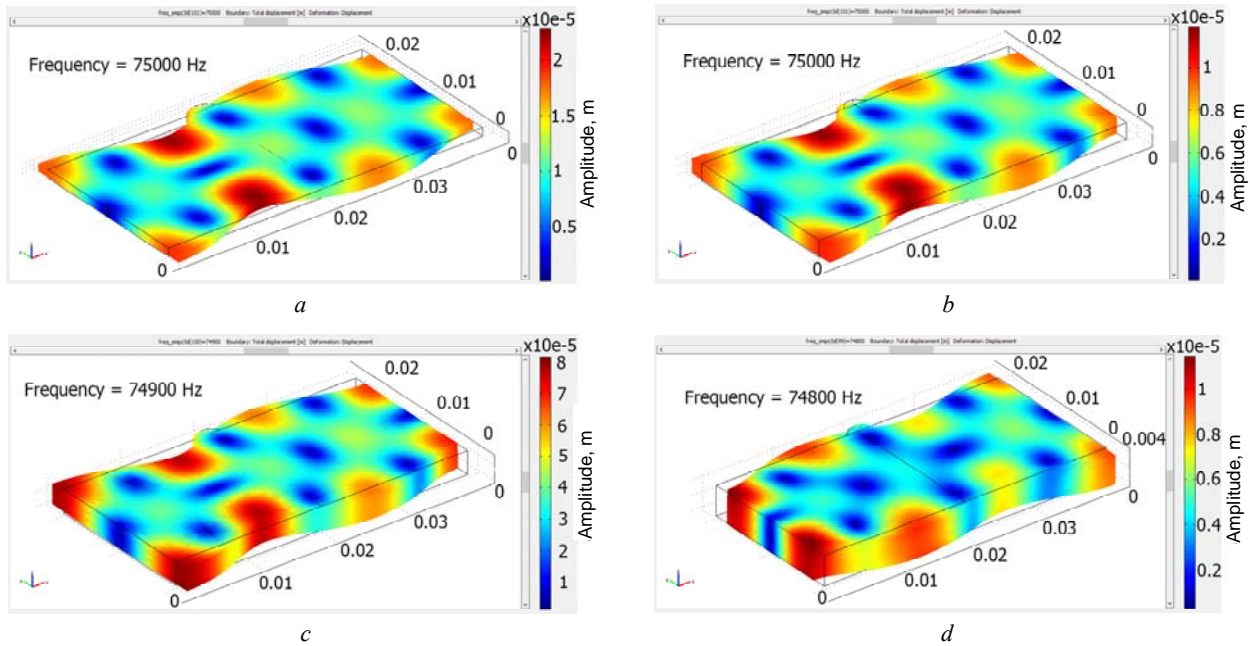


Fig. 6. Some of the results of simulation of amplitude oscillations of a piezoplate of a linear motor with different thickness at constant parameter:  $K = 0.5$ :  $a - h = 1$ ;  $b - h = 2$ ;  $c - h = 3$ ;  $d - h = 4$

The dependence presented in this Figure was approximated by the Gauss function, which has the form:

$$\delta = ae^{-\frac{(h-b)^2}{2c^2}}, \quad (4)$$

where  $\delta$  is the pusher oscillation amplitude,  $h$  is the piezoelectric plate thickness,  $a = 53.247361$ ,  $b = 2.9480015$ ,  $c = 0.50561783$  are the coefficients.

This model is adequate in the range of variation of the piezoceramic plate thickness from 2 to 4 mm.

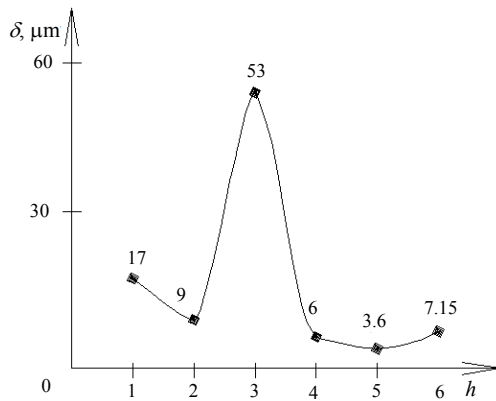


Fig. 7. The dependence of the amplitude of oscillations of the pusher on the piezoceramic plate thickness  $h$  at the parameter  $K = 0.5 = \text{const}$

To choose rational sizes of a piezoceramic plate, it is advisable to use graphic (Fig. 5, 7) and analytical (3), (4) dependencies. Guided by the graphs for the maximum amplitude of the pusher, you can choose a rational ratio of the parameters  $K$  and thickness  $h$ . If necessary, in the absence of piezoelectric ceramics of necessary sizes, the choice of rational sizes of  $K$  and  $h$  can be made using analytical dependencies. In this case, the oscillation amplitude of the pusher is chosen as close to the maximum.

According to the selected rational sizes of the piezoceramic plate, which amounted to  $l = 40$  mm;  $w = 20$  mm;  $h = 3$  mm, an experimental sample of a linear piezoceramic motor was made (Fig. 8). The study of its operation in accordance with the previously described method has confirmed the adequacy of determining the resonant frequency and the performance of the motor. The experimentally determined resonant frequency was  $f_{exp} = 77.2$  kHz, which coincides with the theoretically determined ( $f_{theor} = 74.9$  kHz) using the COMSOL Multiphysics software package (Fig. 4, b and Fig. 6, c) with acceptable accuracy not exceeding 3 %.



Fig. 8. Experimental sample of linear piezoceramic motor

### Conclusions.

1. By numerical modeling of the operation of a linear piezoceramic motor, the influence of the geometric parameters of the motor piezoelectric element on its amplitude characteristics was determined, graphic and analytical dependencies were established to select their rational ratios.

2. The results of investigations can be used in the design of piezoceramic linear motors.

### REFERENCES

1. Sharapov V. *Piezoceramic sensors*. Heidelberg, Dordrecht, London, New York, Springer Verlag, 2011. 498 p. doi: 10.1007/978-3-642-15311-2.
2. Panich A.E., Zhukov S.N. *P'ezoelektricheskoe priborostroenie. T.4. P'ezoelektricheskie aktuatory* [Piezoelectric instrument making. T.4. Piezoelectric actuators]. Rostov-on-Don, TsVVR Publ., 2008. 159p. (Rus).

3. Petrenko S.F. *P'ezoelektricheskii dvigatel'* [Piezoelectric motor]. Kiev, Korniiichuk Publ., 2002. 96 p. (Rus).
4. *Theodolite*. Available at: <https://en.wikipedia.org/wiki/Theodolite> (accessed on 13 July 2018).
5. Smirnov A.B. *Mekhatronika i robototekhnika. Sistemy mikroperemeshchenii s p'ezoelektricheskimi privodami* [Mechatronics and Robotics. Micro-movement systems with piezoelectric drives]. St. Petersburg, SPbGPU Publ., 2003. 160 p. (Rus).
6. Khmelev V.N. *Istochniki ul'trazvukovogo vozdeistviya. Osobennosti postroyeniya i konstruktzii* [Sources of ultrasonic action. Features of construction and construction]. Biisk, AGTU Publ., 2013. 196 p. (Rus).
7. Spanner K., Wishnewskiy O., Vyshnevskyy W. New Linear Ultrasonic Micro motors for Precision Mechatronic Systems. *In Proceedings of the 10th International Conference on New Actuators*. Bremen, Germany. 14-16 June 2006, pp. 439-443.
8. Yokoyama K., Tamura H., Masuda K., Takano T. Single-Phase Drive Ultrasonic Linear Motor Using a Linked Twin Square Plate Vibrator. *Japanese Journal of Applied Physics*, 2013, vol.52, no.7S, p. 07HE03. doi: 10.7567/jjap.52.07he03.
9. Vyshnevskiy O., Kovalev S., Wischnewskiy W. A novel, single-mode piezoceramic plate actuator for ultrasonic linear motors. *IEEE Transactions on Ultrasonics, Ferroelectrics and Frequency Control*, 2005, vol.52, no.11, pp. 2047-2053. doi: 10.1109/tuffc.2005.1561674.
10. Petrenko S.F., Filimonov S.A., Filimonova N.V., Batrachenko A.V., Lavdanskii A.A. Linear piezoelectric motor based on circular cylindrical plate. *Bulletin of Cherkasy State Technological University. Series: Technical sciences*, 2014, no.2, pp. 48-52. (Rus).
11. Spanner K., Koc B. Piezoelectric Motors, an Overview. *Actuators*, 2016, vol.5, no.1, p. 6. doi: 10.3390/act5010006.
12. Shafik A., Ben Mrad R. Piezoelectric Motor Technology: A Review. *Nanopositioning Technologies*, 2016, pp. 33-59. doi: 10.1007/978-3-319-23853-1\_2.
13. Zhukov S.N. *Piezoelektricheskaya keramika: printsipy i primeneniye* [Piezoelectric ceramics: principles and applications]. Minsk, OOO FUAuinform Publ., 2003. 112 p. (Rus).
14. Spicci L., Cati M. Ultrasound Piezo-Disk Transducer Model for Material Parameter Optimization. *Excerpt from the Proceedings of the COMSOL Conference*, Paris 2010. Available at: [https://uk.comsol.com/paper/download/63120/spicci\\_paper.pdf](https://uk.comsol.com/paper/download/63120/spicci_paper.pdf) (accessed on 20 May 2018).
15. Maslennikova S., Sitnikov A., Mironova I. Calculating the Ultra-Sound Engine Piezoelectric Element Characteristics. *Radiooptics Scientific Journal*, 2016, vol.16, no.04, pp. 25-40. doi: 10.7463/rdopt.0416.0847731.

Received 13.07.2018

*V.Ya. Halchenko*<sup>1</sup>, *Doctor of Technical Science, Professor,*  
*Yu.Yu. Bondarenko*<sup>1</sup>, *Candidate of Technical Science, Associate Professor,*  
*S.A. Filimonov*<sup>1</sup>, *Candidate of Technical Science, Associate Professor,*  
*N.V. Filimonova*<sup>1</sup>, *Candidate of Technical Science,*  
<sup>1</sup>*Cherkasy State Technological University,*  
 460, Shevchenko Blvd., Cherkasy, 18006, Ukraine,  
 phone +380 472 710092,  
 e-mail: halchvl@gmail.com, s.filimonov@chdtu.edu.ua

How to cite this article:

Halchenko V.Ya., Bondarenko Yu.Yu., Filimonov S.A., Filimonova N.V. Determination of influence of geometric parameters of piezoceramic plate on amplitude characteristics of linear piezomotor. *Electrical engineering & electromechanics*, 2019, no.1, pp. 17-22. doi: 10.20998/2074-272X.2019.1.03.

V. Pliuhin, M. Sukhonos, M. Pan, O. Petrenko, M. Petrenko

## IMPLEMENTING OF MICROSOFT AZURE MACHINE LEARNING TECHNOLOGY FOR ELECTRIC MACHINES OPTIMIZATION

*Purpose.* To consider problems of electric machines optimization within a wide range of many variables variation as well as the presence of many calculation constraints in a single-criteria optimization search tasks. *Results.* A structural model for optimizing electric machines of arbitrary type using Microsoft Azure machine learning technology has been developed. The obtained results, using several optimization methods from the Microsoft Azure database are demonstrated. The advantages of cloud computing and optimization based on remote servers are shown. The results of statistical analysis of the results are given. *Originality.* Microsoft Azure machine learning technology was used for electrical machines optimization for the first time. *Recommendations for modifying standard algorithms, offered by Microsoft Azure are given. Practical value.* Significant time reduction and resources spent on the optimization of electrical machines in a wide range of variable variables. Reducing the time to develop optimization algorithms. The possibility of automatic statistical analysis of the results after performing optimization calculations. References 20, tables 3, figures 7.

*Key words:* electrical machines, optimization, algorithm, data set, machine learning, Microsoft Azure, cloud computing.

*Рассмотрены проблемы оптимизации электрических машин при широком диапазоне варьирования многих переменных, наличии большого числа вычисляемых ограничений, в однокритериальных задачах оптимизационного поиска. Разработана структурная модель оптимизации электрических машин произвольного типа с применением технологии машинного обучения Microsoft Azure. Продемонстрированы результаты, полученные с использованием нескольких методов оптимизации из базы Microsoft Azure. Показаны преимущества облачных расчетов и оптимизации на базе удаленных серверов. Приведенные результаты касаются решения однокритериальной задачи оптимизации с двумя переменными. Даны результаты статистического анализа полученных результатов. Даны рекомендации по применению машинного обучения Microsoft Azure в проектировании и оптимизации электрических машин. Библи. 20, табл. 3, рис. 7.*

*Ключевые слова:* электрические машины, оптимизация, алгоритм, набор данных, машинное обучение, Microsoft Azure, облачные расчеты.

**Introduction.** The task of electrical machine (EM) optimal design or a series of EM can be represented as a general non-linear mathematical problem. This problem follows to finding the minimum or maximum of the optimality criterion in the presence of a certain number of independent variables and limiter functions, which are technical or technological requirements-limitations to the project [1-6].

In computer-aided design (CAD) systems, the optimization of an electrical machine consists in multiple calculations of the dependencies between the main indicators given in the form of an equations system, empirical coefficients and graphical dependencies, which can be considered as a design equation [7]. The optimal design of an EM can be represented as the search for optimal parameters by solving this system of equations. The complexity of the calculation algorithm complicates the optimization task.

Reducing the number of independent variables by increasing the number of stages for solving a design problem makes it much easier to find the optimal variant. However, this loses the accuracy of determining the optimal value of the objective function.

Considering CAD in the context of electric machines, it is possible to distinguish the following system components that are used in modern electrical engineering [1]:

- 1) automated design of an electric machine;
- 2) search for the optimal version of the designed machine;
- 3) software implementation of design project and search for optimum;

4) the choice of the optimal variant from the set of effective one, which have been tested for restrictions.

Known methods for searching the optimum version of calculating object, such as the method of coordinate descent, Nelder-Mead, the method of a deformable polyhedron, etc., do not allow performing calculations while changing all configuration variables [8]. As a rule, many methods allow alternating variation of variables with subsequent adjustment of the convergence calculations region [9-12].

Thus, the issue of improving the search for the optimal variation and reducing the time and technical resources, spent on these tasks as well, becomes relevant. In this regard in the paper the development of an optimization model of electric machines, using cloud-based machine learning technology provided by Microsoft Azure services was considered [13, 14].

**The aim of the work** is the development of a methodology for optimizing electrical machines using Microsoft Azure machine learning technology.

**Formulation of the optimization problem.** At the optimization stage we assume that the basic version of an electric machine is already calculated (Table 1).

In this case, any electric machine, regardless of its type, turns into a set of initial data (or dataset):

- geometric dimensions;
- winding parameters;
- electrical and magnetic values;
- loss, efficiency, etc.

Table 1  
Base machine parameters

Parameter name	Parameter value
Rated power, kW	15
Line voltage, V	380
Rated speed, rev/min	1500
Frequency, Hz	50
Stator core length, mm	130
Stator core inner diameter, mm	185
Efficiency	0.884

The specified dataset, being placed in a one-dimensional vector, can be changed with a given law, obtaining various combinations of the same electric machine. Thus, in order to obtain a machine with the highest efficiency, it was required to find a solution to the following equation:

$$u = f(x_1, x_2, \dots, x_n), \quad (1)$$

where  $x_1, x_2, \dots, x_n$  – varied variables;  $u$  – target function.

The search for the optimal value was not limited to finding the extremum of the objective function (1). During the search, candidates were screened out that do not pass the specified restrictions. The number of equality constraints within one project can be arbitrary and is set by the designer:

$$\begin{cases} g_1(x_1, x_2, \dots, x_n) = 0, \\ g_2(x_1, x_2, \dots, x_n) = 0, \\ \dots \\ g_n(x_1, x_2, \dots, x_n) = 0. \end{cases} \quad (2)$$

Inequality constraints are also used:

$$\begin{cases} \alpha_1 \leq \gamma_1(x_1, x_2, \dots, x_n) \leq b_1, \\ \alpha_2 \leq \gamma_2(x_1, x_2, \dots, x_n) \leq b_2, \\ \dots \\ \alpha_k \leq \gamma_k(x_1, x_2, \dots, x_n) \leq b_k. \end{cases} \quad (3)$$

In general case for target function  $f(x_1, x_2, \dots, x_n)$  the minimum  $m$  is finding in restricted area  $D(x_1, x_2, \dots, x_n \in D)$  [2]. The considered task was replaced by unconditional optimization (minimization) of a one-parameter family of functions:

$$F(x, \beta) = f(x) + \frac{1}{\beta} \varphi(x), \quad x = \{x_1, x_2, \dots, x_n\}, \quad (4)$$

where  $\varphi(x)$  – penalty function;  $\beta$  – penalty factor.

As a penalty function in (4)  $\varphi(x)$  was taken, that become zero when the conditions (2) – (3) are fulfilled:

$$\varphi(x) = \frac{1}{\beta} \left\{ \sum_{i=1}^I g_i^2(x) + \sum_{j=1}^J h_j^2(x) [1 - \text{sign } h_j(x)] \right\}, \quad (5)$$

$$\beta > 0.$$

In expression (5) the limitations of the equality and inequality types are:

$$\begin{cases} g_i(x) = 0, i = 1, 2, \dots, I; \\ h_j(x) > 0, j = 1, 2, \dots, J; x = \{x_1, x_2, \dots, x_n\}. \end{cases} \quad (6)$$

The additional (penalty) function  $\varphi(x)$  is chosen in the way, when  $\beta \rightarrow 0$ , the solution of the auxiliary problem tends to solve the original one, or that their minimums coincide:  $\min F(x, \beta) \rightarrow m$  while  $\beta \rightarrow 0$ .

To solve the optimization problem, a Java program was written, the functionality of which made it possible to solve the following problems [15]:

- design of the base machine;
- setting restrictions;
- setting a set of varied variables with setting their variation relative to the base value and the step of their change;
- selection of optimality criteria.

When changing only two variable values (stator core length and its internal diameter) in the range  $\pm 20\%$  of the base value, 710000 non-repeating combinations of electric machines were found. Only 441 combinations from this value were passed the restrictions, among which the best option was found. On the Intel Core i3 2.54 GHz processor and 8 Gb RAM, the calculation time was 9 min and 8 s. The results of sampling the selected values are shown on Fig. 1.

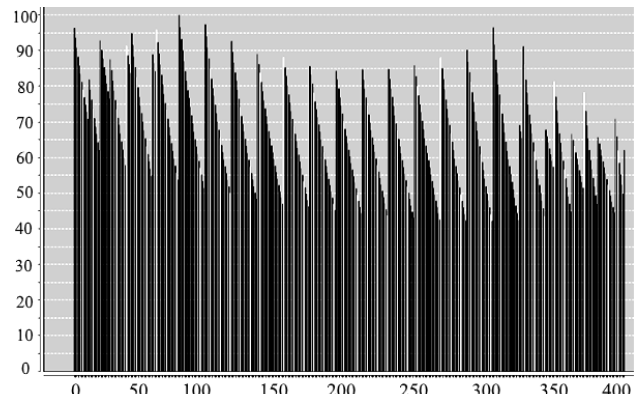


Fig. 1. Sampling combinations diagram of electrical machines in the Java program: Efficiency along the vertical axis and the number of the combination along the X-axis

The obtained optimization results were compared with the experimental data, obtained on two machines with the parameters of the basic and optimized versions, manufactured at «SpecialEnergyService» LLD, Kharkiv, Ukraine. The results of laboratory tests showed a discrepancy with the theoretical no more than 7-8 %.

Performed tests, as well as software solutions of classical optimization methods [2, 3], can be taken for comparison with alternative approaches to optimization.

The disadvantage of the existing method is that the total development time for a Java project was about 3 days (72 hours). In addition, the operating time of the calculated algorithm increases significantly with a change in the range and number of varied values. Fig. 2 shows a comparative chart of the obtained results.

As can be seen from Fig. 2, even at 4 variable variables and the range of their variation  $\pm 20\%$  from the base value, the calculation time was about 8 h.

In real industrial projects of electric machines optimization, it is necessary to vary about 32 parameters, with a range from  $\pm 10\%$  to  $\pm 100\%$  of the base value [3].

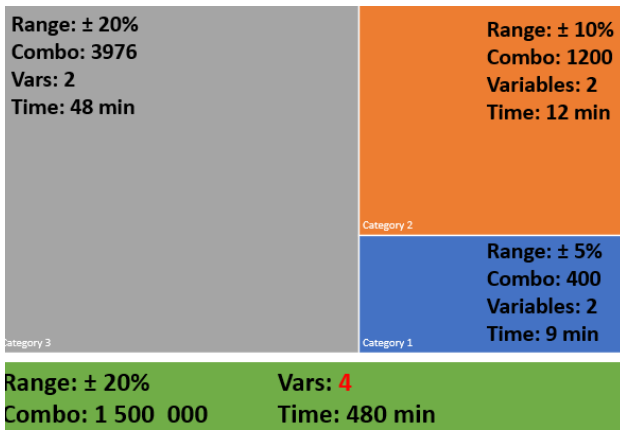


Fig. 2. Comparative chart of time spent on optimization calculations

It is easy to assume that resources of the local PC are not enough to solve such problems, and the debugging time of the project becomes unattainable.

The solution to the problem of operations with large amounts of data (also known as Big Data) and computational operations is the parallelization of calculations and the organization of high-performance computing (HPC) on PC-cluster. However, parallel computing will inevitably entail both changes to the code of an existing program (and an inevitable increase in the debugging time of the program), and will require the presence of the HPC cluster itself.

One solution to this problem is to use the computing power of the Microsoft cloud cluster and machine learning technology based on the Microsoft Azure service.

**Developing Microsoft Azure model.** Azure Machine Learning enables computers to learn from data and experiences and to act without being explicitly programmed. Customers can build Artificial Intelligence (AI) applications that intelligently sense, process, and act on information – augmenting human capabilities, increasing speed and efficiency, and helping organizations achieve more [16].

Machine Learning finds patterns in large volumes of data and uses those patterns to perform predictive analysis. Microsoft offers Azure Machine Learning, while Amazon offers Amazon Machine Learning and Google offers the Google Prediction API. Software products such as MATLAB support traditional, non-cloud-based ML modeling. There are four steps in the process of finding the best parameter set:

- define the parameter space: for the algorithm, first decide the exact parameter values you want to consider;
- define the cross-validation settings: decide how to choose cross-validation folds for the dataset;
- define the metric: decide what metric to use for determining the best set of parameters, such as accuracy, root mean squared error, precision, recall, or  $f$ -score;
- train, evaluate and compare: for each unique combination of the parameter values, cross-validation is carried out by and based on the error metric you define. After evaluation and comparison, you can choose the best-performing model.

To iterate on your model design, you edit the experiment, save a copy if desired, and run it again. When you're ready, you can convert your training experiment to a predictive experiment, and then publish it as a web service so that your model can be accessed by others [17].

Elastic cloud infrastructure is the optimal choice for solutions requiring large design capacities in short periods of time. It allows you not to wait for training models for weeks and at the same time not to keep «supercomputers» on balance.

The source data vector (with parameters of the base machine and its non-repeating combinations) for the investigated electrical machine was saved into a .csv file (comma separated data) and imported into a block of the Microsoft Azure model. In this table (Table 2) for the test task there were 10 variable values (columns) and 442 combinations (rows).

Table 2  
Vector of initial data, imported to Microsoft Azure model

Combo	Diameter	Length	Efficiency	cosφ	...
				...	...
0	175	120	0.8824	0.8618	...
1	175	121	0.8831	0.8679	...
2	175	122	0.8838	0.8739	...
3	175	123	0.8844	0.8787	...
4	175	124	0.8848	0.8828	...
5	175	125	0.8852	0.8866	...
6	175	126	0.8855	0.8896	...
...	...	...	...	...	...

Statistical analysis of the selected optimality criterion (Efficiency) is performed automatically after importing the source data table into the Microsoft Azure workspace (Table 3).

Table 3  
Efficiency statistical performance

Parameter name	Parameter value
Average value	0.8801
Median	0.8817
Minimum value	0.8553
Maximum value	0.8865
Standard deviation	0.0059
Unique values	87
Lost Values	0
Type of analysis	Numeric label

The Microsoft Azure database contains hundreds of computational blocks from which a research task can be made and the complexity of which is limited by the designer's skill [18-20]. Numerous examples of already completed works are available in the Azure cloud. This allow to choose selected one as the basis for the own development.

In this example, the Microsoft Azure project contained the following elements:

- IM\_Data – table of parameters;
- Clean Missing Data – deleting of empty rows;

- Select Columns in Dataset – selection of columns of variable parameters;
- Split Data – initial dataset dividing (70% for model teaching in left port and 30% for model analyses using original data in right port);
- Algorithm (Boosted Decision Tree, Multiclass Neural Network);
- Train Model – blocks for model teaching;
- Score Model – block of selection and analysis of the optimality criterion;
- Evaluate Model – block for calculating of statistical information.

The block-scheme of the project is shown on Fig. 3

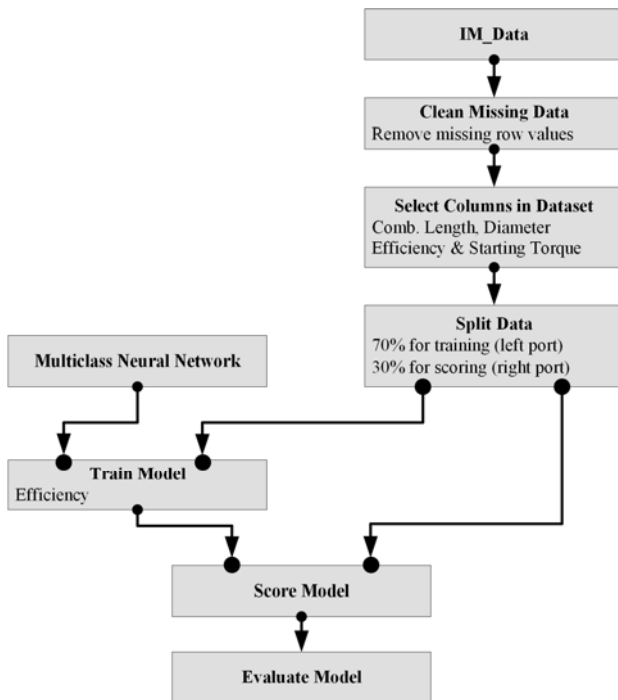


Fig. 3. The project on the optimization of the electric machine in Microsoft Azure workspace

After performing the calculations, related to the system training, testing the sampling algorithm and searching for the optimum, the final results were obtained. We can get access to these results from «Evaluate Model» block (Fig. 3) and receive various reports. The sample of efficiency data is shown on Fig. 4 and Fig. 5.

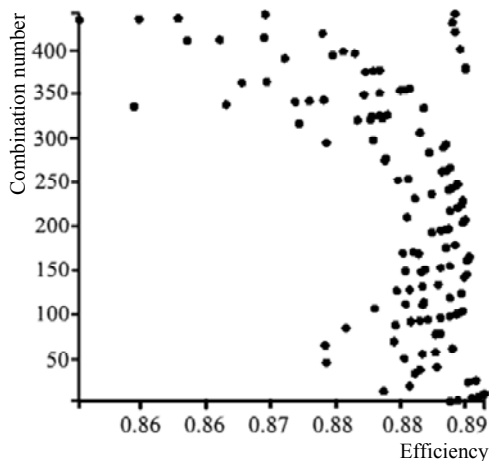


Fig. 4 The dependence of the combinations number vs. efficiency

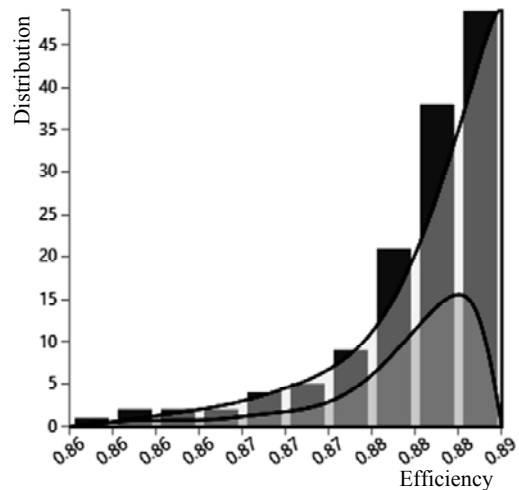


Fig. 5. Efficiency dispersion summary

Fig. 6 shows the report, obtained after analyzing the constructed model in Microsoft Azure using the method of multiclass neural networks. The generated report in tabular format represents the source data sets, followed by columns with calculated deviations from the optimum, as well as statistical indicators (on Fig. 6 only one column (rightmost one) is shown out of 10 available for analysis).

Fig. 7 shows the user project view in the Microsoft Azure workspace, where in addition to the neural network method, the decision tree algorithm, the Poisson regression analysis were included in the analysis of the source data sample.

According to the calculation results, the optimal combination No. 420 was chosen (the choice was made according to the table, the first row of Fig. 6, where the optimization results are sorted in order of increasing error) with the following parameters: stator core length 120 mm, stator core diameter 195 mm, efficiency 0.884.

The computation time was only 1 min 45 s. The metric estimation module built into Microsoft Azure made it possible to determine the quality of the performed calculations. Absolute error 0.000702, standard deviation 0.005926, relative absolute error 0.164582 and relative square error 1.011483 (the lower the value, the better) were obtained.

It should be noted that if the functionality of the embedded Microsoft Azure tools is not enough for some reason, researchers can write and execute their own scripts on *R* or *Python* [13, 14].

Thus, the use of Microsoft Azure in optimizing electrical machines has been demonstrated. In the shown example, only one data vector was used and there were no modules for intermediate processing and data transfer between the modules.

Further research will be focus on creating own *Python* calculating blocks and *R* scripts with a view to transferring to the Microsoft Azure platform not only data set (now this data set is forming based on the results of separate calculations in *Java* program), but also creating a population of source data based on the vector parameters of the base machine.

rows	columns								
133	131	Efficiency	PowerFactor	Induction	StartCurrent	StartTorque	MaxTorque	Temperature	Scored Probabilities for Class "0.8556"
		0.8849	0.9052	0.709	5.65	1.35	2.53	90.6	0
		0.8828	0.8793	0.73	5.61	1.39	2.59	92.9	0.000001
		0.8778	0.8582	0.729	5.61	1.42	2.66	96.2	0.000792
		0.8696	0.8256	0.659	5.12	1.36	2.57	95.9	0.001181
		0.8779	0.8524	0.768	5.76	1.48	2.76	98.9	0.00042
		0.8811	0.8598	0.769	5.72	1.46	2.72	96.8	0.000045
		0.8835	0.9042	0.684	5.54	1.32	2.49	89.7	0
		0.8765	0.8627	0.676	5.36	1.35	2.55	93.1	0.000138
		0.88	0.8829	0.683	5.48	1.34	2.53	91.6	0.000021
		0.8831	0.8805	0.743	5.7	1.41	2.63	93.8	0.000004

Fig. 6. Results of the neural network sampling algorithm in the Microsoft Azure report table (screenshot of the project table in the browser workplace)

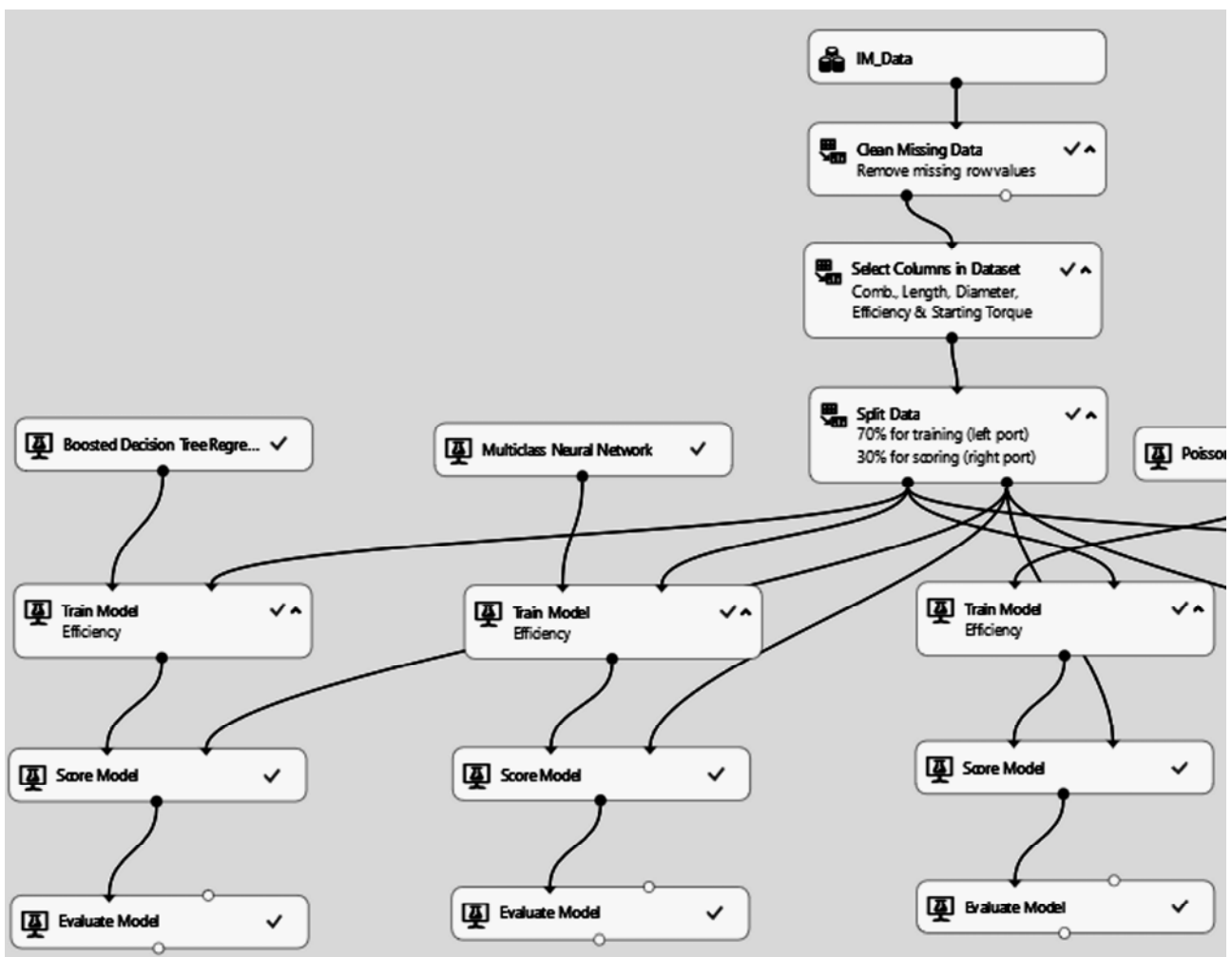


Fig. 7. Full project model in Microsoft Azure (Screenshot of the project model in the browser workplace)

## Conclusions.

The application of Microsoft Azure machine learning technology in electrical machines optimizing is shown for the first time.

As a result of the performed optimization using Microsoft Azure cloud services, the computation time was reduced by more than 300 times (from 480 minutes to 2 minutes) when solving the same task compared to calculations on a stationary PC.

The project development time of an electric machine, on the example of an induction motor with a squirrel-cage rotor, was reduced from several working days to 30 minutes.

The complexity of project developing (induction motor parameters optimization task) has significantly decreased compared to direct *Java* programming, due to the use of ready-made analysis units provided by Microsoft Azure.

The Microsoft Azure platform for the implementation of machine learning technology can be recommended in solving optimization problems of various electric machine types.

## REFERENCES

1. Sen S.K. *Principles Of Electrical Machine Design With Computer Programs*. Oxford, IBH Publishing Company Pvt. Limited, 2006. 415 p.
2. Rekleitis G., Reivindran A., Regsdel K. *Optimizatsiia v tekhnike* [Optimization in technology]. Moscow, Mir Publ., 1986. 351 p. (Rus).
3. Goriagin V.F., Zagriadskii V.I., Sycheva T.A. *Optimal'noe proektirovanie asinkhronnykh vzryvozashchishchennykh dvigatelei* [Optimal design of asynchronous explosion-proof motors]. Kishinev, Shtiitsa Publ., 1980. 200 p. (Rus).
4. Zablodskiy N., Lettl J., Pliugin V., Buhr K., Khomitskiy S. Induction Motor Optimal Design by Use of Cartesian Product. *Transactions on electrical engineering*, 2013, no.2, pp. 54-58.
5. Zablodskiy N., Lettl J., Pliugin V., Buhr K., Khomitskiy S. Induction Motor Design by Use of Genetic Optimization Algorithms. *Transactions on electrical engineering*, 2013, no.3, pp. 65-69.
6. Zablodskii N.N., Pliugin V.E., Petrenko A.N. Using object-oriented design principles in electric machines development. *Electrical engineering & electromechanics*, 2016, no.1, pp. 17-20. doi: **10.20998/2074-272X.2016.1.03**.
7. Papalambros P.Y., Wilde D.J. *Principles of optimal design*. Cambridge University Press, 2017. doi: **10.1017/9781316451038**.
8. Severin V.P., Nikulina E.N. *Metody odnomernogo poiska* [Methods of one-dimensional search]. Kharkiv, NTU KhPI Publ., 2013. 124 p. (Rus).
9. Todorov E. Optimal control theory. *Bayesian Brain: Probabilistic Approaches to Neural Coding*, 2006, chap. 12, pp. 268-298. doi: **10.7551/mitpress/9780262042383.003.0012**.
10. Kappen H.J. Optimal control theory and the linear Bellman equation. *Bayesian Time Series Models*, 2011, pp. 363-387. doi: **10.1017/cbo9780511984679.018**.
11. Kanemoto Y. *Theories of urban externalities*. Holland, North-Holland Publ., 1980. 189 p.
12. Satit Owatchaiphong, Nisai Fuengwarodsakul. Multi-Objective Design for Switched Reluctance Machines Using Genetic and Fuzzy Algorithms. *The ECTI Transactions on Electrical Engineering, Electronics, and Communications*, 2013, vol.11, no.2, pp. 1530-1533.
13. Chappel D. *Introduction Azure machine learning: a guide for technical professionals*. Chappel & Associates, 2015.
14. Collier M., Shahan R. *Microsoft Azure Essentials*. Microsoft Press, 2016.
15. Bloch J. *Effective Java*. Canada, Sun Microsystems, 2008.
16. *What is Azure machine learning studio?* Available at: <https://docs.microsoft.com/en-us/azure/machinelearning/studio/what-is-ml-studio> (Accessed 10 May 2018).
17. Hayakawa S., Hayashi H. Using Azure Machine Learning for Estimating Indoor Locations. *2017 International Conference on Platform Technology and Service (PlatCon)*, Busan, 2017, pp. 1-4. doi: **10.1109/platcon.2017.7883736**.
18. *Azure Machine Learning*. Available at: <https://azure.microsoft.com/en-us/services/machine-learning-studio/> (Accessed 22 April 2018).
19. *Dig Deep with Azure Machine Learning*. Available at: <https://studio.azureml.net/> (Accessed 16 February 2018).
20. Microsoft Azure Machine Learning: Algorithm Cheat Sheet. Available at: <http://aka.ms/MLCheatSheet> (Accessed 05 March 2018).

Received 17.10.2018

V. Pliuhin<sup>1</sup>, Doctor of Technical Sciences, Professor,  
M. Sukhonos<sup>1</sup>, Doctor of Technical Sciences, Professor,  
M. Pan<sup>1</sup>, Candidate of Technical Sciences, Professor,  
O. Petrenko<sup>1</sup>, Doctor of Technical Sciences, Associate Professor,  
M. Petrenko<sup>2</sup>, Candidate of Technical Sciences, Associate Professor,

<sup>1</sup>O.M. Beketov National University of Urban Economy in Kharkiv,  
17, Marshal Bazhanov Str., Kharkiv, 61002, Ukraine,  
e-mail: petersanya1972@gmail.com

<sup>2</sup>National Technical University «Kharkiv Polytechnic Institute»,  
2, Kyrpychova Str., Kharkiv, 61002, Ukraine.

## How to cite this article:

Pliuhin V., Sukhonos M., Pan M., Petrenko O., Petrenko M. Implementing of Microsoft Azure machine learning technology for electric machines optimization. *Electrical engineering & electromechanics*, 2019, no.1, pp. 23-28. doi: **10.20998/2074-272X.2019.1.04**.

D.O. Volontsevich, E.A. Veretennikov, I.V. Kostianik, A.S. Iaremchenko, A.I. Efremova, V.O. Karpov

## DETERMINATION OF THE ELECTRIC DRIVE POWER FOR LIGHTLY ARMORED CATERPILLAR AND WHEELED VEHICLES USING SINGLE- OR TWO-STAGE MECHANICAL GEARBOXES

*When designing electromechanical transmissions (EMT) for lightly armored caterpillar and wheeled vehicles (LACWV), there is often a problem that the coefficient of adaptability of the traction motor (TM) at the minimum design power is not sufficient to meet the requirements for the power range of the transmission. In the literature, several ways have been worked out to solve this problem, however, there was not found a single algorithm allowing to formalize and step by step pass the process of choosing the most rational structure of the EMT. The purpose of the proposed work is the formation of scientifically based methodology for evaluating the possibility of using single-stage gearboxes in EMT for LACWV and calculation of the required TM power of the selected type for single- or two-stage mechanical gearboxes. Methodology. To carry out the research, the theory of motion of caterpillar and wheeled vehicles was used. Result. A formalized methodology for determining the required mechanical power of the electric drive for the LACWV is proposed, depending on the power capabilities of the motor-generator set, the torque characteristics of the selected TM and the number of stages in the mechanical gearboxes. Scientific novelty. For the first time, a formalized connection has been established between the tactical and technical requirements for LACWV, the characteristics of the selected TM, the structure and parameters of the mechanical gearboxes. Practical value. The toolkit for the engineering and design personnel developing the EMT for the LACWV was obtained. Work with the algorithm is illustrated by the example of power selection and gear ratios of mechanical gearboxes for the multi-purpose lightly armored caterpillar tractor MT-LB. References 10, tables 3, figures 4.*

**Key words:** electromechanical transmissions, lightly armored caterpillar and wheeled vehicles, traction electric motor, mechanical gearbox, power transmission range.

*При проектуванні електромеханічних трансмісій (EMT) для легкоброньованих гусеничних і колісних машин (ЛБГКМ) часто виникає проблема недостатці коефіцієнта пристосованості тягового електродвигуна (ТЕД) мінімальної розрахункової потужності для задоволення вимогам до силового діапазону трансмісії. У літературі напрацьовано кілька способів рішення цієї проблеми, однак не було знайдено єдиного алгоритму, що дозволяє формалізувати й покроково провести процес вибору найбільш раціональної структури EMT. Метою запропонованої роботи є формування науково обгрунтованої методики оцінки можливості використання одноступінчастих редукторів в EMT для ЛБГКМ і розрахунку необхідної потужності ТЕД обраного типу для одно- або двоступінчастих механічних редукторів. Методика. Для проведення досліджень використовувалися положення теорії руху гусеничних і колісних машин. Результат. Запропонована формалізована методика визначення необхідної механічної потужності електродвигуна ЛБГКМ залежно від енергетичних можливостей мотор-генераторної установки, моментної характеристики обраних ТЕД і кількості ступенів у механічних редукторах. Наукова новизна. Уперше встановлено формалізований зв'язок між тактико-технічними вимогами до ЛБГКМ, характеристиками обраних ТЕД, структурою і параметрами механічних редукторів. Практична цінність. Отримано інструментарій для інженерно-конструкторського персоналу, що розробляє EMT для ЛБГКМ. Робота з алгоритмом проілюстрована на прикладі вибору потужності і передатних відношень механічних редукторів для багатопільового легкоброньованого транспортера тягача МТ-ЛБ. Бібл. 10, табл. 3, рис. 4.*

**Ключові слова:** електромеханічні трансмісії, легкоброньовані гусеничні і колісні машини, тяговий електродвигун, механічний редуктор, силовий діапазон трансмісії.

*При проектировании электромеханических трансмиссий (ЭМТ) для легкобронированных гусеничных и колесных машин (ЛБГКМ) часто возникает проблема нехватки коэффициента приспособляемости тягового электродвигателя (ТЭД) минимальной расчетной мощности для удовлетворения требованиям к силовому диапазону трансмиссии. В литературе разработано несколько способов решения этой проблемы, однако не было найдено единого алгоритма, позволяющего формализовать и пошагово провести процесс выбора наиболее рациональной структуры ЭМТ. Целью предложенной работы является формирование научно обоснованной методики оценки возможности использования одноступенчатых редукторов в ЭМТ для ЛБГКМ и расчета необходимой мощности ТЭД выбранного типа для одно- или двухступенчатых механических редукторов. Методика. Для проведения исследований использовались положения теории движения гусеничных и колесных машин. Результат. Предложена формализованная методика определения необходимой механической мощности электродвигателя ЛБГКМ в зависимости от энергетических возможностей мотор-генераторной установки, моментной характеристики выбранных ТЭД и количества ступеней в механических редукторах. Научная новизна. Впервые установлена формализованная связь между тактико-техническими требованиями к ЛБГКМ, характеристиками выбранных ТЭД, структурой и параметрами механических редукторов. Практическая ценность. Получен инструментарий для инженерно-конструкторского персонала, разрабатывающего ЭМТ для ЛБГКМ. Работа с алгоритмом проиллюстрирована на примере выбора мощности и передаточных отношений механических редукторов для многоцелевого легкобронированного транспортера тягача МТ-ЛБ. Библ. 10, табл. 3, рис. 4.*

**Ключевые слова:** электромеханические трансмиссии, легкобронированные гусеничные и колесные машины, тяговий електродвигатель, механический редуктор, силовый диапазон трансмиссии.

**Introduction.** Electromechanical transmissions not only in civilian vehicles, but also in military (EMT) have recently become increasingly widespread, equipment [1-7]. This is due to the fact that EMT can

provide a number of significant advantages, which were formulated in [8, 9]:

- the stepless change of speed, traction force and turning radius;
- ease of automating the transmission and ensuring the control of the vehicle by any crew member and remote control;
- enhanced capabilities for recovering energy from slowing down, turning, oscillations of sprung masses, etc.;
- the possibility of short-term movement without an operating internal combustion engine;
- the possibility of short-term summation of the power of the generator unit and energy storage devices;
- absence of rigid mechanical connections between the main units, facilitating the layout.

Classic stepped mechanical transmissions with hydrodynamic elements almost completely selected their technical potential for increasing the power density and mobility of both tracked (caterpillar) and all-wheel drive wheeled vehicles. In addition, with such transmissions on multi-axle all-wheel vehicles, there is an unjustified complexity in implementing a system for maintaining road holding and thrust control in order to avoid slipping.

All this made the task of designing the EMT for lightly armored caterpillar (tracked) and wheeled vehicles (LACWV) relevant and timely.

**Brief analysis of the issue, the goal and definition of the problem.** The characteristics of modern traction motors (TMs), in particular induction TMs with frequency control, allow to obtain a hyperbolic characteristic of constant power close to ideal. However, as a rule, it is still not enough to produce an electric drive with stepless regulation in the whole range that is required for vehicles moving not only on paved roads, but also off-road [8, 9]. This is due to the limitation of the maximum torque of the TM, which is dictated by the value of the maximum current in the windings and overheating.

In existing foreign designs, usually to solve this problem, TMs with large power reserve are used, which cannot even be ensured at all by the total power of the generator and storage device [2-4, 6]. This leads to an additional increase in the weight, size and cost of such a transmission and reduces in aggregate the advantages that could be obtained when introducing an electric drive for military armored vehicles. In the works [8, 9], the traction balance of vehicles with EMT was calculated using the example of the MT-LB tracked multipurpose conveyor-tractor and the BTR-4 wheeled armored personnel carrier. However, a coherent and relatively universal algorithm that allows determining the limits of the possibility of using single-stage gearboxes in the EMT for the LACWV and the power of the TM required for this purpose has not been found in the scientific literature.

**The goal of the work** is the formation of a scientifically based methodology for assessing the possibility of using single-stage gearboxes in EMT for LACWVs and calculating the required power of a TM of the selected type for one- or two-stage mechanical gearboxes.

Tasks solved to achieve the goal:

- formalization of requirements for the kinematic and force ranges of EMT for LACWV;

- determination of the required mechanical power of selected TMs for use in transmissions with single-stage mechanical gearboxes while ensuring the specified mobility parameters;

- determination of rational values of transmission ratios of both stages of mechanical gearboxes and the minimum possible value of the required mechanical power of the selected TMs for transmission with two-stage mechanical gearboxes.

**Algorithm for determining the power and choice of characteristics of the gearbox.** According to their functional purpose, LACWVs perform diverse tasks for conducting combat operations in direct contact with the enemy, for transporting personnel, military cargo, towing artillery and other systems both in conditions of paved roads and in full off-road conditions.

If we try to summarize the modern requirements for mobility of these vehicles in relation to electromechanical transmissions, then, first of all, the following should be highlighted:

- 1) the achievement and long-term maintenance of the maximum speed  $v_{\max}$  when driving on the highway;
- 2) the ability to climb on the soil sodded slope with angle of  $\alpha_{\max}$  with speed of at least  $v_{\min}$ ;
- 3) the acceleration time to maximum speed when driving on the highway;
- 4) the acceleration time up to speed of 20 m/s for wheeled vehicles (WV) and up to 12 m/s for caterpillar (tracked) vehicles (CV) when driving on the highway;
- 5) the acceleration time up to speed of 10 m/s when driving on the dry dirt road;
- 6) the long-term implementation of the dynamic factor  $D_{\max}^{LL}$  for CV and WV with the power organization of rotation on the principle of CV, as a rule, not less than 0.8 and for WV with kinematic rotation of not less than 0.7.

The proposed algorithm contains the following sequence of actions:

1. The first requirement allows to determine the minimum required mechanical power of the electric drive, necessary for its implementation. In accordance with [8, 9] for the first requirement

$$N_{v_{\max}} = \frac{(G_M f + k F v_{\max}^2) v_{\max}}{\eta_{WG} \eta_{CD}},$$

where  $G_M$  is the weight of the vehicle (N);  $v_{\max}$  is the maximum speed on the highway (m/s);  $f$  is the coefficient of resistance to movement on the horizontal surface, depending on the quality and microrelief of the terrain and type of propulsion;  $k$  is the coefficient of flow around the body of the vehicle ( $N \cdot s^2/m^4$ );  $F$  is the area of the frontal projection of the vehicle ( $m^2$ );  $\eta_{WG}$  is the efficiency of the mechanical wheel gear;  $\eta_{CD}$  is the efficiency of the caterpillar propulsion, which at maximum speed is calculated by the formula

$$\eta_{CD} = a_1 - a_2 v_{\max},$$

where the coefficients  $a_1$  and  $a_2$  depend on the type of hinge of the caterpillar propulsion and for the metal hinge (MH) are  $a_1 = 0.95$  and  $a_2 = 0.018$  s/m, and for the rubber metal hinge (RMH)  $a_1 = 0.98$  and  $a_2 = 0.012$  s/m.

2. According to the calculated power value, the TMs of the adopted type are selected, the total long-term

operating mechanical power of which is not less than the required value:

$$N_{\Sigma TM} \geq N_{v_{\max}}$$

3. By given or accepted dimensions of the driving wheels  $R_{DW}$  and the maximum angular velocity of the TM  $\omega_{TM_{\max}}$ , we determine the gear ratio of the mechanical wheel gears, allowing the vehicle to move at given maximum speed  $v_{\max}$  on the road with hard surface:

$$i_{WG} = \frac{\omega_{TM_{\max}} R_{DW}}{v_{\max}}$$

4. Knowing the value of the gear ratio of the wheel gears and specifying the value of their efficiency depending on the structure, we determine the maximum values of the traction force  $P$  and the dynamic factor  $D$  of the vehicle at the moment of start at  $v = 0$  for the short-term mode and at  $v=v_{\min}$  for the long-term mode

$$P_{v=0}^{AST} = \frac{M_{\Sigma TM_{\max}}^{AST} i_{WG} \eta_{WG} \eta_{CD}}{R_{DW}} \quad \text{and} \quad D_{v=0}^{AST} = \frac{P_{v=0}^{AST}}{G_M};$$

$$P_{v=v_{\min}}^{LL} = \frac{M_{\Sigma TM_{\max}}^{LL} i_{WG} \eta_{WG} \eta_{CD}}{R_{DW}} \quad \text{and} \quad D_{v=v_{\min}}^{LL} = \frac{P_{v=v_{\min}}^{LL}}{G_M},$$

where  $M_{\Sigma TM_{\max}}^{AST}$  is the maximum total short-term allowable torque of all TMs, and  $M_{\Sigma TM_{\max}}^{LL}$  is the maximum total long-term torque of all TMs.

5. We check the value  $D_{v=v_{\min}}^{LL}$  for compliance with requirements 6 and 2 at the selected value of the gear ratio of the wheel gear. To do this, we calculate the gear ratio of additional gearboxes

$$i_{add}^{D_{\max}} = \frac{D_{\max}^{LL}}{D_{v=v_{\min}}^{LL}} \leq 1 \quad \text{and} \quad i_{add}^{\alpha} = \frac{f_{\Sigma}}{D_{v=v_{\min}}^{LL}} \leq 1,$$

where  $f_{\Sigma}$  is the total coefficient of resistance to movement, which is determined by the formula

$$f_{\Sigma} = f \cdot \cos \alpha + \sin \alpha,$$

where  $\alpha$  is the slope angle equal to  $\alpha_{\max}$  – the specified in tactical and technical characteristics of the LACWV maximum slope angle on a soil sodded slope.

If one or both conditions are not fulfilled, then it is necessary to take the larger of the values  $i_{add}^{\alpha}$  and  $i_{add}^{D_{\max}}$  found and, in this number of times by the available method, increase the maximum total long-term operating torque of all TMs or install a reduced stage in the wheel gears with the additional transmission ratio found.

6. Assess the capabilities of the intended power plant, generator and storage devices by the possibilities of long-term and short-term power supply to the transmission.

7. Check the fulfillment of requirements 2 – 5 by carrying out a traction calculation in the appropriate road conditions taking into account the limitations on the possibilities of the power plant, generator and storage devices. If, in the course of the calculation, lower stages were introduced in the wheel gears, then the traction calculation should be carried out in two modes – first estimate the acceleration time at the start immediately from the second gear, and then, if conditions are not met,

consider acceleration with sequential gears up starting with down one.

We illustrate the above methodology with an example of the development of an electromechanical transmission for the MT-LB multi-purpose conveyor tractor.

Initial data for calculations on the vehicle are presented in Table 1, regarding TM – in Table 2.

Table 1

Initial data on the conveyor tractor		
Indicator name	Value	
Vehicle weight $G_M$ , N	117720	
Maximum velocity on the highway $V_{\max}$ , m/s (km/h)	18.06 (65)	
Average velocity of movement, m/s (km/h)	on the highway $V_{av}$	11.11 (40)
	on the dirt road $V_{av}^*$	8.33 (30)
Maximum slope angle on the ground $\alpha_{\max}$ , °	35	
Rise velocity with slope 35° not less, m/s (km/h)	1.39 (5)	
Vehicle height $H$ , m	2.035	
Track width $B$ , m	2.5	
Clearance $h$ , m	0,4	
Driving wheel radius $R_{DW}$ , m	0.265	
Flow rate $k$ , (N·s <sup>2</sup> )/m <sup>4</sup>	0.65	
Calculated acceleration time on the highway, s (no more) to velocity $0.95 v_{\max} - 17.153$ m/s (61.75 km/h)	60	
Calculated acceleration time on the highway, s (no more) to velocity 11.11 m/s (40 km/h)	15	
Calculated acceleration time on the dirt road, s (no more) to velocity 8.33 m/s (30 km/h)	10	
Maximum value of the dynamic factor (not less)	0.8	

Table 2

Characteristics of the TM M73	
Indicator	Value
TM mass, kg	88
Dimensions (diameter × length), mm	483 × 232
TM maximum power, kW	150
TM maximum long-term power, kW	120
Maximum rotation speed, rpm	3100
Maximum long-term torque, Nm	1050
Maximum short-term torque (less than a minute), Nm	2050

In accordance with the proposed algorithm:

1. Power required to reach maximum velocity

$$N_{v_{\max}} = \frac{(G_M f + k F v_{\max}^2) v_{\max}}{\eta_{WG} \eta_{CD}} = \frac{\left( 117720 \cdot 0.045 + 0.65 \cdot 4.0875 \cdot \left( \frac{65}{3.6} \right)^2 \right) \frac{65}{3.6}}{0.98 \cdot \left( 0.95 - 0.018 \frac{65}{3.6} \right)} = 181692 \text{ W},$$

where the frontal area of the vehicle is

$$F = B(H - h) = 2.5(2.035 - 0.4) = 4.0875 \text{ m}^2.$$

2. For the TM M73, having a long-term power of 120 kW, two TMs will suffice – one for each driving wheel (board).

3. The gear ratio of the wheel gears for these TMs will be

$$i_{WG} = \frac{\omega_{TM \max} R_{DW}}{v_{\max}} = \frac{\pi \cdot 3100}{\frac{30}{65} \cdot 0.265} = 4.765.$$

4. We determine the maximum values of the traction force and the dynamic factor of the vehicle at the moment of start at  $v = 0$  for the short-term mode and at  $v = v_{\min}$  for the long-term mode:

$$P_{v=0}^{AST} = \frac{M_{\Sigma TM \max}^{AST} i_{WG} \eta_{WG} \eta_{CD}}{R_{DW}} = \frac{2 \cdot 2050 \cdot 4.765 \cdot 0.98 \cdot 0.95}{0.265} = 68636 \text{ N};$$

$$D_{v=0}^{AST} = \frac{P_{v=0}^{AST}}{G_M} = \frac{68636}{117720} = 0.583;$$

$$P_{v=v_{\min}}^{LL} = \frac{M_{\Sigma TM \max}^{LL} i_{WG} \eta_{WG} \eta_{CD}}{R_{DW}} = \frac{2 \cdot 1050 \cdot 4.765 \cdot 0.98 \cdot \left(0.95 - 0.018 \frac{5}{3.6}\right)}{0.265} = 34230 \text{ N};$$

$$D_{v=v_{\min}}^{LL} = \frac{P_{v=v_{\min}}^{LL}}{G_M} = \frac{34230}{117720} = 0.291.$$

5. We calculate the gear ratios of additional gearboxes:

$$i_{add}^{D_{\max}} = \frac{D_{\max}^{LL}}{D_{v=v_{\min}}^{LL}} = \frac{0.8}{0.291} = 2.75 > 1;$$

$$i_{add}^{\alpha} = \frac{f_{\Sigma}}{D_{v=v_{\min}}^{LL}} = \frac{0.065 \cdot \cos 35^{\circ} + \sin 35^{\circ}}{0.291} = 2.154 > 1.$$

The values obtained indicate that in this configuration, the electromechanical drive for the conveyor tractor will not meet the requirements of either point 2 or point 6.

6. To solve this problem, it is necessary either to increase by 2.75 times the total torque at the TM, or to introduce an additional reduced stage in the wheel gears with an additional gear ratio of 2.75.

Consider the first solution of the issue.

The increase in the total long-term TM torque is possible either by switching to a higher torque TM or increasing their number. In our case, there is only an opportunity to apply a larger number of TMs M73 accepted for calculation.

We estimate the power that will be consumed by 6 TMs M73 when implementing  $D_{v=v_{\min}}^{LL} = 0.8$ . In this case, the traction force should be

$$P_{v=v_{\min}}^{LL} = D_{v=v_{\min}}^{LL} G_M = 0.8 \cdot 117720 = 94176 \text{ N}.$$

Accordingly, the total torque of all six TMs will be

$$M_{\Sigma TM \max}^{LL} = \frac{P_{v=v_{\min}}^{LL} R_{DW}}{i_{WG} \eta_{WG} \eta_{CD}} = \frac{94176 \cdot 0.265}{4.765 \cdot 0.98 \cdot \left(0.95 - 0.018 \frac{5}{3.6}\right)} = 5778 \text{ Nm}.$$

Their rotation speed will be

$$\omega_{TM} = \frac{v_{\min} i_{WG}}{R_{DW}} = \frac{5}{3.6} \cdot 4.765 / 0.265 = 24.97 \text{ s}^{-1}.$$

The mechanical power consumed will be just

$$N_{D \max} = \omega_{TM} M_{\Sigma TM \max}^{LL} = 24.97 \cdot 5778 = 144299 \text{ W},$$

which is completely valid.

We consider the second solution.

In this case, we leave two TMs M73 and add a lower stage in the wheel gears with gear ratio

$$i_L = i_{WG} \cdot i_{add}^{D_{\max}} = 4.765 \cdot 2.75 = 13.1.$$

7. Let us check the fulfillment of requirements 2 – 5 for both options by carrying out traction calculation in appropriate road conditions taking into account the limitations on the possibilities of the power plant, generator and storage devices. We take the maximum total long-term mechanical power of all six TMs M73 equal to 200 kW.

Then the dependence of the total torque of all 6 TMs on the rotation speed of the armature will correspond to the curve shown in Fig. 1. And, respectively, the graph of the dynamic factor for a vehicle with 6 TMs M73, calculated by the formula

$$D = \frac{\frac{M_{\Sigma TM}^{LL} i_{WG} \eta_{WG} \eta_{CD}}{R_{DW}} - k F v^2}{G_M},$$

will have the form shown in Fig. 2.

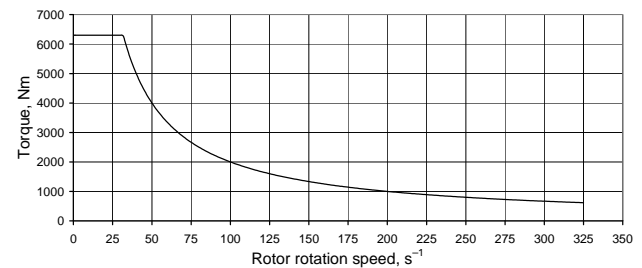


Fig. 1. Total torque of 6 TMs M73 at power limit 200 kW

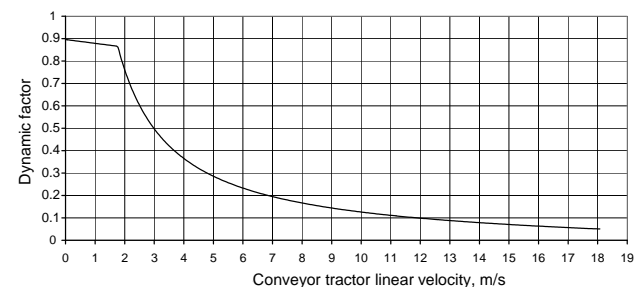


Fig. 2. Dynamic factor of the conveyor tractor with 6 TMs M73 at power limit 200 kW

Respectively, for two TMs M73 and two-stage wheel gear, graphs of the total torque and dynamic factor are presented in Fig. 3, 4.

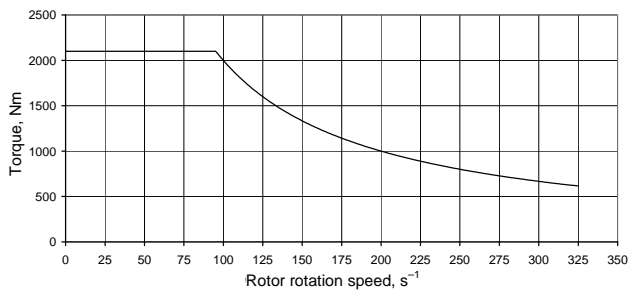


Fig. 3. Total torque of 2 TMs M73 at power limit 200 kW

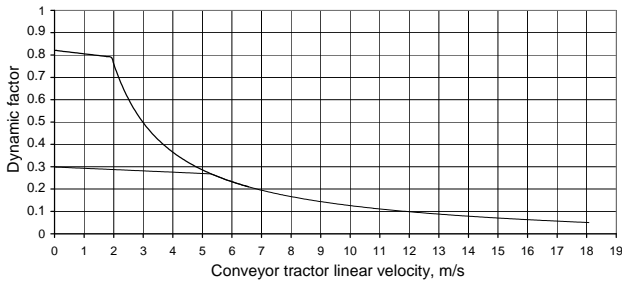


Fig. 4. Dynamic factor of the conveyor tractor with 2 TMs M73 at power limit 200 kW

To verify the requirements of 2-5, 3 variants of calculations were carried out for the vehicle accelerating on a horizontal surface:

- 6 TMs M73, single-stage wheel gears with  $i_{WG} = 4.765$ ;
- 2 TMs M73, two-stage wheel gears with gear ratios – reduced  $i_L = 13.1$  and normal  $i_{WG} = 4.765$ , acceleration from the transmission of the normal series without switching in the process of movement;
- 2 TMs M73, two-stage wheel gears with gear ratios – reduced  $i_L = 13.1$  and normal  $i_{WG} = 4.765$ , acceleration from the lower stage with switching during movement.

Also, calculations were carried out to determine the maximum velocity of the vehicle to climb 35° on the dirt road in two versions:

- 6 TMs M73, single-stage wheel gears with  $i_{WG} = 4.765$ ;
- 2 TMs M73, two-stage wheel gears with gear ratios – reduced  $i_L = 13.1$  and normal  $i_{WG} = 4.765$ , acceleration and movement in low gear.

The results of the calculations are given in Table 3.

**Analysis of the results obtained.** The variant of construction of the EMT for the MT-LB conveyor tractor with two TMs M73 and single-stage wheel gears was removed from consideration as not allowing to provide for points 2 and 6 of the «Requirements».

The remaining three options for construction suggest:

- six TMs M73 (three per board) with two single-stage wheel gears (one per board);
- two TMs M73 (one per board) with two two-stage wheel gears (one per board) with the possibility of activating a lower row when stopping the vehicle to drive in heavy road conditions;
- two TMs M73 (one per board) with two two-stage wheel gears (one per board) with the possibility of sequential activation of the reduced and normal rows in motion, both during acceleration and deceleration.

The requirements for mobility of LACWV, prescribed in [1, 2], are underestimated and, in fact, repeat the parameters of a vehicle with a classic mechanical manual transmission. All three retained for consideration options for building EMT confidently meet the requirements.

The best performance of the mobility of the conveyor tractor has EMT, consisting of six TMs M73 (three TMs per board) with two single-stage wheel gears (one per board). However, its use leads to an increase in the drive mass by 352 kg and cost – at the cost of four additional TMs M73 compared to a transmission containing 2 TMs M73 and 2 single-stage wheel gears.

Table 3

Results of calculations of the mobility of the conveyor tractor at power limit of 200 kW

Indicator name	Requirement	6 TMs M73		2 TMs M73			
				Acceleration in the normal row		Acceleration with switching	
		MH	RMH	MH	RMH	MH	RMH
Rise velocity with slope 35° not less, m/s (km/h)	1.389 (5)	2.408 (8.67)	2.522 (9.08)	–	–	2.408 (8.67)	2.522 (9.08)
Calculated acceleration time on the highway, s (no more) to velocity 0.95 $v_{max}$ – 17.153 m/s (61.75 km/h)	60	29.622	20.335	30.64	21.286	29.629	20.341
		100 %	100 %	–3.4 %	–4.7 %	–0.02 %	–0.03 %
Calculated acceleration time on the highway, s (no more) to velocity 12 m/s (43.2 km/h)	15	8.153	7.063	9.17	8.014	8.159	7.069
		100 %	100 %	–12.5 %	–13.5 %	–0.07 %	–0.08 %
Calculated acceleration time on the dirt road, s (no more) to velocity 10 m/s (36 km/h)	10	5.879	5.141	7.064	6.245	5.884	5.147
		100 %	100 %	–20.2 %	–21.5 %	–0.09 %	–0.12 %
Maximum long-term value of the dynamic factor (not less)	0.8	0.896	0.924	0.299	0.308	0.821	0.847
		100 %	100 %	–	–	–8.37 %	–8.33 %

The smallest weight and cost when losing the first option in mobility from 3 % to 21.5 %, depending on the indicator and the type of hinge of the tracked propulsion, has the option with two TMs M73 and two two-stage wheel gears with the ability to turn on the reduced row

when stopping the vehicle for movement only at heavy road conditions. In this case, it is possible to avoid friction discs in a two-stage planetary gearbox, and to organize switching by means of gear couplings by analogy with the reversing onboard gear of the fighting

vehicle «Oplot». In contrast to the first option, an increase in the mass of the drive is expected to be in the range of only 160–165 kg compared to a transmission containing 2 TMs M73 and 2 single-stage wheel gears.

The most promising, in our opinion, is the third option, which very slightly loses to the first option in mobility (from 0.02 % to 8.37 %), but in the case of a properly designed wheel gear, it is possible to combine the functions of stopping brakes and control range switching clutches on the same friction devices. In this case, weight increase is expected to 200 kg.

#### Conclusions and recommendations.

As a result of the presented work, a scientifically based method was developed, which allows to find the required power of the TM of the selected type when using single- or two-stage mechanical gearboxes.

The obtained method allows the developer of an electromechanical transmission to determine rational limits for using single-stage mechanical gearboxes and, if necessary, to choose a method for using two-stage mechanical gearboxes sufficient to provide the specified tactical and technical characteristics of military equipment.

#### REFERENCES

1. Walentynowicz Je. Hybrid and electric power drive combat vehicles. *Journal of KONES Powertrain and Transport*, 2011, vol.18, no.1, pp. 471-478.
2. Colyer Ron E. The use of electric and hybrid-electric drives in military combat vehicles. *Journal of Battlefield Technology*, 2003, vol.6, no.3, pp. 11-15.
3. *All Electric Combat Vehicles (AECV) for Future Applications* / Report of the Research and Technology Organization (RTO) of NATO Applied Vehicle Technology Panel (AVT) Task Group AVT-047 (WG-015). 2004. 234 p.
4. Galvagno E., Rondinelli E., Velardocchia M. Electro-mechanical transmission modelling for series-hybrid tracked tanks. *International Journal of Heavy Vehicle Systems*, 2012, vol.19, no.3, pp. 256-280. doi: 10.1504/ijhvs.2012.047916.
5. Glebov V.V., Klimov V.F., Volosnikov S.A. Assessment of the Possibility to Use Hybrid Electromechanical Transmission in Combat Tracked Platforms. *Mechanics, Materials Science & Engineering*, 2017, vol.8, pp. 99-105. doi: 10.2412/mmse.83.5.981.
6. Erkhart P. Elektrische Kraftübertragung – Technologie und praktische Anwendung. *Soldat und Technik*, 2003. pp. 22-27. (Ger).
7. Ilijevski Ž. *A Hybrid-Electric Drive Concept For High Speed Tracked Vehicles*. Brodarski Institut, Zagreb, Croatia. 2006. 9 p.
8. Sivakumar P., Reginald R., Venkatesan G., Viswanath H., Selvathai T. Configuration Study of Hybrid Electric Power Pack for Tracked Combat Vehicles. *Defence Science Journal*, 2017, vol.67, no.4, pp. 354-359. doi: 10.14429/dsj.67.11454.
9. Volontsevich D.O., Veretennikov E.A., Yefremova A.I., Yaremchenko A.S., Prokop'ev M.I. Traction balance for perspective tracked multipurpose carrier-truck with electromechanical transmission is located on the sides. *Bulletin of NTU «KhPI». Series: Transport machine building*, 2017, no.5(1227), pp. 162-167. (Rus).
10. Volontsevich D.O., Veretennikov E.A., Mormilo Ya.M., Yaremchenko A.S., Karpov V.O. Traction balance for perspective wheeled armored personnel carrier with electromechanical transmission. *Bulletin of NTU «KhPI». Series: Transport machine building*, 2017, no.5(1227), pp. 168-173. (Rus).

Received 27.08.2018

D.O. Volontsevich<sup>1</sup>, Doctor of Technical Science, Professor,  
E.A. Veretennikov<sup>1</sup>, Candidate of Technical Science,  
I.V. Kostianik<sup>1</sup>, Candidate of Technical Science, Associate Professor,  
A.S. Iaremchenko<sup>1</sup>, Postgraduate Student,  
A.I. Efremova<sup>1</sup>, Postgraduate Student,  
V.O. Karpov<sup>1</sup>, Postgraduate Student,  
<sup>1</sup>National Technical University «Kharkiv Polytechnic Institute»,  
2, Kyrpychova Str., Kharkiv, 61002, Ukraine,  
phone +380 57 7076355,  
e-mail: vdo\_khpi@ukr.net

#### How to cite this article:

Volontsevich D.O., Veretennikov E.A., Kostianik I.V., Iaremchenko A.S., Efremova A.I., Karpov V.O. Determination of the electric drive power for lightly armored caterpillar and wheeled vehicles using single- or two-stage mechanical gearboxes. *Electrical engineering & electromechanics*, 2019, no.1, pp. 29-34. doi: 10.20998/2074-272X.2019.1.05.

O.V. Bialobrzheskyi, D.I. Rodkin

## ALTERNATIVE INDICATORS OF POWER OF ELECTRIC ENERGY IN A SINGLE-PHASE CIRCUIT WITH POLYHARMONIC CURRENT AND VOLTAGE

*Introduction.* Many electrical engineering issues use a power balance. It is compiled from averaged power values, and equivalent power is used to characterize power of transient processes. To account electricity, both mono- and polyharmonic currents and voltages use active and reactive power, the quality of electricity is not taken into account. *Problem.* A number of works are declared a certain number of power components that reflect indicators of quantity and quality of electrical energy. These components of power are subject to criticism. The order of determining power components requires algorithmization, as well the task of determining indicators that will reflect poor quality of energy. *Goal.* Development of a technique for determining the components of power in single-phase circuits with polyharmonic current and voltage, for definition electrical energy transmission indicators. *Methodology.* Based on analysis of power components determined in known papers and order of their calculation, the features of taking sign of sine and cosine orthogonal components are marked, depending on combination of numbers a current and voltage harmonics. Using Fourier theory of series and elements of the logic algebra, an algorithm for determining components of electric power energy is developed. *Results.* Highlighting active and reactive powers of the fundamental harmonic of current and voltage; active and reactive power; canonical power components; non-canonical power components, and proposed indicators of quality of transmission of electrical energy. *Originality.* Based on analysis of power represented by trigonometric Fourier series, the specific calculation of canonical and non-canonical components with use of a number of indicators of electric energy transmission is proposed that reflect its quality. *Practical value.* The proposed power components of transmission of electrical energy can be used in technical accounting systems. References. 12, figures 6.

*Key words:* power of electric energy, quality indicators, power norm, quantity and quality of electric energy.

*Мета.* Розробка методики визначення компонент потужності, в однофазних колах з полігармонійними струмом та напругою, для формування показників передачі електричної енергії. *Методика.* Використовуючи теорію рядів Фур'є та елементи алгебри логіки, відмічені особливості винесення знаку ортогональних компонент потужності в залежності від комбінації номеру гармонік струму та напруги. *Результати.* Відокремлюючи активну та реактивну потужності основної гармоніки струму та напруги; активну та реактивну потужності; канонічні компоненти потужності; неканонічні компоненти потужності, запропоновано показники якості передачі електричної енергії. *Наукова новизна.* Потужність, представлена тригонометричним рядом Фур'є, містить канонічні та неканонічні компоненти, які відбивають якість електричної енергії. *Практична значимість.* Компоненти потужності, та показники передачі електричної енергії можуть бути використаними в системах технічного обліку для вимірювання обсягів якісної та неякісної енергії. Бібл. 12, рис. 6.

*Ключові слова:* потужність електричної енергії, показники якості, норма потужності, кількість та якість електричної енергії.

*Цель.* Разработка методики определения компонент мощности, в однофазных цепях с полигармоническом током и напряжением, для формирования показателей передачи электрической энергии. *Методика.* Используя теорию рядов Фурье и элементы алгебры логики, отмеченные особенности вынесения знака ортогональных компонент мощности в зависимости от комбинации номера гармоник тока и напряжения. *Результаты.* Отделяя активную и реактивную мощности основной гармоник тока и напряжения; активную и реактивную мощности; канонические компоненты мощности; неканонические компоненты мощности, предложены показатели качества передачи электрической энергии. *Научная новизна.* Мощность, представленная тригонометрическим рядом Фурье, содержит канонические и неканонические компоненты, которые отражают качество электрической энергии. *Практическая значимость.* Компоненты мощности, и показатели передачи электрической энергии могут быть использованы в системах технического учета для измерения объемов качественной и некачественной энергии. Библ. 12, рис. 6.

*Ключевые слова:* мощность электрической энергии, показатели качества, норма мощности, количество и качество электрической энергии.

**Introduction.** In the electric power, electromechanical and electrical engineering systems and complexes, when solving the problems associated with the transformation of electric energy into other types of energy, the balance of energy or power is used. This allows to check the result of the task solution and estimate the distribution of power flows. In most cases, the balance consists of values averaged over a certain period of time. For a category of problems with stationary processes, such an approach is rational.

In the case of a transient process, such as transforming the power of electric motors in an automated electric drive of technological mechanisms characterized by variable power consumption, additional parameters are

introduced that characterize the mode – S1-S8 [1]. Here, a certain period of time – a cycle is considered. Equivalent mode parameters are used for the cycle, in particular – equivalent power [2].

In modern systems, the generation, transportation and consumption of electric energy are carried out by alternating current except for traction networks of direct current, onboard networks of vehicles, and specialized inserts of direct current [3]. The latter only in a certain approximation operate with direct current, in the general case, the current is alternating.

When operating networks that provide electric energy consumers, regardless of the nature of the current,

© O.V. Bialobrzheskyi, D.I. Rodkin

problems arise in the account of electrical energy. For DC networks, the average (at a specified interval) power value is used as the accounting indicator, for AC networks – active and reactive power [4, 5]. In this way, the volume of electric energy is accounted, and reactive power in some way characterizes poor quality. The reactive power is uniquely determined for periodic monoharmonic currents and voltages. In case of distortion of current or voltage, for accounting indicators determined by averaged current and voltage are used. The resulting poor quality of electric energy is estimated by certain indicators, normalizing their acceptable values [6], but accounting low-quality energy is not performed.

**Analysis of previous research.** A well-known Standard [7], which is a product of many years of work by a group of scientists, declares a certain number of components of electric energy power, each of which reflects characteristic indicators. The determination of the power components of electric energy occurs on the basis of the currents and voltages presented in the trigonometric form of the Fourier series. Using well-known vector forms and concepts of full, active, inactive, reactive power, distortion power, for three-phase circuits of corresponding fundamental powers of direct, zero and reciprocal sequences, the authors sufficiently multifaceted define a characteristic of the electric energy flux. These power components are based on the Budeanu concept and are criticized [8, 9] from the standpoint of determining the harmonic components of power based on harmonic current and voltage. In [10] the question of the formation of power components, both as power source and elements of electric circuits, both with linear and nonlinear characteristics, is considered in various ways. As in the works previously mentioned, the authors are based on the representation of periodic currents and voltages in the trigonometric form of the Fourier series. The substantiated [11] procedures for the determination of the volt-ampere characteristics of nonlinear elements are also based on the representation of current, voltage and power by periodic polyharmonic functions. The last group of works emphasizes the observance of the law of conservation of energy and the implementation of the Tellegen theorem.

**Problem definition.** The differentiation of the power component provides an opportunity for a certain assessment of the energy process [7]. The analysis of processes in electric circuits using the representation of currents, voltages and powers by polyharmonic functions is used for tasks of identifying parameters and characteristics of circuit elements [11]. In spite of the fact that in both cases the polyharmonic current and voltage are the basic, the determination procedure and the resulting power components are different. In the latter case, the law of conservation of energy is provided, which makes it more favorable for assessing the indicators of transmission of electricity. But the order of determining the components of power requires algorithmization, and as a consequence the problem of determining the indicators that reflect the poor quality of the flow of electric energy, arises.

**The goal of the work** is the development of a method for determining the components of power of

electric energy in single-phase circuits with polyharmonic current and voltage, for the formation of indicators of transmission of electric energy.

**Main material and results of investigations.** In the theory of linear circuits with energy sources which determine the monoharmonic currents in the branches and the corresponding monoharmonic voltages in the nodes, for example

$$u = \sqrt{2}U \sin(\omega t + \psi_u);$$

$$i = \sqrt{2}I \sin(\omega t + \psi_i),$$

where  $U, I$  are the effective values of voltage and current;  $\psi_u, \psi_i$  are the initial phases of voltage and current;  $\omega$  is the angular frequency, based on the corresponding power, active  $P$ , reactive  $Q$  and full  $S$  powers are introduced:

$$p = ui = \sqrt{2}U \sin(\omega t + \psi_u) \sqrt{2}I \sin(\omega t + \psi_i) =$$

$$= UI \cos(\psi_u - \psi_i) \cos(0) - UI \cos(\psi_u + \psi_i) \cos(2\omega t) -$$

$$- UI \sin(\psi_u - \psi_i) \sin(0) + UI \sin(\psi_u + \psi_i) \sin(2\omega t) =$$

$$= P \cos(0) - Q \sin(0) - S \cos(2\omega t + \psi_u + \psi_i).$$

We emphasize the well-known fact that the full power in this case is determined by the product of effective values of current and voltage. At that, obviously

$$\left[ (UI \cos(\psi_u - \psi_i))^2 + (UI \sin(\psi_u - \psi_i))^2 \right] = [UI]^2;$$

$$\left[ P^2 + Q^2 \right] = S^2.$$

In the case of polyharmonic currents and voltages

$$u = \sum_k \sqrt{2}U_k \sin(k\omega t + \psi_{uk}) =$$

$$= \sqrt{2} \sum_k (U_k \cos(\psi_{uk}) \sin(k\omega t) + U_k \sin(\psi_{uk}) \cos(k\omega t)) =$$

$$= \sum_k (U_{a,k} \sin(k\omega t) + U_{b,k} \cos(k\omega t));$$

$$i = \sum_n \sqrt{2}I_n \sin(n\omega t + \psi_{in}) =$$

$$= \sqrt{2} \sum_n (I_n \cos(\psi_{in}) \sin(k\omega t) + I_n \sin(\psi_{in}) \cos(k\omega t)) =$$

$$= \sum_n (I_{a,n} \sin(n\omega t) + I_{a,n} \cos(n\omega t)),$$

where  $k, n$  are the numbers of harmonics of voltage and current;  $U_k, I_n$  are the effective values of harmonics of voltage and current;  $\psi_{uk}, \psi_{ik}$  are the initial phases of voltage and current;  $U_{a,k}, U_{b,k}$  are the amplitudes of cosine and sine components of harmonics of voltage;  $I_{a,k}, I_{b,k}$  are the amplitudes of cosine and sine component of harmonics of current, expression for power is considerably complicated

$$p = \sum_{k,n} U_k I_n \cos[(k-n)\omega t + \psi_{uk} - \psi_{in}] -$$

$$- \sum_{k,n} U_k I_n \cos[(k+n)\omega t + \psi_{uk} + \psi_{in}]; \quad (1)$$

As indicated in [12] from the last expression, the instantaneous power function contains harmonics whose order ( $s$ ) is defined as the difference  $(k-n)$  and the sum  $(k+n)$  of the orders of the harmonics of voltage and current, that is  $s = k \pm n$ . Thus, instantaneous power

$$p = \sum_s P_s = P_0 + P_1 + \dots + P_{k-n} + \dots + P_{k+n} + \dots + P_z, \quad (2)$$

where the numbers of harmonics are defined by the set  $Z = \{0, 1, 2, \dots, s, \dots, z\}$ . The spectrum of the harmonics of the power function depends on which harmonic numbers are represented in the voltage and current spectrum. It must be borne in mind that different, but certain combinations of harmonics of voltage and current form harmonics of power of one order (for example, if  $k = n + 1$ , then the difference  $s = k - n$  equals one for any numbers  $s = k$  and  $s = n$ ), so the actual number of harmonics of power may be less than maximum, but not less than twice the number of harmonics of voltage or current.

In this case, it is accepted to use active, reactive and full power in the form

$$P = p_0 = \sum_{k=n} U_k I_n \cos(\psi_{uk} - \psi_{in});$$

$$Q = \sum_{k=n} U_k I_n \sin(\psi_{uk} - \psi_{in});$$

$$S = \sqrt{P^2 + Q^2},$$

but as is known from the functional analysis, the Cauchy-Budianovsky-Schwartz inequality is fulfilled [6] and in the case under consideration, as noted in [4, 12]:

$$S \neq UI.$$

Without going into Budeanu theory and its generalization in work [4] in the part of inactive power and components of the distortion power, we consider the order of formation of the power components of (2) based on (1).

In [12] the conditional distribution of the power components is used in the form of the sum:

$$p = p_0 + \sum_{\substack{s=k+n \\ s=2k=2n}} (p_{a.c.s} + p_{b.c.s}) +$$

$$\left[ \sum_{\substack{s=k \pm n \\ s=2k \cap 2n}} (p_{a.pc.s} + p_{b.pc.s}) + \sum_{\substack{s=k \pm n \\ s \neq 2k \cap 2n}} (p_{a.nc.s} + p_{b.nc.s}) \right], \quad (3)$$

where  $p_0$  is the zero component of power (active power) for all harmonics;  $p_{a.c.s}$  are the cosine canonical components;  $p_{b.c.s}$  are the sine canonical components;  $p_{a.pc.s}$  are the cosine components of non-canonical order – pseudo-canonical components;  $p_{b.pc.s}$  are the sine components of non-canonical order – pseudo-canonical components;  $p_{a.nc.s}$  are the cosine noncanonical components;  $p_{b.nc.s}$  are the sine noncanonical components.

Direct calculation and differentiation of indicated power components by expression (1) requires a lot of time and effort. Therefore, an algorithm for calculating the power components, the general form of which is shown in Fig. 1, is developed. The algorithm can be divided into four stages: preparation of measured signals of current and voltage; fast Fourier transform of voltage and current; definition of power components; calculation of indicators of transmission of power of electric energy.

At the first stage, the measurement of current and voltage, depending on the characteristics of the equipment, setting the discretization rate, discretization time and the maximum number of harmonics. Also, instantaneous power and its quadratic norm are

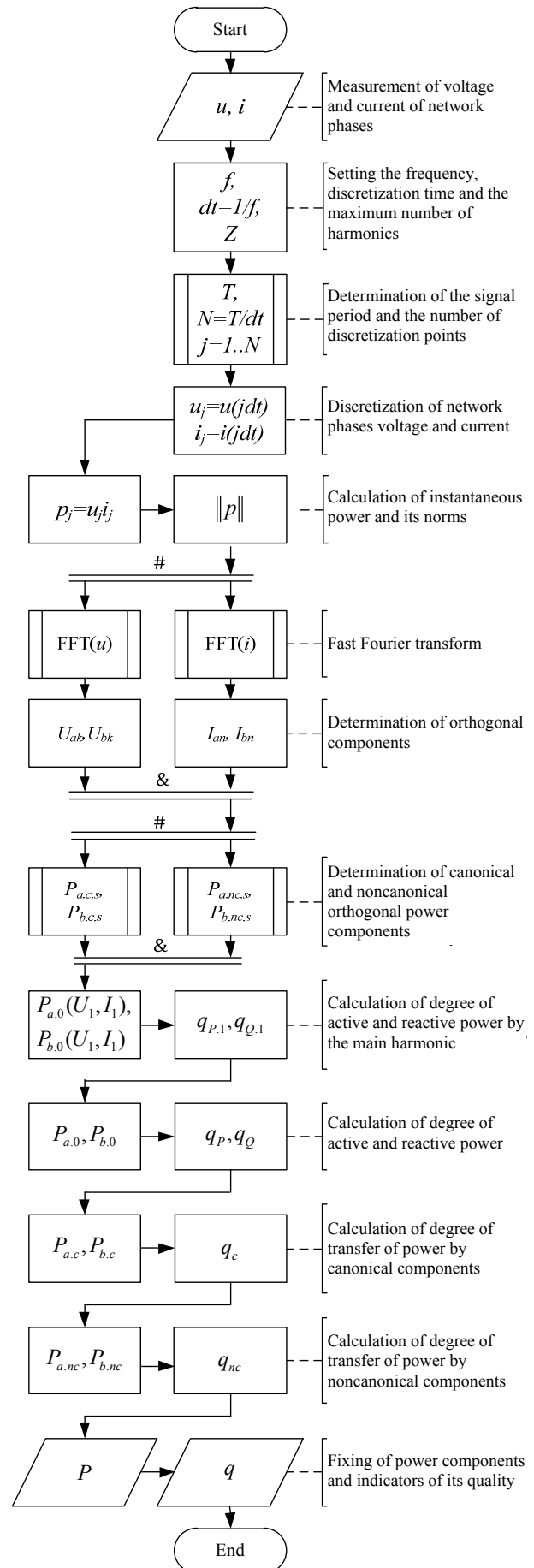


Fig. 1. The algorithm for determination of power and its qualitative indicators

determined. At the second stage, fast Fourier transform of voltage and current is performed, as a result of which their orthogonal components are determined. On the basis of this, at the third stage, the definition of canonical and noncanonical power components is performed. The procedure for determining these components has a certain peculiarity and can be implemented by performing the algorithm shown in Fig. 2.

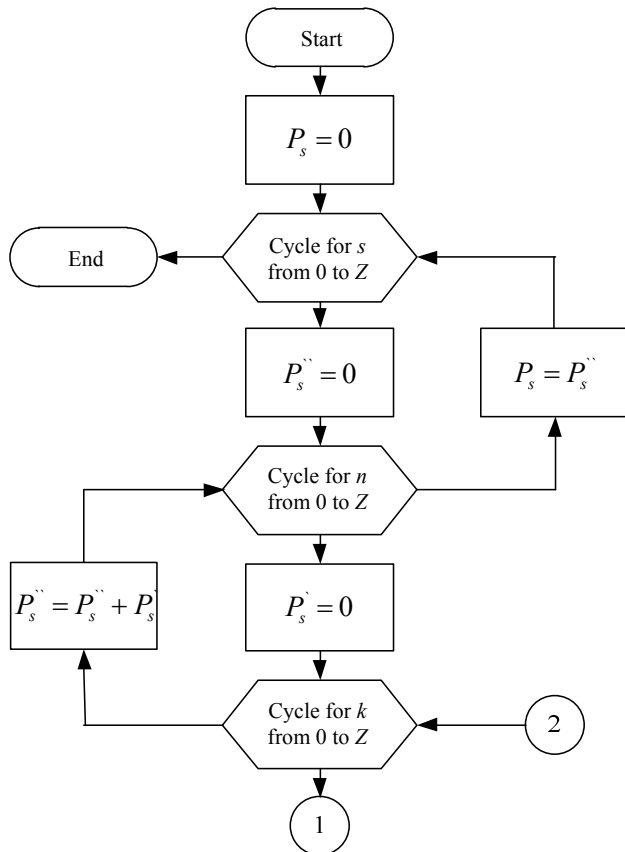


Fig. 2. The algorithm for determining orthogonal power components

Cycles of the definition of orthogonal power components, the input in each of which is indicated by the number 1, and output by the number 2 (see Fig. 2), by the structure are the same. The specified cycles differ in the essence of the conditions and are shown in Fig. 3-6. As a result of calculations by the algorithm (Fig. 2) using cycles (Fig. 3-6), for all combinations of harmonics of current and voltage, the following components of power are determined:

1. Active and reactive power of the main harmonic of current and voltage

$$\begin{cases} P_{a,1-1} = 0.5(U_{a,1}I_{a,1} + U_{b,1}I_{b,1}); \\ P_{b,1-1} = 0.5(U_{a,1}I_{b,1} - U_{b,1}I_{a,1}). \end{cases} \quad (4)$$

2. Active and reactive powers

$$\begin{cases} P_{a,0} = 0.5 \sum_{k-n=0} (U_{a,k}I_{a,n} + U_{b,k}I_{b,n}); \\ P_{b,0} = 0.5 \sum_{k-n=0} (U_{a,k}I_{b,n} - U_{b,k}I_{a,n}). \end{cases} \quad (5)$$

3. Canonical power components ( $k = n$ )

$$\begin{cases} P_{a.c.s} = \begin{cases} 0.5 \sum_{|k+n|=s} (U_{b,k}I_{b,n} - U_{a,k}I_{a,n}); \\ 0.5 \sum_{|k-n|=s} (U_{b,k}I_{b,n} + U_{a,k}I_{a,n}); \end{cases} \\ P_{b.c.s} = \begin{cases} 0.5 \sum_{|k+n|=s} (U_{a,k}I_{b,n} + U_{b,k}I_{a,n}); \\ 0.5 \sum_{|k-n|=s} (U_{a,k}I_{b,n} - U_{b,k}I_{a,n}) \text{sign}(k-n). \end{cases} \end{cases} \quad (6)$$

4. Noncanonical power components  $P_{a.nc.s}$ ,  $P_{b.nc.s}$ , which are calculated by the system of equations (6) at the condition ( $k \neq n$ ).

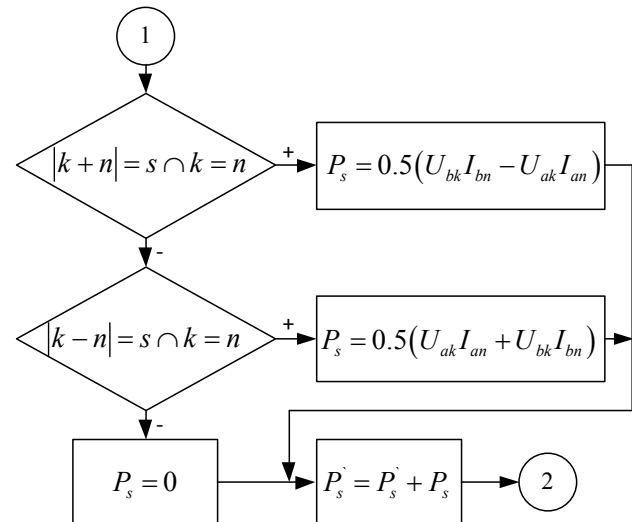


Fig. 3. The cycle of definition of cosine canonical components

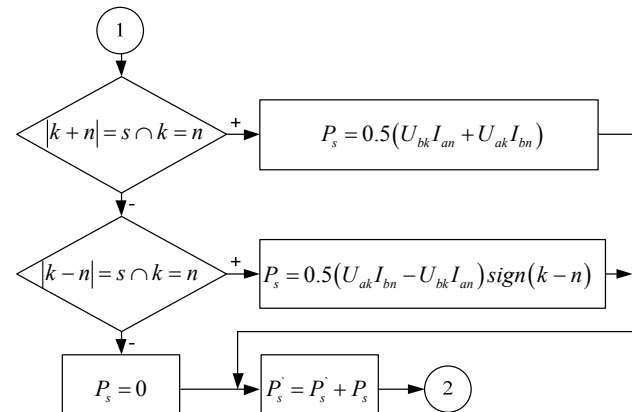


Fig. 4. The cycle of definition of sine canonical components

Thus, the power can be represented in a trigonometric form by the following series

$$p = P_{a,0} \cos(0) + \sum_{s \neq 0} (P_{a.c.s} + P_{a.nc.s}) \cos(s\omega t) + P_{b,0} \sin(0) + \sum_{s \neq 0} (P_{b.c.s} + P_{b.nc.s}) \sin(s\omega t),$$

The above-mentioned power components characterize in a certain way the process of transmission of electric energy. In general, this process can be characterized using a quadratic power norm

$$\|p\| = \sqrt{\frac{1}{T} \int_t^{t+T} p^2 dt}.$$

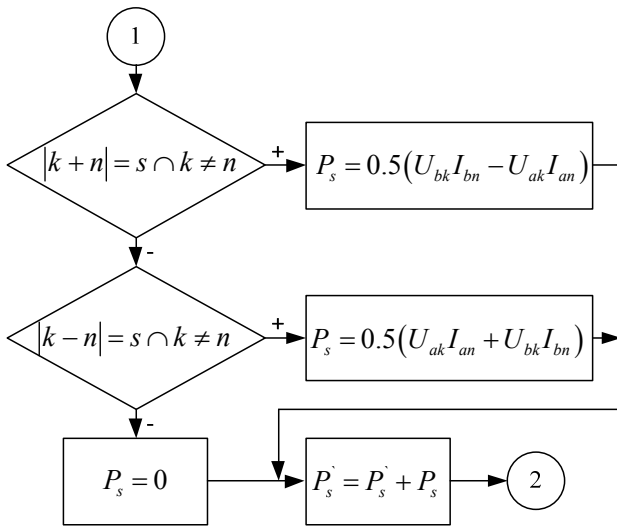


Fig. 5. The cycle of definition of cosine noncanonical components

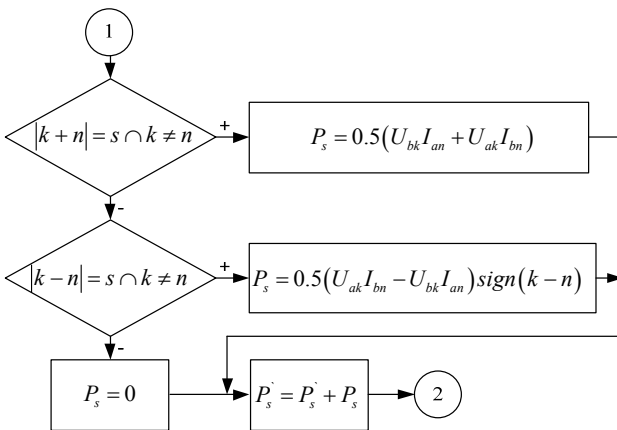


Fig. 6. The cycle of definition of sine noncanonical components

Using similar relations and previously used power components, a number of indicators have been proposed that characterize the process of energy transmission:

1. The degree of active and reactive power by the main harmonic

$$q_{P,1} = \frac{P_{a,1-1}}{\|P\|}; q_{Q,1} = \frac{P_{b,1-1}}{\|P\|}.$$

2. The degree of active and reactive power

$$q_P = \frac{P_{a,0}}{\|P\|}; q_Q = \frac{P_{b,0}}{\|P\|}.$$

3. The degree of transfer of power by canonical components

$$q_c = \frac{\sqrt{\sum P_{a.c.s}^2 + \sum P_{b.c.s}^2}}{\|P\|}.$$

4. The degree of transfer of power by noncanonical components

$$q_{nc} = \frac{\sqrt{\sum P_{a.nc.s}^2 + \sum P_{b.nc.s}^2}}{\|P\|}.$$

These indicators reflect the quality of the transmission of energy, both in the case of its consumption and generation, taking into account

components that are caused by higher harmonics of current and voltage. These indicators require a detailed substantiation from the standpoint of the processes of energy conversion in electric circuits and can be expanded, in particular, in part with regard to the influence of the transition of pseudo-canonical harmonics of power on canonical harmonics, the order of which coincides.

#### Conclusions and directions of further research.

The methodology and procedure for determining the power based on the measured current and voltage are proposed, as a result of which the power components and indicators of its quality are recorded.

For circuits with polyharmonic currents and voltages on the basis of their orthogonal components, using known power distribution division into constant, canonical, noncanonical components, a calculation algorithm and corresponding cycles for each of the components are developed.

A set of indicators characterizing the process of electric energy transmission taking into account quality is determined: the degree of active and reactive power by the main harmonic; the degree of active and reactive power; the degree of power transfer by canonical components; the degree of power transfer by noncanonical components.

The proposed indicators need to be substantiated from the standpoint of the physical processes of the distribution of electric energy in the elements of electric circuits, and more importantly, the power supply systems.

#### REFERENCES

1. Belov M.P., Novikov A.D., Rasudov L.N. *Avtomatizirovannyi elektroprivod tipovykh proizvodstvennykh mekhanizmov i tekhnologicheskikh kompleksov* [Automated electric drive of standard production mechanisms and technological complexes]. Moscow, Publishing Center «Akademiya», 2007. 576 p. (Rus).
2. Wang J., Duan C. Equivalent Power Spectrum Analysis Method for Feature Extraction. *2010 International Conference on Measuring Technology and Mechatronics Automation*, Changsha City, 2010, pp. 120-123. doi: 10.1109/ICMTMA.2010.222.
3. Tugay D.V. Power electronics devices in the Smart Grid. *Lighting engineering and power engineering*, 2016, no.2, pp. 10-26. (Rus).
4. Emanuel A.E. *Power Definitions and the Physical Mechanism of Power Flow*. John Wiley & Sons Ltd, The Atrium, Southern Gate, Chichester, West Sussex, United Kingdom, 2010. doi: 10.1002/9780470667149.
5. Zhemerov G.G., Tugay D.V. Physical meaning of the «reactive power» concept applied to three-phase energy supply systems with non-linear load. *Electrical engineering & Electromechanics*, 2015, no.6, pp. 36-42. (Rus). doi: 10.20998/2074-272X.2015.6.06.
6. «IEEE Recommended Practice for Monitoring Electric Power Quality» in IEEE Std 1159-2009 (Revision of IEEE Std 1159-1995), 2009, 81 p. doi: 10.1109/IEEESTD.2009.5154067.
7. «IEEE Standard Definitions for the Measurement of Electric Power Quantities Under Sinusoidal, Nonsinusoidal, Balanced, or Unbalanced Conditions» in IEEE Std 1459-2010 (Revision of IEEE Std 1459-2000), 2010, 50 p. doi: 10.1109/IEEESTD.2010.5439063.
8. Jeltsema D. Budeanu's concept of reactive and distortion power revisited. *2015 International School on Nonsinusoidal*

*Currents and Compensation (ISNCC)*, 2015, pp. 1-6. doi: **10.1109/ISNCC.2015.7174697**.

9. Willems J.L. Budeanu's Reactive Power and Related Concepts Revisited. *IEEE Transactions on Instrumentation and Measurement*, 2011, vol.60, no.4, pp. 1182-1186. doi: **10.1109/TIM.2010.2090704**.

10. Zagirnyak M., Korenkova T., Kovalchuk V. Estimation of electromechanical systems power controllability according to instantaneous power components. *2014 IEEE International Conference on Intelligent Energy and Power Systems (IEPS)*, Kyiv, 2014, pp. 266-272. doi: **10.1109/IEPS.2014.6874192**.

11. Rodkin D.I. Particularities of the using the energy method to identifications of induction motors at psevdopoligarmonical signal, *Electromechanical and energy saving systems*, 2009, iss.1/2009(5), pp. 7-20. (Rus).

12. Bialobrzheskyi O., Rod'kin D., Gladyr A. Power components of electric energy for technical and commercial

electricity metering. *Naukovyi Visnyk Natsionalnoho Hirnychoho Universytetu*, 2018, no.2, pp. 70-79. doi: **10.29202/nvngu/2018-2/10**.

Received 29.08.2018

O.V. Bialobrzheskyi<sup>1</sup>, Candidate of Technical Science, Associate Professor,

D.I. Rodkin<sup>1</sup>, Doctor of Technical Science, Professor,

<sup>1</sup>Kremenchuk Mykhailo Ostrohradskyi National University, 20, Pershotravneva Str., Kremenchuk, Poltava region, 39600, Ukraine,

e-mail: seemA1@kdu.edu.ua, saue@kdu.edu.ua

How to cite this article:

Bialobrzheskyi O.V., Rodkin D.I. Alternative indicators of power of electric energy in a single-phase circuit with polyharmonic current and voltage. *Electrical engineering & electromechanics*, 2019, no.1, pp. 35-40. doi: **10.20998/2074-272X.2019.1.06**.

O. Makarchuk, D. Calus, V. Moroz, Z. Gałuszkiewicz, P. Gałuszkiewicz

## TWO-DIMENSIONAL FEM-ANALYSIS OF EDDY CURRENTS LOSS IN LAMINATED MAGNETIC CIRCUITS

*Purpose.* One of the solutions of the problem of taking into account losses in laminated magnetic circuits caused by eddy currents was examined. The proposed solution is intended for use in specialized mathematical models, which are based on a two-dimensional description of the electromagnetic field. The algorithm for calculating the equivalent value of the specific electrical resistance of the material of the magnetic circuit is based on the FEM analysis of the spatial distribution of the current density vector in the laminated magnetic core model, as well as the magnetic and electrical properties which are as close as possible to electrotechnical steel. The principal possibility of using the proposed approach was confirmed by comparing the calculated and experimental time dependences of the regime values, for example, of a single-phase transformer operating at different voltage supply frequencies. References 11, tables 3, figures 6.

*Key words:* eddy current losses, laminated magnetic core, two-dimensional FEM analysis, single-phase transformer.

*Розглядається одне з вирішень проблеми врахування втрат потужності в шихтованих магнітопроводах, що викликані вихровими струмами. Запропоноване рішення призначене для використання у спеціалізованих математичних моделях, які ґрунтуються на двовимірному описі електромагнітного поля. Алгоритм розрахунку еквівалентного значення питомого електричного опору матеріалу магнітопроводу побудовано на підставі FEM-аналізу просторового розподілу вектора густини струму в шихтованому взірці, магнітні та електричні властивості якого максимально наближені до електротехнічної сталі. Принципова можливість використання запропонованого підходу підтверджується порівнянням розрахункових та експериментальних часових залежностей режимних величин, на прикладі однофазного трансформатора, що працює за різних частот напруги живлення. Бібл. 11, табл. 3, рис. 6.*

*Ключові слова:* втрати від вихрових струмів, шихтований магнітопровід, двовимірний FEM-аналіз, однофазний трансформатор.

**Introduction.** Despite the fact that the methods of calculating the field of the vector of current density in electrically conductive areas of arbitrary configuration are well known, mathematical models that are intended for analysis of energy conversion processes in objects with laminated magnetic cores are usually based on assumptions about the absence of losses from them. There are several reasons for this discrepancy between the theoretical level and the practical implementation of the algorithms of mathematical models of electromechanical energy converters, in particular, the need for an extremely high level of discretization of the calculated area. Also, the directions of vectors of current density and vector magnetic potential do not always coincide in the modes close to saturation.

Both of these factors lead to the need to use powerful computing technology, which is far from always guaranteeing the creation of mathematical models with desirable performance indicators – fast performance, acceptable RAM and precision.

**The analysis of recent research.** The relevance of this issue is evidenced by numerous publications.

The approaches described in [1-3] are based on the results of the calculation of the magnetic field obtained by a specific conversion of the characteristics of the magnetization of materials, and are intended for further determination of losses in the steel.

The authors apply the principle of overlay in relation to the non-linear system.

Attempts for analytical calculation of losses in laminated areas of simple form are described in [4, 5]. In 3 the importance of taking into account the distribution of the current density field at least in several outer sheets of the laminated packet is emphasized.

In 5 the mutual influence of hysteresis losses and eddy current losses is investigated. It is pointed out that

this effect is fairly significant, but unfortunately, the question of creating adequate models for its inclusion in dynamic regimes is not considered. Similarly, in 6, solving the problem in terms of the magnetic scalar potential, the authors propose a method for replacing a laminated medium so that an adequate reflection of the magnetic field is achieved in the problems of magneto-statics. The issue of determining the losses in these materials remains open.

This problem is solved, but in a three-dimensional space in 7. For field problems, it is proposed to use homogeneous materials, anisotropic in both electrical and magnetic terms.

The authors of the paper 8 are engaged in the study of the dependences of specific losses in the laminated cores, depending on the field intensity and in the wide frequency domain (20÷2000 Hz). The influence of the interaction of these factors is shown. The paper contains interesting experimental material.

In terms of the classical theory of circles, the problem of taking into account losses in the material, which considers both hysteresis and eddy currents, is solved in 9. Non-linear properties of the material are specified using additional elements of the sub-scheme.

The publication 10 directly addresses the issues outlined above. For relatively geometrically simple forms of magnetic conductors, it is proposed to apply the original numerical calculation algorithm for surface integrals that the finite element method (FEM) operates. Thus, the field of the densities of currents for equivalent homogeneous structures, deprived of air gaps, is determined. The method is quite attractive, but the plane of the calculation area should be located perpendicular to the main magnetic flux. In the most tasks of

electromechanics of practical interest, this plane should be oriented parallel to the direction of flux.

**Formulation of the problem.** It is clear that in the transition from a real three-dimensional to two-dimensional description of the quantities describing the spatial distribution of losses in laminated electric conductive cells, the picture of physical phenomena varies on a qualitative level. Replacing the laminated magnetic core with a homogeneous medium, in a two-dimensional approximation, changes the real direction of the current density vector to one that is perpendicular to the surface of the calculated domain. The phenomena associated with the dumping of the magnetic flux by the «current layer» are to some extent distorted.

The logical question arises whether it is possible to replace the laminated magnetic core with a homogeneous medium with some calculated values of the specific electrical resistance, so that for a two-dimensional magnetic field approximation, the loss from eddy currents in this medium is equal to the losses in the volume of the real magnetic core? How to determine the value of this equivalent specific resistance?

**The purpose of the study.** An analysis of the fundamental possibility of creating mathematical models of EMPE, which, in the two-dimensional approximation of a quasi-steady-state magnetic field, will adequately consider the losses from eddy currents in the laminated elements of the magnetic conductors in both the established and transient operating modes.

**The subject of study.** The processes are related to the spatial distribution of the vector of current density and power losses in laminated magnetic cores of electric machines and apparatuses.

**Methods.** To achieve the goal, two mathematical models have been created. They both have the same purpose: the calculation of the fields of current density and losses in the conductive model, located in the time variable magnetic field.

The sample is a parallelepiped loaded with sheets of electrotechnical steel of rectangular shape. The sheets are separated from each other by air spaces. In the future, we will call it «model of type 3D» or «3D».

In it, the sample is a rectangular plane of a homogeneous material, which corresponds to the size and magnetic properties of a sheet from a three-dimensional model, and its specific electrical resistance is calculated. Let's call it «model of type 2D» or «2D».

All dimensions, fill factor and electrical resistance of samples' material can vary widely. Also, the models parameters are the magnetization characteristic of the material as a table-defined function.

The mathematical formulation of these tasks is based on Maxwell equations and uses the Coulomb gauge. In invariant notation, it is reduced to the expression

$$\nabla^2 \bar{A} = \sigma \nabla U + \sigma \frac{\partial \bar{A}}{\partial t}, \quad (1)$$

where  $\nabla$  is a differential operator of Hamilton;  $\bar{A}$  is a vector magnetic potential;  $U$  is a scalar electric potential;  $\sigma$  is the specific electrical conductivity of the medium.

The field of the vector of current density is determined by the formula

$$\bar{J} = \sigma \left( -\nabla U - \sigma \frac{\partial \bar{A}}{\partial t} \right). \quad (2)$$

The solution (1), (2) provided using the finite element method using the specialized software Ansys. After that, the power losses in the volume of the conductive area are found as

$$P_{cr} = \sigma^{-1} \int_V |\bar{J}|^2 dV = \sigma^{-1} \sum_{e=1}^E \left( \frac{V^{[e]}}{K} \sum_{k=1}^K |J_k|^2 \right), \quad (3)$$

where  $dV$  is the volume of the elementary domain;  $J_k$  is a module of the node value of the current density vector;  $k = \overline{1, K}$  is a current node number of the finite element;  $e = \overline{1, E}$  is a current finite element number, which belongs to conductor volume  $V$ ;  $V^{[e]}$  is the volume of  $e$ -th finite element.

For a two-dimensional case in (3),  $V$  should be replaced with  $S$  and  $V^{[e]}$  with  $S^{[e]}l$ , where  $S$ ,  $S^{[e]}$  is the area of the calculated domain and finite element domain respectively;  $l$  is the length of the calculated area in the direction  $z$  coordinates.

In a three-dimensional model, there exists a number of planes, for which the field of vector potential is symmetric. Using this property, the calculated area occupies only 1/4 of the volume of the complete model, which allows to reduce the dimension of the problem by 4 times. The view of the calculated area and its binding to the coordinate system is shown in Fig. 1, a.

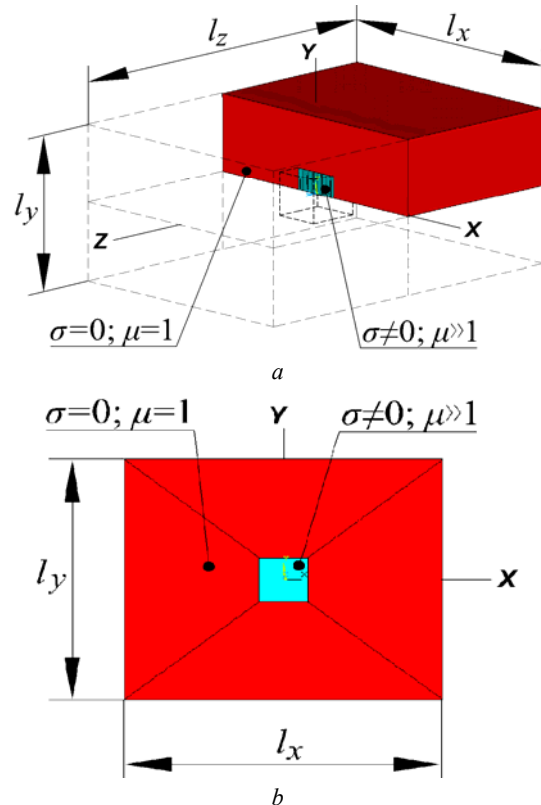


Fig. 1. Calculated areas of models: 3D (a); 2D (b)

The boundary condition and symmetry condition for this problem are summarized in Table 1. The level of discretization of the volume of the calculated area is schematically shown in Fig. 2, a.

Table 1  
The boundary conditions and symmetry conditions

Dimension of the problem – 3D	
Plane equation	Boundary condition
$x = -0.5l_x; x = 0.5l_x$	$A_{xi} = \frac{2z_i}{l_z} A_m \sin(\omega t); A_{yi} = 0; A_{zi} = 0$
$y = 0.5l_y$	$A_{xi} = \frac{2z_i}{l_z} A_m \sin(\omega t); A_{yi} = 0; A_{zi} = 0$
$z = -0.5l_z$	$A_{xi} = -A_m \sin(\omega t); A_{yi} = 0; A_{zi} = 0$
Plane equation	Symmetry condition
$z = 0$	$A_{xi} = 0, A_{yi} = 0$ (condition of parallel flow); $U = 0$
$z = 0$ and $\sigma \neq 0$	$U = 0$
$y = 0$	$A_{yi} = 0$ (condition of perpendicular flow)
Dimension of the problem – 2D	
Equation of line	Boundary condition
$x = -0.5l_x; x = 0.5l_x$	$A_{zi} = \pm A_m \sin(\omega t)$
$y = -0.5l_y; y = 0.5l_y$	$A_{zi} = \frac{-2x_i}{l_x} A_m \sin(\omega t)$

**Marks:**  $A_{xi}, A_{yi}, A_{zi}$  are the values of the projections of the vector of the magnetic potential in the  $i$ -th node;  $A_m$  is the amplitude of vector magnetic potential;  $x_i, z_i$  are coordinates of  $x$  or  $z$  for  $i$ -th node.

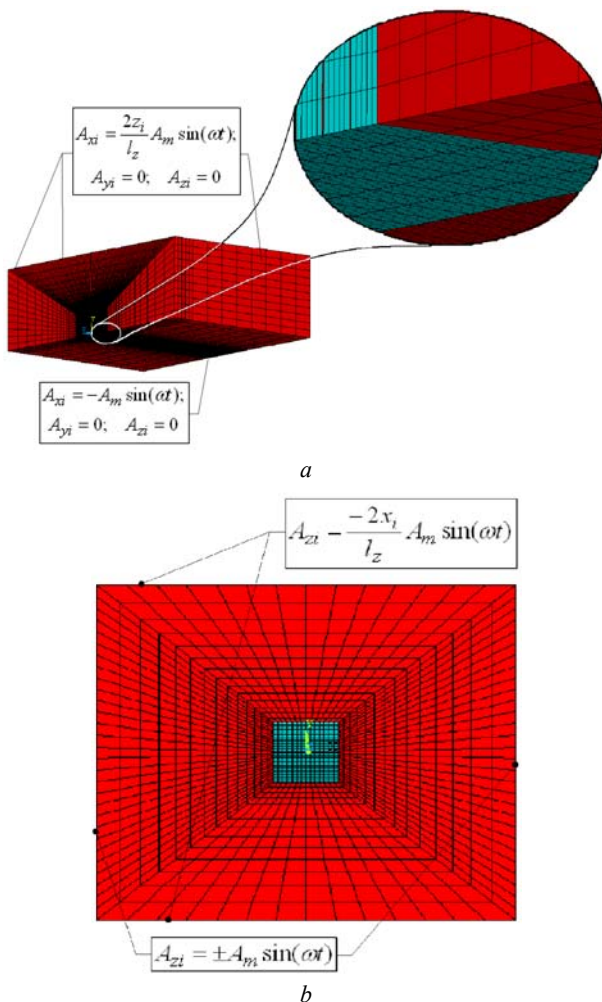


Fig. 2. Finite elemental models: 3D (a); 2D (b)

For a two-dimensional model of binding to the coordinate system is shown in Fig. 1,b, the boundary condition is shown in Table 1, the level of sampling is given in Fig. 2,b.

By processing the results of numerical simulation, which changed the dimensions of the electrotechnical steel 2013 sample (3÷20 mm, the thickness of the sheet is 0.35÷1.0 mm), the material resistivity (0.14÷0.50  $\mu\Omega\cdot m$ ) and the intensity of the magnetic field (0.7÷2.0 T), the empirical dependence has been obtained which allows determining the equivalent resistivity of the magnetic core material, depending on the ratio of dimensions

$$\rho_e = \frac{1}{\sigma_e} = k_f \left(\frac{l}{t}\right)^2 \rho_m, \quad (4)$$

where  $\rho_m$  is the specific electrical resistivity of the material of the magnetic core (according to reference data, for example GOST 21427.2-83),  $l$  is the size of the area of the magnetic core in the direction perpendicular to the direction of passage of the main magnetic flux (for the toothed areas – the average width of the teeth, for a jar of electric machines – the thickness of the yoke in the radial direction);  $t$  is thickness of the sheet of the laminated core;  $k_f$  is a coefficient of the form of the core (correction coefficient). If the ratio of sizes  $l/t$  belongs to the range 3÷20, we suggest that its value be calculated according to the formula

$$k_f = 4.02 - 0.276\left(\frac{l}{t}\right) + 0.0044\left(\frac{l}{t}\right)^2. \quad (5)$$

and if exceeds 20 – choose from Table 2.

It is (4) that we propose to use to account for the losses in laminated magnetic circuits in field 2D models.

Table 2

The value of the form factor				
$l/t$	5	10	20	>40
$k_f$	2.75	1.7	0.27	0.075

**Results and discussion.** For a laminated test component of 10×10×10 mm with a sheet thickness of 0.5 mm, a material fill factor of 0.95, with magnetic properties corresponding to the electrotechnical steel 2013 and a specific electrical resistance of 0.14  $\mu\Omega\cdot m$ , using the 3D type model, dependences on the specific power losses [W/m<sup>3</sup>] from the active value flux density, averaged over the volume of the whole model (Fig. 3) were obtained. Similar dependencies are obtained on the model 2D, but the resistivity of the material, in this case, is increased by 109 times, to a value of 15.26  $\mu\Omega\cdot m$ .

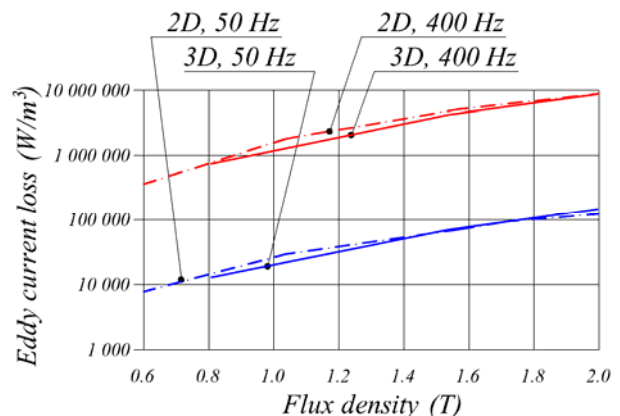


Fig. 3. Dependences of specific losses in the laminated model from flux density

The comparison of these dependencies, for the frequency changes of the 50 and 400 Hz field, shows a good convergence of results. This comparison and analysis of the results of mathematical experiments carried out using the above-mentioned models 3D and 2D allow to declare the following:

- known methods for calculating the losses in the laminated cores, for example, according to the Krug formula, in conditions close to the saturation of the material make a significant error both at the industrial and higher frequencies of field change;
- two-dimensional approximation of the magnetic field allows considering the effect of eddy currents in the laminated cores by converting the value of the resistivity of the material.

Fig. 4 shows the distribution of instantaneous values of the module of the current density vector in a three-dimensional laminated model (Fig. 4,a) and a two-dimensional model (Fig. 4,b), where the resistivity of the material is determined by (4). As can be seen from Fig. 4, the distribution of the vector of current density in 2D and 3D cases varies, but the average for the period of power loss in the two samples is practically the same, as illustrated in Fig. Note, that the negative value in Fig. 4,b corresponds to the direction  $z$ -projections of the current density vectors, directed from the observer.

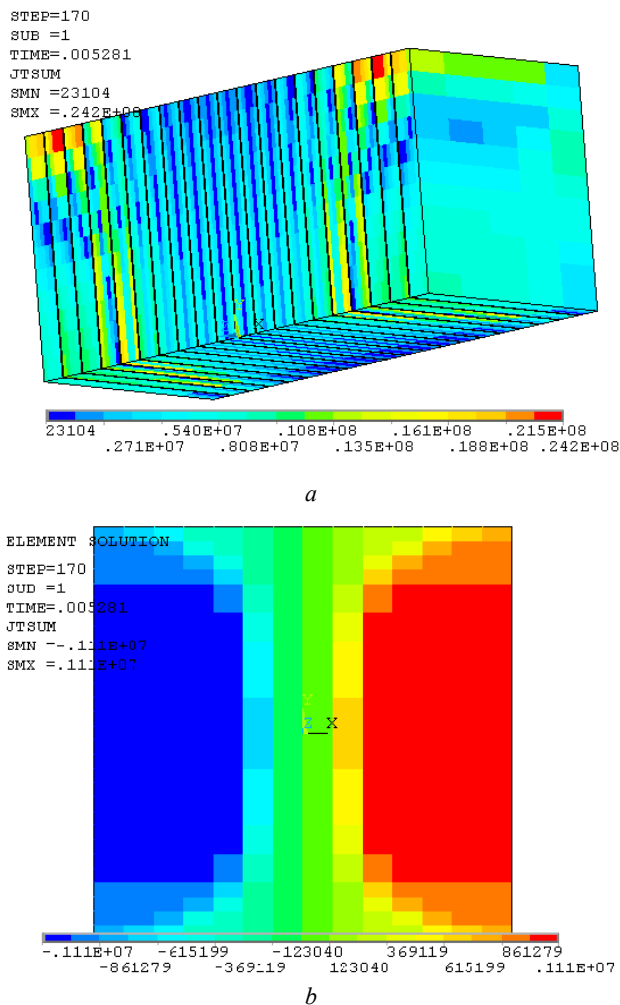


Fig. 4. Current density vector field ( $t = 5.281$  ms,  $f = 400$  Hz): 3D (a); 2D (b)

To verify the correctness of the accepted assumptions, a physical experiment has been performed to record the instantaneous steady-state values of current and voltage in the primary winding of a single-phase transformer in idle mode. The experiment has been conducted for two frequencies of supply voltages. For a frequency of 50 Hz, the current voltage of 150 V is applied to a winding that had 609 turns. The active resistance of this winding is 18.3 Ohms. For a frequency of 495 Hz, the value of the voltage is 40 V, the number of turns of the winding is 170 and its resistance is 0.585 Ohms. Overall dimensions of the core of the investigated transformer are  $94 \times 81 \times 26.7$  mm (Fig. 5), and its magnetic properties correspond to the electrotechnical steel 2411.

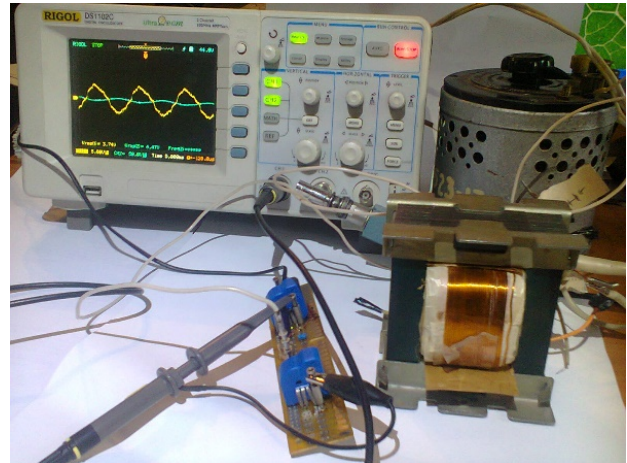
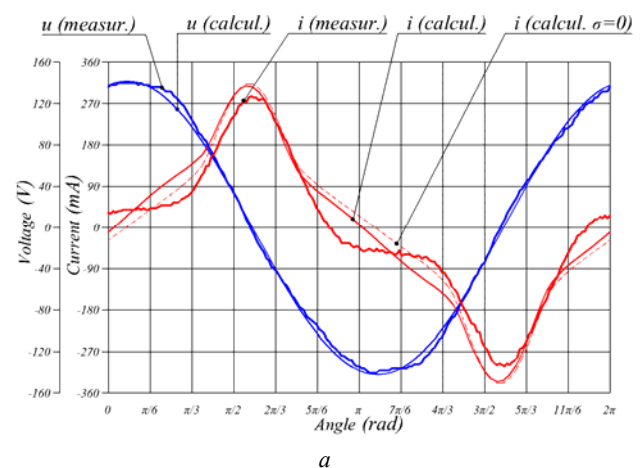


Fig. 5. Investigated transformer and measuring equipment

The results of the experiment are compared with the calculated values of the non-operating current, obtained on a specially created mathematical model of the aforementioned transformer. This model calculates the two-dimensional approximation of the magnetic field constructed based on approach (1) and uses the core material with magnetic properties of 2411 and equivalent to the specific electrical resistance of  $190.8 \mu\Omega \cdot m$ , obtained on the basis of (4) and with subsequent correction of its value.

The results of this comparison are shown in Fig. 6. It also depicts the calculated current dependencies in windings from time to time, provided that there are no eddy currents in the core ( $\sigma = 0$ ).



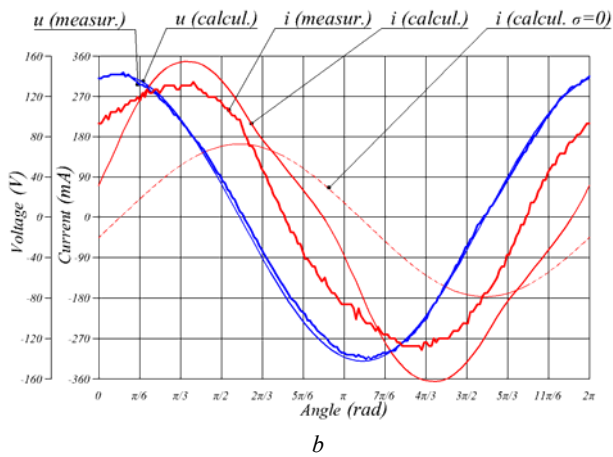


Fig. 6. Dependences of currents and voltages of the transformer on: 50 Hz (a); 495 Hz (b)

The comparison of average values of power consumed in these regimes is summarized in Table 3.

Table 3  
Comparison of average values of power consumption

Frequency, Hz	Calculation (2D), W	Experiment, W	Discrepancy, %
50	1.692	1.893	11.9
495	13.16	17.25	31.1

### Conclusion.

1. Our studies allow for taking into account the effects of eddy currents in a magnetic circuit by bringing its laminated parts to a homogeneous medium with the calculated values of the specific electrical resistance, so that it ensures the loss of power due to the effect of eddy currents in the real laminated axis and in the design two-dimensional modeling plane.

2. Analysis of the saturation influence of the laminated magnetic circuit and its shape on the spatial distribution of his current density vector allow to establish an empirical relationship between the equivalent and actual specific electrical resistance of the material, size and shape of the sample.

3. Using the obtained equivalent resistance value for description the materials properties of objects with laminated magnetic circuits makes it possible to take into account the effects of eddy currents and corresponding power losses, in the two-dimensional approximation of the magnetic field, both in transitions and in steady-state mode.

### REFERENCES

- Gyselinc J., Vandeveld L., Melkebeek J., Dular P., Henrotte F., Legros W. Calculation of eddy currents and associated losses in electrical steel laminations. *IEEE Transactions on Magnetics*, 1999, vol.35, no.3, pp. 1191-1194. doi: 10.1109/20.767162.
- Gyselinc J., Sabariego R.V., Dular P. A nonlinear time-domain homogenization technique for laminated iron cores in three-dimensional finite-element models. *IEEE Transactions on Magnetics*, 2006, vol.42, no.4, pp. 763-766. doi: 10.1109/TMAG.2006.872034.

### How to cite this article:

Makarchuk O., Calus D., Moroz V., Gałuszkiewicz Z., Gałuszkiewicz P. Two-dimensional FEM-analysis of eddy currents loss in laminated magnetic circuits. *Electrical engineering & electromechanics*, 2019, no.1, pp. 41-45. doi: 10.20998/2074-272X.2019.1.07.

- Kaimori H., Kameari A., Fujiwara K. FEM computation of magnetic field and iron loss in laminated iron core using homogenization method. *IEEE Transactions on Magnetics*, 2007, vol.43, no.4, pp. 1405-1408. doi: 10.1109/TMAG.2007.892429.
- Zheng W., Cheng Z. An Inner-Constrained Separation Technique for 3-D Finite-Element Modeling of Grain-Oriented Silicon Steel Laminations. *IEEE Transactions on Magnetics*, 2012, vol.48, no.8, pp. 2277-2283. doi: 10.1109/TMAG.2012.2191591.
- Pippuri J., Belahcen A., Dlala E., Arkkio A. Inclusion of eddy currents in laminations in two-dimensional finite element analysis. *IEEE Transactions on Magnetics*, 2010, vol.6, no.8, pp. 2915-2918. doi: 10.1109/TMAG.2010.2044490.
- Dlala E., Belahcen A., Pippuri J., Arkkio A. Interdependence of hysteresis and eddy-current losses in laminated magnetic cores of electrical machines. *IEEE Transactions on Magnetics*, 2010, vol.46, no.2, pp. 306-309. doi: 10.1109/TMAG.2009.2032930.
- Niyonzima I., Sabariego R.V., Dular P., Geuzaine C. Finite Element Computational Homogenization of Nonlinear Multiscale Materials in Magnetostatics. *IEEE Transactions on Magnetics*, 2012, vol.48, no.2, pp. 587-590. doi: 10.1109/TMAG.2011.2174210.
- Koch S., Gerssem H., Weiland T., Fischer E., Moritz G. Transient 3D Finite Element Simulations of the SIS100 Magnet Considering Anisotropic, Nonlinear Material Models for the Ferromagnetic Yoke. *IEEE Transactions on Applied Superconductivity*, 2008, vol.18, no.2, pp. 1601-1604. doi: 10.1109/TASC.2008.921892.
- Ionel D.M., Popescu M., McGilp M.I., Miller T.J.E., Dellinger S.J., Heideman R.J. Computation of core losses in electrical machines using improved models for laminated steel. *IEEE Transactions on Industry Applications*, 2007, vol.43, no.6, pp. 1554-1564. doi: 10.1109/TIA.2007.908159.
- Wei Chen, Jien Ma, Xiaoyan Huang, Youtong Fang. Predicting Iron Losses in Laminated Steel with Given Non-Sinusoidal Waveforms of Flux Density. *Energies*, 2015, vol.8, no.12, pp. 13726-13740. doi: 10.3390/en81212384.
- Hollaus K., Hannukainen A., Schöberl J. Two-scale homogenization of the nonlinear eddy current problem with FEM. *IEEE Transactions on Magnetics*, 2014, vol.50, no.2, pp. 413-416. doi: 10.1109/TMAG.2013.2282334.

Received 02.07.2018

Makarchuk Oleksandr<sup>1,2</sup>, Doctor of Technical Science, Associate Professor,  
Calus Dariush<sup>1</sup>, PhD, Associate Professor,  
Moroz Vlodimir<sup>1,2</sup>, Doctor of Technical Science, Professor,  
Gałuszkiewicz Zbigniew<sup>1</sup>, Mgr. Inż.,  
Gałuszkiewicz Patryk<sup>1</sup>, Mgr. Inż.  
<sup>1</sup>Czestochowa University of Technology,  
Faculty of Electrical Engineering,  
Institute of Electrical Power Engineering,  
17, Armii Krajowej Avenue, p.o. box 42-200 Czestochowa,  
Poland,  
e-mail: o.makarchuk@el.pcz.czest.pl; dc@el.pcz.czest.pl  
<sup>2</sup>Lviv Polytechnic National University,  
Institute of Power Engineering and Control Systems,  
12, S. Bandera Str., Lviv, 79013, Ukraine,  
phone +380 97 2259180,  
e-mail: oleksandr.v.makarchuk@lpnu.ua

A.G. Guryn, O.V. Golik, V.V. Zolotaryov, S.Yu. Antonets, L.A. Shchebeniuk, O.M. Grechko

## A STATISTICAL MODEL OF MONITORING OF INSULATION BREAKDOWN VOLTAGE STABILITY IN THE PROCESS OF ENAMELED WIRES PRODUCTION

*This paper is devoted to non-destructive technological monitoring of defects of insulation of enameled wires with polyimide polymer. The authors present a statistical method for processing, comparison and analysis of outcomes of measurements of parameters of insulation of enameled wires. A mathematical model of trend for application in active technological monitoring is developed to develop recommendations for parameters of such monitoring. It is theoretically justified and the possibility of a diminution of dependence of an error on the velocity of movement of a wire for want of quantifying defects of enameled insulation using non-destructive tests by high voltage is shown. The dependence of average value of amount of defects for enameled wires with two-sheeted polyimide insulation in a range of nominal diameter 0.56 mm is experimentally determined. The technological monitoring purpose is to reduce quantifying defects of enameled insulation. References 12, figures 4.*

*Key words:* enameled wire, polyimide insulation, insulation defectiveness, technological monitoring, statistical model, voltage tests.

*Представлено результати технологічного контролю напруги пробую ізоляції емаль проводу на основі поліімідного полімеру. Розглянуто застосування статистичного аналізу результатів вимірювання показників контролю за допомогою інтервальної статистичної моделі для використання результатів в активному технологічному контролі. Запропоновано рекомендації щодо практичного використання інтервальної статистичної моделі для визначення гарантованого рівня відносної дисперсії контрольованого параметру. Представлена кількісна оцінка відносної дисперсії  $\delta$  напруги пробую  $U$  впродовж тривалого технологічного циклу. Теоретично показана і вимірюваннями підтверджена можливість надійної кількісної оцінки тенденції зміни дефектності емаль ізоляції для проводу ПЭЭИДХ2 – 200 з двошаровою поліімідною ізоляцією номінальним діаметром 0,56 мм впродовж тривалого технологічного циклу. Визначення кількісної оцінки тенденції зміни дефектності емаль ізоляції дозволяє також виділити і кількісно оцінити випадкову похибку технологічного процесу – сумарну похибку результатів технологічного контролю, яка є кількісною характеристикою випадкової складової стабільності технологічного процесу. Застосування методів інтервальної статистики дозволяє одержувати достовірні (надійна ймовірність дорівнює одиниці) числові оцінки навіть для окремої серії невеликої кількості вимірів, до яких не ставлять вимоги ні статистичної сталості, ні взаємної незалежності. Бібл. 12, рис. 4.*

*Ключові слова:* емаль провід, поліімідна ізоляція, дефектність ізоляції, технологічний контроль, статистична модель, випробування напругою.

*Представлены результаты определения напряжения пробоя изоляции эмаль провода на основе полиимидного полимера. Выполнен статистический анализ результатов с помощью методов интервальной статистики с целью использования интервальной статистической модели в активном технологическом контроле. Представлена количественная оценка относительной дисперсии  $\delta$  напряжения пробоя  $U$  в течение длительного технологического цикла. Теоретически показана и экспериментально подтверждена возможность количественной оценки тенденции изменения дефектности эмальизоляции для провода ПЭЭИДХ2 – 200 с двухслойной полиимидной изоляцией номинальным диаметром 0,56 мм в течение технологического цикла. Это позволяет выделить и количественно оценить случайную ошибку технологического процесса – суммарную ошибку результатов технологического контроля, которая является количественной характеристикой случайной составляющей стабильности технологического процесса. Использование методов интервальной статистики дает возможность получать достоверные (доверительная вероятность единица) интервальные оценки даже для небольшого количества измерений, к которым не предъявляют требования ни статистической устойчивости, ни взаимной независимости. Библ. 12, рис. 4.*

*Ключевые слова:* эмаль провод, полиимидная изоляция, дефектность изоляции, технологический контроль, статистическая модель, испытания напряжением.

**Problem definition.** The introduction of enameled wires based on polyimide synthetic copolymers with a temperature index of 200 °C, which have the highest modern level of electrical, mechanical strength and minimum thickness of insulation [1, 2], encountered contradictions characteristic of innovation in cable products. This is a contradiction between the relatively high cost of products and the need to organize the use of advanced state-of-the-art monitoring technologies. In the case of the mentioned wires it is an online monitoring of insulation defectiveness immediately after the exit from the enamel furnace by non-destructive test on passage with high constant voltage. The system of this monitoring is part of the automatic lines with high speeds (MAG unit up to 1000 m/min) [2].

Active online defectiveness monitoring by non-destructive test on the pass is one of the most promising methods of monitoring in cable production, which is characterized by significant lengths of products with high homogeneity along the length. Particularly relevant online defect monitoring by non-destructive test on the pass is for enameled wires, for which the length to the diameter ratio reaches tens of millions.

The effectiveness of using such monitoring for a particular manufacturer when introducing enameled wires on the base of polyimide synthetic copolymers leads is that the control parameters must be determined by the user from wide available ranges (for example, test voltage of 400 V to 4000 V every 100 V) that should be defined for each type of product. Consequently, the analysis of

results and the development of technical requirements for each type of product is a separate scientific and technical task, the solution of which requires considerable time and cost.

As a result, one of the most promising methods of monitoring in cable production, for which there is a ready-made modern verified equipment, remains unused in real production.

The problem is the need to develop and implement a system of technical and organizational solutions for the use of a modern online monitoring system for insulation defectiveness during tests on the passage under production conditions with the obligatory connection of technical parameters of monitoring to the achieved level of technology and technical requirements, which requires significant additional costs.

The problem, at first glance, is such that for manufacturers during the development period of known in the world, but innovative for these product manufacturers, there is no solution from an economic point of view. The well-known concept of «Six Sigma» («6 $\sigma$ ») [3] can serve as an indirect but real confirmation of this pessimistic conclusion. In it, the criterion for the quality of mass products or services in marketing is the ratio of the size of the range of admissible values of the main parameter to the experimentally determined root of the square of the dispersion ( $\sigma = \sqrt{D}$ ). The concept of «Six Sigma Methodology» is a demonstration of the achievements of leading manufacturers and does not include a methodology for achieving achievements (why not «7 $\sigma$ »?). And the more the technological cycle is automated, the problem of organizing the use of the modern system of technological online defectiveness monitoring is more urgent, since between the tasks of receiving and current technological monitoring there is a significant theoretical and technical difference [4]. The problem of organizing active online technological monitoring is conceptualized for automated mass production.

**Analysis of literature.** The first works devoted to the tasks of technological monitoring, dated from the beginning of 60-ies of the twentieth century, and the result is formulated in [5], where the main thing is that in the very formulation of the question of technological monitoring, it was recorded the possibility of changes in the technological process and the need to identify and quantify these changes [1]. In theory, this means that each measurement result is an element of an unknown statistical array. Therefore, the classical (canonical) measurement model, which requires the fulfillment of three conditions below, is not applicable to the results of the measurements of technological monitoring. These conditions are [3]:

- measurement time is not limited;
- measured value retains the true value unchanged throughout the measurement cycle;
- all factors affecting the result are identified.

None of these conditions can be a condition for the implementation and analysis of the results of technological monitoring.

Since the problem of organizing the use of the modern system of technological online monitoring is

closely linked to the economic component of innovation in mass production, in [11] it is proposed to resolve the contradiction between the high cost of products and the price factor as a liquidity criterion precisely for wires with poliimide insulation by reducing the level of requirements for voltage breakdown agreed with the customer. In essence, it is an announcement of capitulation to the problem of the introduction of this innovative product due to the complexity of the organization of the use of the modern system of technological online defectiveness insulation monitoring, with which enamel aggregates of world manufacturers of the equipment are equipped.

Technological monitoring in automated high-speed continuous cycles of modern cable production requires, apart from practically instantaneous efficiency (online mode) [2, 3, 5], the separation of the deterministic and random components of the array of measurement results.

Therefore, for the purposes of technological monitoring, firstly, a statistical model of measurements is acceptable, in which the measured value is a sequence of reflections of the current state of the object of measurement. Here, the true value of the measured value is uncertain [2], but their interval in this segment of the technological time is completely determined.

The interval approach to the statistical determination of technical parameters is proposed by the concept «6 $\sigma$ » [3], whereby the coefficient of homogeneity  $K\sigma$  is determined by the dispersion of the controlled parameter  $X$ :  $K\sigma = |CL - X_{av}|/(D[X])^{0.5}$  at the lower limit,  $K\sigma = |CS - X_{av}|/(D[X])^{0.5}$  at the upper limit, where  $CL$ ,  $CS$  are, respectively, the lower and upper limits, agreed with the customer of the product. A step forward in the concept of «6 $\sigma$ » is the definition of the coefficient of homogeneity by the value of the permissible margin of the parameter, agreed with the customer of the product. But, firstly, for the determination of  $K\sigma$ , large arrays of data obtained under the same conditions are required, which makes it impossible to make decisions in the conditions of operational technological monitoring.

Secondly, in this concept there are no components that would allow a gradual reduction of the dispersion of the controlled parameter that should be the main objective of operational technological monitoring in a stable production environment.

Modern methods of interval statistics are based on axioms, the first of which is: for all the restricted features  $f$ , belonging to  $J_{00} = \{f: \sup|f(x)| < \infty\}$  there are interval means  $M_{\min}(f)$ ;  $M_{\max}(f)$  which are within the limits of values of  $f$ . According to the axiom of the transform [6] for all the lower bounds of the features:  $M_{\min}(-f) = -M_{\max}(f)$ . That is, the replacement of a sign in the class features  $J_{00}$  leads to the class  $-J_{00}$ , which has lower means  $M_{\min}(f)$ , and there are interval means on the section of these classes [6].

The unambiguous connection between the lower and upper means, by replacing the array sign, convenient for the mathematical description [6], is not applicable to many control technical parameters. In the tasks of technological monitoring in cable technology, a situation is typical where the measured parameter  $x$  only accepts positive values, and the technological boundary can be both bi-sided and one-sided. In particular, when defectiveness control is monitored on MAG in online

mode, the number of defects  $er$  on the length of 100 m is positive ( $er \geq 0$ ) [4] (EFHP system of the MAG-ECOTESTER Company).

In this case, the entire set of functions of the primary features  $f_j(x)$  of the technological monitoring can be represented by the weighting functions  $g_{j,i}(x) \geq f_j(x)$ , each of which belongs to a semi-linear shell with non-negative coefficients  $c_i^+$  and an arbitrary substitution  $c$  for each feature  $j$ :  $g(x) = c + \sum c_i^+ g_i(x)$ . The approximation is more precise if  $Mg$  is known, in particular, if  $Mg = 0$ , i.e. the major function  $g(x)$  is centered [6]. This can be achieved by using the difference between the measured and the mean values as the primary feature  $Y = x - M[x]$ .

The construction of secondary features consists in the choice of the values of arbitrary  $C$  and the non-negative coefficients  $C_i^{(+)}$ , so that the secondary features are minimally (as far as possible) majored primary ones, that is,  $g(Y_j) \geq f_j(Y_j)$ . This scheme can be applied to any parameter. Therefore, we will simply denote  $g(Y), f(Y)$ .

If the primary function  $f(Y) = Y^2$ , when the majored one  $g(Y) = C + C_2^{(+)} Y^2$ . If the upper bound as a limit of possible values of  $Y$  equals to  $E_{\max}$ , when at  $C = 0$ ;  $C_2^{(+)} = 1/E^2$ .  $g(Y)$  at  $Y \geq E_{\max}$  majors  $A(Y)$ , which is a relative number of feature  $Y = [E, E_{\max}]$  values:

$$A\{E \leq Y \leq E_{\max}\} \leq Y^2/E^2. \quad (1)$$

By the axiom of the conservation of order, if  $g(Y)$  majors  $A(Y)$ , then its upper average is no less than the upper average  $A(Y)$ , this inequality can be written for the corresponding mathematical expectations:

$$M_{\max}[A\{E \leq Y \leq E_{\max}\}] \leq M_{\max}[Y^2]/E^2, \quad (2)$$

where in the left part of the inequality the upper average of the relative number of measurements in which the parameter has taken values in the specified interval is nothing more than the upper limit of the interval probability of exceeding the boundary  $E$ . Substituting in (2) the statistical estimate of the upper mean  $M_{\max}[Y^2] = M^*[Y^2]$  gives a statistical estimate of the probability of exceeding the limit:

$$P_{\max}\{E \leq Y \leq E_{\max}\} \leq M^*[Y^2]/E^2. \quad (3)$$

If the initial feature is  $Y = x - M[x]$ , then its mean is zero  $M[Y - M^*[Y]] = 0$ . Then the majoring function can be selected in the form of a parabola with three parameters:

$$g(Y - M^*[Y]) = C + C_2^{(+)} ((Y - M^*[Y]) - C_1)^2, \quad (4)$$

that after transformations gives the formula for maximum probability of output of the parameter  $Y$  from the upper technological limit  $\alpha$ :

$$P_{\max}\{0 \leq Y \leq \alpha\} \leq (1 + \alpha^2/M_{\max}[(\Delta Y)^2])^{-1}. \quad (5)$$

The use of (5) gives a reliable (reliable probability equal to one) numerical estimates of  $P_{\max}$  for a separate series of small amounts of measurements, which are not subject to either statistical stability or mutual independence. Inequality (1) is analogous to the well-known Chebyshev inequality, that is, the interval model (5) extends the possibilities of applied statistical methods without contradiction with the fundamental probability theory [6].

The main point is that the use of interval models allows to create unified statistical models that are

adequate to the essence of the tasks of technological monitoring, since these tasks question the statistical stability of the measured features.

In [12], based on model (5), a method is proposed for controlling the output of a technical parameter from the normative limit. The technical tool of the method is a control card based on the application of (5) for determining the maximum probability of  $P_{\max}$  of that the control technical parameter (for example, breakdown voltage of the enamel or other) will go beyond the prescribed normative limit. The  $P_{\max}$  control card can be applied to any technical specification that is appropriate to control. Primary in this approach is the mean value of the feature, and the concept of probability corresponds to the average value of the relative number of such values (incidence).

**The goal of the work.** In order to increase the efficiency of technological monitoring in automated cable production (online mode is provided with innovative equipment), it is necessary to separate the deterministic and random components of the array of measurement results of the technological parameter:

- the deterministic trend of the parameter is evidence of changes in technology, the causes of which must be determined and a corresponding technological solution must be adopted;
- the random component is the sum of the statistical errors of the technological process, the individual reasons of which in the online mode is practically impossible to determine; this component must be reliably estimated for the entire set of control parameters as a comparable dimensionless value, for example, the relative variance of the parameter.

To obtain a reliable (reliable probability equal to one) numerical estimates of the relative parameter dispersion, to develop, based on the use of interval statistical models, a statistical control card applicable to the entire set of parameters that are controlled during the manufacture of the enameled wire and to verify its applicability in the production conditions.

Using the control card of the relative dispersion of the parameter in the system of ensuring homogeneity of the enterprise products will unify the definition of the random component for the whole set of parameters (in the manufacture of enamel wires based on polyimide synthetic copolymers of more than 10 parameters), which significantly reduces the amount of processing procedures for technological monitoring data and increases its efficiency.

**Main results.** The results of technological monitoring are a discrete array of numerical values  $\chi$ . This array is the vector of primary features  $\chi = \{x_1, \dots, x_r\}$ , each element of which can be matched to the frequency of occurrence of this value, the average values of which for this array form the probability vector:

$$P = \{p_1, \dots, p_r\},$$

where  $r$  is the number of the measured values.

Vector of secondary features:  $f = \{fx_1, \dots, fx_r\}$ .

The mean value of the secondary feature of the array  $\chi$  is the scalar product of the vectors  $f$  and  $P$ :

$$Mf = \sum fx_i \cdot p_i, \text{ where } i = 1, \dots, r. \quad (6)$$

This formula is valid at the exact fulfillment of the condition

$$\sum p_i = 1, \text{ where } i = 1, \dots, r, \quad (7)$$

which in reality is impossible, first of all, due to the limited data. Therefore, for the mean value of the secondary feature of the array  $\chi$ , the only reliable estimate is the interval:

$$M_{\min} f = \inf Mf_i; \quad M_{\max} f = \sup Mf_i. \quad (8)$$

The choice of indicators and the required boundary of the evaluation interval is a purely technical task.

For example, an experimental study during the technological cycle of the breakdown voltage  $U$  of insulation of the wire with a nominal diameter of 0.56 mm indicates that during different technological periods the dynamics of the diametrical thickness  $t$  of the enamel can vary significantly (Fig. 1).

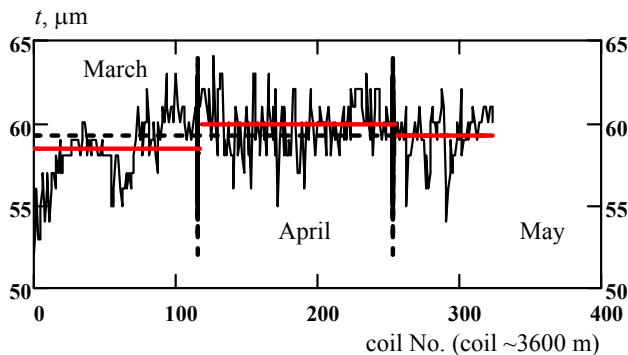


Fig. 1. Dynamics of diametrical thickness  $t$  change of enamel of wire with nominal diameter of 0.56 mm during different technological periods

One of the main indicators of the quality of the enameled wire is the breakdown voltage  $U$ . Therefore, the evaluation of the effect of this change in the diametrical thickness  $t$  of the enamel on the breakdown voltage is crucial in selecting the control parameters and the required boundaries of the evaluation interval and is of great practical importance in the production conditions.

For the breakdown voltage the vector is the primary feature is  $\chi = \{U_1, \dots, U_r\}$ , the vector of the secondary feature:  $f = \{fU_1, \dots, fU_r\}$ , where  $fU_i = [(U_{i+1} - U_i)/U_{i+1}]^2 = \delta_i$  from point of view of the need to center the feature and technically feasible restriction on top.

It also solves the problem of comparing the results of measuring various control parameters.

By (6) the average value of the secondary feature of the array  $\chi$  is the scalar product of the vectors  $f$  and  $P$ :

$$Mf = \sum \delta_i p_i, \text{ where } i = 2, \dots, r, \quad (9)$$

and for the purpose of determining  $p_i$  we used of a normal law of distribution of probabilities, the suitability of which in this case is illustrated by Fig. 2, the suitability test on condition (7) is illustrated by Fig. 3, where the experimental points of the relative dispersion of the breakdown voltage are plotted on the derivative of the normal distribution function.

Condition (7) (Fig. 3) is approximated, which further indicates the necessity of using interval estimates in the monitoring of technical parameters. In the example given, condition (7) is reliably executed for  $r \geq 17$ , so  $r$  can not be arbitrarily selected, but must be chosen as  $r = \inf r (\sum p_i = 1)$ .

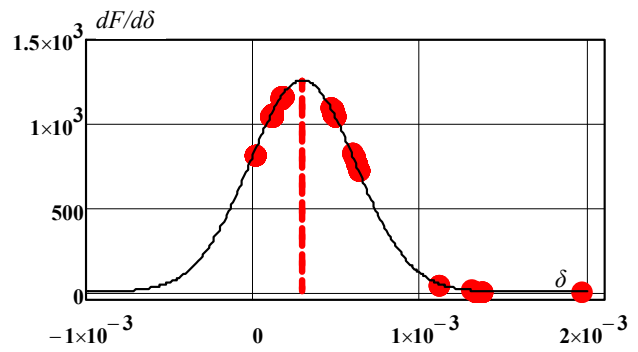


Fig. 2. Comparison of the theoretical density of normal distribution (solid curve) and approximation of the distribution density of experimentally determined values of  $\delta_i$  by normal distribution (324 experimental values)

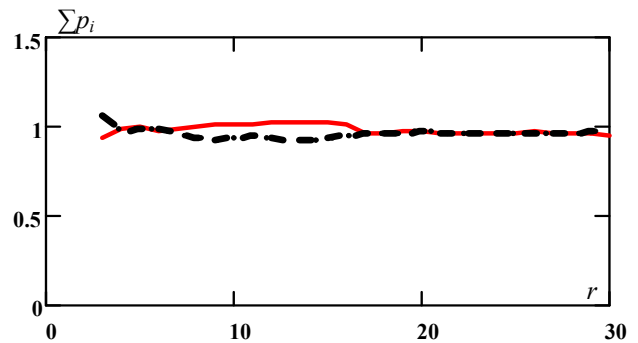


Fig. 3. On checking the fulfillment of condition (7) for the interval estimation of the relative breakdown voltage dispersion of the wire with nominal diameter of 0.56 mm

The average values of the secondary features for the data arrays at  $r = 30$  determined by (8) in different technological periods are shown in Fig. 3, which confirms that condition (7) is reliably executed for  $r \geq 17$ .

Estimates  $Mf_{\max} = \sup(Mf_i)$  for  $r = 30$  indicate that in the various technological periods (see Fig. 1), the upper average relative dispersions of the breakdown voltage are different:

$$\begin{aligned} Mf_{\max 1} (i = 1, \dots, 117) &= \sup(Mf_i(i=1, \dots, 117)) = 4.2 \cdot 10^{-4}; \\ Mf_{\max 2} (i = 118, \dots, 255) &= \sup(Mf_i(i=118, \dots, 255)) = 4.3 \cdot 10^{-4}; \\ Mf_{\max 3} (i = 256, \dots, 324) &= \sup(Mf_i(i=256, \dots, 324)) = 4.0 \cdot 10^{-4}. \end{aligned}$$

The dependence  $Mf(\delta)$  for  $r = 30$  over a long-term technological period is presented in Fig. 4, which shows a stable decrease in the relative dispersion of the breakdown voltage for  $i = 148, \dots, 255$ , that is, during a period with a higher average thickness of the insulation (see Fig. 1). Fig. 4 is an image of the control card of the relative dispersion of the breakdown voltage, on which the rigid boundaries of regulation based on normal distribution [12], corresponding to the range  $M[\delta] \pm \sigma[\delta]$ , which is up to 30 % of the values, are applied. For technical reasons, the relative dispersion should be limited only to the maximum allowable value.

Fig. 4 shows that  $Mf_{\max} < M[\delta] + 3 \sigma[\delta]$ , in normal distribution, that is, corresponds to the known criterion of maximum product homogeneity [12].

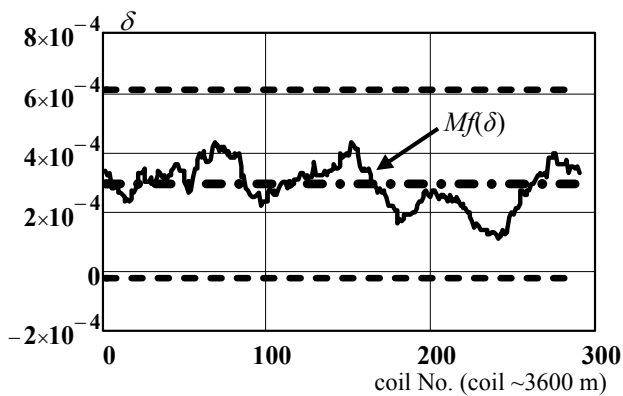


Fig. 4. Statistical control card of the dependence  $Mf(\delta)$  for  $r = 30$ , which shows a stable decrease in the relative dispersion  $\delta$  of the breakdown voltage during April (Fig. 1) when there was a tendency to decrease the thickness of the enamel

### Conclusions.

1. To obtain reliable (reliable probability equal to one) numerical estimates of the relative dispersion of the parameter on the basis of the use of interval statistical models, a unified statistical control card of the relative dispersion of the parameter, applicable to the whole set of parameters that are controlled during the manufacture of the enameled wire, has been developed. The verification of its applicability in the production conditions is carried out on the example of the monitoring of breakdown voltage  $U$  of the wire with two-layer polyimide insulation with nominal diameter of 0.56 mm. Using the unified control card of the relative dispersion of the parameter in the system of ensuring homogeneity of the enterprise products will significantly reduce the amount of processing procedures for technological control data (more than 10 parameters).

2. For three months, the relative dispersion of the breakdown voltage of the wire did not exceed 0.05 % (reliability of the estimation is equal to one), which testifies, firstly, to the stability of the technological process in relation to the electrical strength of the enamel of insulation, and, secondly, on the appropriateness of the use of interval statistical models in the analysis of technological control results.

3. Centering the feature and technically expedient upper restriction for it allow to solve the problem of comparing the results of measurement of various control parameters.

4. Estimates of the maximum average  $Mf_{\max}$  of the relative dispersion  $\delta$  of the breakdown voltage  $U$  of the wire over a long-term period in the conditions of production and comparison of these estimates with the dynamics of diametrical thickness of the enamel wire  $t$  change showed that one of the reasons for the growth of the dispersion of the breakdown voltage is an increase in the thickness of the enamel of insulation.

5. The use of interval statistical models to obtain reliable (reliable probability equal to one) numerical estimates, even for individual series with a small number of measurements

(a multiple sample of 30), which are not subject to either statistical stability or mutual independence, is a promising method of analysis the results of technological monitoring in the conditions of the current production.

### REFERENCES

- Zolotaryov V.M., Antonets Yu.P., Antonets S.Yu., Golik O.V., Shchebeniuk L.A. Online technological monitoring of insulation defects in enameled wires. *Electrical engineering & electromechanics*, 2017, no.4, pp. 55-60. doi: 10.20998/2074-272X.2017.4.09.
- Shchebeniuk L.A., Antonets S.Yu. Statistical method purpose is the reduce of quantifying defects of enameled wire. *Bulletin of NTU «KhPI»*, 2012, no.23, pp. 166-169. (Ukr).
- Golik O.V. Quantifying of defects for enameled wire with two-sheeted polyimide isolation by tests by high voltage. *Ukrainian metrological journal*, 2009, no.1, pp. 15-18. (Rus).
- Golik O.V. Statistical procedures for two-sided limit of a controlled parameter in the process of production of cable and wire products. *Electrical Engineering & Electromechanics*, 2016, no.5, pp. 47-50. (Rus). doi: 10.20998/2074-272X.2016.5.07.
- Gnedenko B.V., Belyaev Yu.O., Solovjev A.D. *Matematicheskie metody v teorii nadezhnosti* [Mathematical methods in theory of reliability]. Moscow, Nauka Publ., 1965. 524 p. (Rus).
- Kuznetsov V.P. *Interval'nye statisticheskie modeli* [Interval statistical models]. Moscow, Radio i sviaz' Publ., 1991. 352 p. (Rus).
- Tutubalin V.N. *Statisticheskaya obrabotka riadov nabliudenii* [Statistical analysis of observation series]. Moscow, Znanie Publ., 1973. 64 p. (Rus).
- Andrianov A.V., Andrianov V.K., Bykov E.V. About the statistics of pin-hole damages of winding wires and inter-turn short-circuits in windings. *Cables and wires*, 2013, no.5, pp. 28-31. (Rus).
- Technical Report IVA Laboratories: Breakdown voltage. – classified: October 2007. – p. 18.
- Mary Walton. *The Deming Management Method*. Foreword by W. Edward Deming. New York: NY 10016 Copyright, 1986. 262 p.
- Zelenetsky Yu.A. About the improvement of technical documentation for enameled wires. *Cables and wires*, 2013, no.5, pp. 19-23. (Rus).
- Karpushenko V.P., Shchebeniuk L.A., Antonets Yu.O., Naumenko O.A. *Sylovi kabeli nyz'koyi ta seredn'oyi napruhy. Konstruyuvannya, tekhnolohiya, yakist'* [Power cables of low and medium voltage. Designing, technology, quality]. Kharkiv, Region-inform Publ., 2000. 376 p. (Ukr).

Received 28.02.2018

A.G. Guryn<sup>1</sup>, Doctor of Technical Science, Professor,  
O.V. Golik<sup>1</sup>, Candidate of Technical Science, Associate  
Professor,

V.V. Zolotaryov<sup>2</sup>, Candidate of Technical Science,  
S.Yu. Antonets<sup>2</sup>, Candidate of Technical Science,  
L.A. Shchebeniuk<sup>1</sup>, Candidate of Technical Science, Professor,  
O.M. Grechko<sup>1</sup>, Candidate of Technical Science, Associate  
Professor,

<sup>1</sup>National Technical University «Kharkiv Polytechnic Institute»,  
2, Kyrpychova Str., Kharkiv, 61002, Ukraine,  
e-mail: agurin@kpi.kharkov.ua, unona928@gmail.com,  
a.m.grechko@gmail.com

<sup>2</sup>Private Joint-stock company Yuzhcable works,  
7, Avtogenyaya Str., Kharkiv, 61099, Ukraine,  
phone +380 57 7545248, e-mail: zavod@yuzhcable.com.ua

### How to cite this article:

Guryn A.G., Golik O.V., Zolotaryov V.V., Antonets S.Yu., Shchebeniuk L.A., Grechko O.M. A statistical model of monitoring of insulation breakdown voltage stability in the process of enameled wires production. *Electrical engineering & electromechanics*, 2019, no.1, pp. 46-50. doi: 10.20998/2074-272X.2019.1.08.

Zh.V. Samokhvalova, V.N. Samokhvalov

## MAGNETIC-PULSE PRESSING OF ELECTRICAL CONNECTIONS FOR STRANDED WIRES

*Purpose. The research of the process peculiarities of magnetic-pulse fitting of electric stranded conductor joints, made of different materials, using couplings. Evaluation of loading optimal parameters, providing high operational reliability of electric connecting units. Methodology. In order to carry out simulation and research of the process of magnetic-pulse fitting of electric stranded conductor joints CRUG24 software package was used, which was developed to estimate impact interaction. Handling the problem was carried out numerically using finite differences. Metallographic study of collected cross-sectional cuts was performed with the use of optical microscope METAM JB-71, equipped with digital-still camera, connected to the computer, which used image analysis system IMEGE Expert Pro3. The electrical tests of wire joints were carried out using the thermal bench from exposure to two factors: heating with rated current and expansion by operating load. Results. It was ascertained that magnetic-pulse pressing of electric joints was followed by partial self-purification and bedding component contacting surfaces of electric joints. Oxides and contaminating impurities were expelled into small localized zones between wires, between a wire and a coupling, which resulted in the contact of juvenile surfaces. Upon mutual deformation and displacement of metal wire surface capacity size and coupling tight mechanical contact was created, which provided minimal transient resistivity. The existence of residual compression stress provides the longstanding high-quality electric contact in joints. While using magnetic-pulse pressing of electric joints, due to high speed of deformation and impact of great inertial forces, deformation containment of connected components takes place in the zone of load action. The wires in contact with each other and with couplings generate faceting, but coupling sidewall hardly has any thinning. Filled density of cross-section is approximately 100 %. This fact provides a high degree of sealing capacity of joints, which to a wide extent prevents the oxidation of contacting surfaces and the rise of transient resistivity of electric joints in the operational process. As a result of processing of the results of thermal and electrical tests it was ascertained that pressed joint factors of defectiveness with all types of wires according to thermal impact and resistivity, are significantly lower than unity. Practical value. Magnetic-pulse pressing of unattended joints in electric stranded monometallic, bimetallic and composite conductors provides high operational reliability of connecting units and it may be used while mounting overhead system of railways, transmission lines and fitting connecting components of electrical transport electric circuits. References 9, figures 6.*

*Key words: magnetic-pulse assembly, connection of stranded wires, numerical simulation, electrical tests.*

*Розглянуто метод створення потужнострумів електричних з'єднань багатодротяних проводів при пресуванні затискачів імпульсним магнітним полем. Представлені результати чисельного моделювання та експериментальних досліджень процесу складання стикових з'єднань монометалевих, біметалевих та комбінованих проводів, в тому числі при отриманні перехідних з'єднань алюміній-мідь. Викладено результати теплових та електричних випробувань з'єднань. Бібл. 9, рис. 6.*

*Ключові слова: магнітно-імпульсна збірка, з'єднання багатодротяних проводів, чисельне моделювання, електричні випробування.*

*Рассмотрен метод создания сильноточных электрических соединений многопроволочных проводов при прессовании зажимов импульсным магнитным полем. Представлены результаты численного моделирования и экспериментальных исследований процесса сборки стыковых соединений монометаллических, биметаллических и комбинированных проводов, в том числе при получении переходных соединений алюминий-медь. Изложены результаты тепловых и электрических испытаний соединений. Библ. 9, рис. 6.*

*Ключевые слова: магнитно-импульсная сборка, соединение многопроволочных проводов, численное моделирование, электрические испытания.*

**Problem definition.** The analysis of the number of violations by types of technical devices and elements of the contact network of electrified railways of JSC Russian Railways for the period from 2003 to 2010 presented in the monograph [1] shows that in terms of the frequency of failures, wires and terminals occupy the first and the third place among all types of contact network devices (about 40 % of all failures not caused by external causes). Heating in the terminals of electrical connectors, fatigue in the attachment points, weakening due to short-circuit are the main causes of failures. A large proportion of such damage is due to unacceptable temperature rises and the burnout of stranded wires in the spot-bolted connecting joints. To solve this problem, pressable terminals are

used. The compressed terminals of the electrical connection joints are durable, lightweight, economical, require no maintenance, have non-degrading quality of the current-carrying connections, are resistant to corrosion and the effects of short-circuit currents.

**Analysis of recent investigations and publications.** Mechanical pressing of terminals is carried out using portable hydraulic presses using local indentation methods, as well as continuous or combined crimping using round or hexagonal dies. However, this results in an irregular crimping of the strands of the wire over its cross section. To improve the operational reliability of stranded copper wire connections with lugs

in the electrical and aviation industry, the method of magnetic-pulse pressing of joints is used [2-4]. The connection is made during the high-speed crimping of the handpiece to the stranded wire. When a current pulse is passed through the inductor, transient magnetic field is excited, which induces eddy currents in the skin layer of the handpiece material. When the eddy current interacts with the inductor's magnetic field, forces arise that cause plastic deformation of the handpiece shell. This method can be applied in electric transport and in power supply systems of railways for butt joining of copper, aluminum, bimetallic and combined wires or press-on of handpieces.

Unlike mechanical pressing of terminals, when pulsed magnetic field is applied, the cylindrical part of the connecting sleeve or handpiece is deformed uniformly around the circumference, ensuring its electrical contact over all the conductors of the external strand of the wire. As a result of the high speed of the impact of the connected elements, as well as surface heating of the connectors with eddy currents and their subsequent cooling, additional compressive stresses arise that improve the quality of the connection of the sleeve and the stranded wire.

**The goal of the work** is investigation of the peculiarities of the process of formation of butt joints of stranded wires of various materials, including heterogeneous, determination of optimal parameters of magnetic-pulse loading, ensuring high operational reliability of electrical connecting joints.

**Experimental investigations of stranded wire connections.** During magnetic-pulse pressing, the parameters of the stranded wire connections are determined both by the initial dimensions of the connecting sleeve and the space-time characteristics of the magnetic field pressure pulse during the formation of the joint. The working tool that determines the plot of pressure in a magnetic-pulse assembly is an inductor. The experiments used multi-turn inductors with interchangeable magnetic field concentrators [5]. The working hole in the magnetic field concentrators was made for the sleeves with diameter of 16 to 28 mm, which allowed to cover the entire size of the selected stranded wires. The width of the working area of the concentrator varied from 6 to 15 mm. This made it possible to change the zone of action of the pulsed pressure of the magnetic field, as well as to additionally vary the value of the specific energy of the charge of the magnetic-pulse installation when receiving the connections of the wires. Variable parameters were the length and wall thickness of the connecting sleeve. The diameter of the sleeve and the minimum thickness of its wall in this case were set from the following conditions: the cross-sectional area of the sleeve is not less than the cross-sectional area of the wire; sleeve strength is not lower than the breaking strength of the wire.

An experimental study of the process of assembling the connection of wires was carried out on the magnetic-pulse installation МНУ-30 (manufactured by the Kharkiv Polytechnic Institute). The own inductance of the

installation is  $L = 0.004 \mu\text{H}$ , the capacitance of capacitor batteries is  $C = 168 \mu\text{F}$ , the maximum charge voltage of capacitors is  $U = 19 \text{ kV}$ , the maximum charge energy is  $W = 30.3 \text{ kJ}$ .

Metallographic studies of the cross-sections of the stranded wire connections obtained on the Gripo IV grinding and polishing machine were carried out using METAM JIB-71 optical microscope equipped with a digital camera connected to a computer using the IMEGE Expert Pro3 image analysis system. Studies of the macrosections of the joints obtained have shown that during magnetic-pulse pressing, due to high-speed collisions, the inner surface of the connecting sleeve (handpiece) is strongly deformed. This leads to an increase in the contact area of the sleeve and the wire in the joint compared with compression by hydraulic presses and, consequently, a decrease in the transient electrical resistance.

The cross-sections of the wire connections, obtained at the optimum value of the specific energy, showed that the wire has a contact across the entire wire surface (Fig. 1).

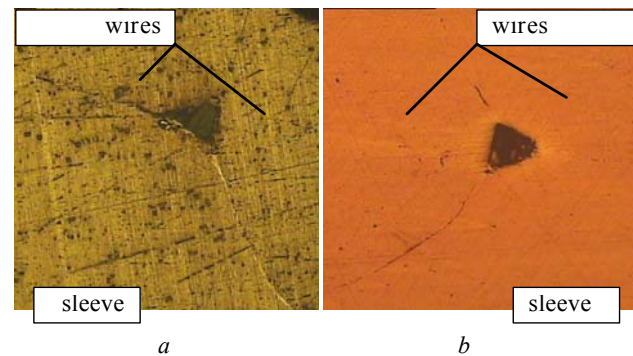


Fig. 1. View of contact of wires and the connecting sleeve at magnetic-pulse pressing of the joint:

- a) aluminum wire and aluminum sleeve;
- b) copper wire and copper sleeve

Oxides and dirt are forced into small local areas between the wires, wires and the sleeve, contact of juvenile surfaces occurs.

The state of the boundaries between the individual wires, as well as between the wires and the sleeve in the joint depends mainly on the specific energy of the charge of the magnetic-pulse installation and the initial gap between the outer layer of wires and the inner surface of the connecting sleeve, determining the speed of the collision of the sleeve with the wire.

Upon receipt of the transitional joints of aluminum and copper stranded wires, the principal differences in the process of forming the joint of copper wire M-120 with an A0 aluminum sleeve and aluminum A-185 wire with an M1 copper sleeve were revealed. In the first case, the contact area of the sleeve with the external strand of the wire is much larger than in the joint of the aluminum wire A-185 with the copper sleeve. This is due to the «leakage» of the material of the soft aluminum sleeve between the copper wires, due to the effect of high-speed

collision. In the second case, a more durable copper sleeve strongly crumples aluminum wires, but in both cases a high degree of tightness of the joint is ensured (Fig. 2).

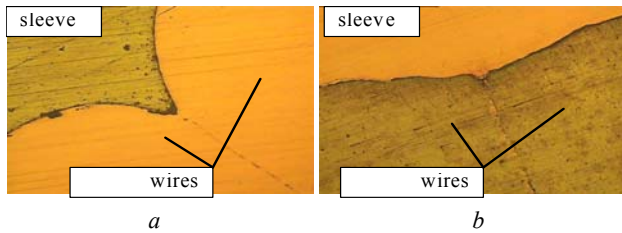


Fig. 2. Copper-aluminum transitional joint:  
a) copper wire and aluminum sleeve,  
b) aluminum wire and copper sleeve

**Numerical simulation of the process of magnetic-pulse pressing of joints.** To study the basic laws of the process of obtaining electrical joints by pulsed magnetic field, representatives of the main types of stranded wires of the power supply systems of railways and power lines were taken. This is supporting copper cable M-120 and aluminum auxiliary wire A-185; steel-copper bimetallic wire ПБСМ-95 (supporting cable of chain hangers, electric traction connectors, jumpers of choke transformers, etc.) and steel-aluminum combined wire AC-50/8 (suspension on overhead power lines). Materials of connecting sleeves are copper M1 and aluminum A0.

For the numerical simulation and study of the magnetic-pulse assembly of stranded wires joints using connecting sleeves, the software package CRUG24 was used developed for calculating shock interactions [6]. According to the method similar to [3, 4], the problem of deforming a system of cylindrical bodies enclosed in a circular shell (connecting sleeve or handpiece) was considered in 2D formulation. A pulsed magnetic field inductor is located around the shell. The connection is carried out in the process of high-speed crimping of the tubular connector or the handpiece to the stranded wire with the pressure of the pulsed magnetic field. The solution of this problem was carried out numerically using the finite difference method. The visual display of the process made it possible to control the calculation, to evaluate the parameters and features of the interaction of the sleeve and the wires.

For each element of the developed computational model, its individual physic-mechanical properties were specified. For example, in the numerical simulation of the magnetic-pulse assembly of the ПБСМ-95 steel-copper wires joint, inside each wire, the grid areas of the steel core and its copper shell were separated. In the numerical simulation of the assembly process of the steel-aluminum wires AC-50/8 with pressure of the pulsed magnetic field, various characteristics of the material of the central steel wire and its outer aluminum wires were specified.

In numerical modelling, the features of the formation of joints were studied:

a) «copper-copper» – connection of the M-120 or ПБСМ-95 wire with the copper connecting sleeve (or handpiece);

b) «aluminum-aluminum» – connection of the wire A-185 or AC-50/8 with the aluminum connecting sleeve;

c) «copper-aluminum» transitional joints – M-120 wire with aluminum sleeve, A-185 wire with copper sleeve.

In the numerical simulation of the assembly processes, as in the experimental studies, the energy of the charge of the magnetic-pulse installation and the wall thickness of the connecting sleeve were varied. The process of assembling the connection of wires was modeled using the МНУ-30 magnetic-pulse installation used in the calculations with parameters, which was used during the full-scale experiments.

When conducting numerical simulation of the processes of a magnetic-pulse assembly, the coefficient of filling of the section  $K_z$  in the terminal was calculated, which indirectly determines the mechanical strength of the joint and the transient electrical resistance [3]:

$$K_z = 4F / \pi d^2,$$

where  $F$  is the total cross-sectional area of the sleeve and wire,  $d$  is the outer diameter of the sleeve after assembly of the joint.

The criterion for the efficiency of the assembly process was chosen to be the minimum specific energy of the charge of the magnetic-pulse installation, necessary to achieve complete compaction of the wires in the joint ( $K_z \approx 1$ ). The specific energy  $W_u$  on the assembly of the wire joint was determined as the ratio of the charge energy of the magnetic-pulse installation  $W$  to the volume of the deformed material in the joint:

$$W_u = W / (F / l), \text{ J/mm}^3,$$

where  $l$  is the width of the working zone of the inductor (magnetic field concentrator), which determines the length of the crimping zone in the resulting joint.

As shown by the results of numerical simulation of the assembly of joints by pressure of the pulsed magnetic field and the results of metallographic studies of the joints obtained, the interaction of the sleeve with the monometallic wires of the M-120 and A-185 wires at optimum specific energy leads to a uniform deformation of the majority of the wires, their complete compaction and cutting (Fig. 3).

In the steel-aluminum combined wire AC-50/8, its central steel wire is deformed slightly, the compaction of the joint is ensured by the deformation of aluminum wires.

In joints of steel-copper wires ПБСМ-95 using copper sleeves, there is a slight deformation of the steel core of the wires in the bimetallic wires, and their copper shell is deformed to a much greater degree, which coincides with the results of numerical simulation. Due to this, there is a fairly strong leakage of the material of the copper sleeve in the cavity between the wires, which further increases the contact area of the sleeve and wire in the joint (Fig. 4).

In case of insufficient specific energy, the wires are not fully compacted in the joint ( $K_z < 1$ ), which does not provide the desired quality of the joint. With a

rational mode of magnetic-pulse loading, the deformation of the wires and the final compression of the entire wire occur at the stage of maximum acceleration of the connecting sleeve (handpiece), which ensures the closing of all the wires and filling the entire cross-section of the joint ( $K_z \approx 1$ ).

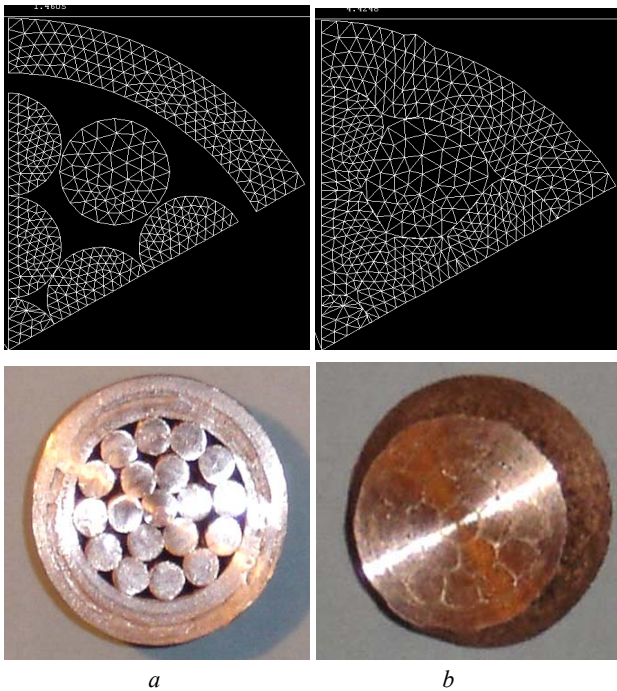


Fig. 3. View of joint of the wire M-120 and the copper sleeve in the numerical simulation and full-scale experiment: a) before crimping, b) after assembling

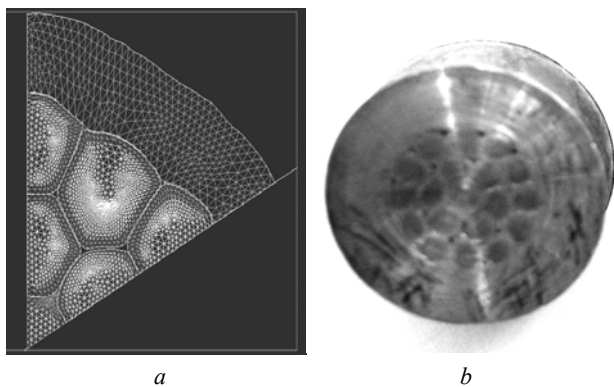


Fig. 4. View in cross section of the wire ПБСМ-95 and copper connecting sleeve in magnetic-pulse assembly: a) numerical simulation, b) experiment

This is achieved if the maximum of the first half-wave of the pressure of the pulsed magnetic field coincides with the maximum of the speed of deformation of the connecting sleeve. As shown by the simulation of the process, the speed of deformation of the connecting sleeve, in the process of assembling (crimping) the joint, reaches 150 ... 200 m/s, and the process time is 18 ... 25  $\mu$ s, depending on the material and wall thickness of the connecting element (sleeve, handpiece). With an excess of the specific energy of the charge of the magnetic-pulse installation, the maximum deformation speed of the connecting sleeve does not

coincide with the maximum of the first half-wave of pressure of the pulsed magnetic field. There is an overrun of the energy of the charge of the magnetic-pulse installation and an irrational force effect on the resulting joint which does not increase its quality.

As a result of processing the calculation results, we obtained the dependencies of the minimum calculated specific energy of the joint of wires on the thickness of the connecting sleeve, at which  $K_z \approx 1$  is reached, using sleeves with different wall thicknesses having a tensile strength not lower than the wire strength (Fig. 5).

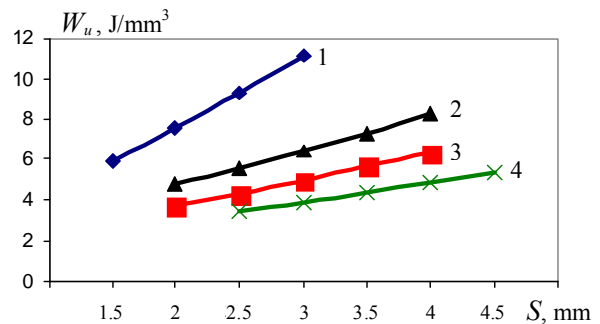


Fig. 5. Dependence of the minimum specific energy of the assembly of the joint of wires on the thickness of the connecting sleeve.

Wire: 1) AC 50/8, 2) ПБСМ-95, 3) M-120, 4) A-185

#### Electrical testing of the obtained wire joints.

Electrical tests were conducted indoors using a thermal bench. Quality control of the joints of stranded wires produced by the pressure of the pulsed magnetic field was carried out in accordance with GOST 12393-77 [7]. The properties of the stranded wire joints were evaluated according to standard indicators, as well as under the influence of two factors: heating with rated current and tension by the working load. For complex tests, a special device for mechanical loading of joints was manufactured. The device is equipped with interchangeable collet clamps for gripping wires of different diameters installed in dielectric (textolite) plates (Fig. 6).

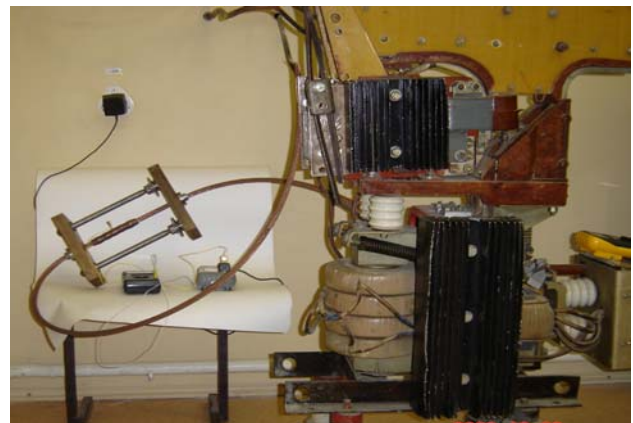


Fig. 6. Thermal bench and device for mechanical loading of butt joints of wires

Textolite plates are interconnected by two racks, one end of which is rigidly connected to the first plate and the other end enters the hole of the second plate. The distance

between the plates was changed due to the rotation of the nuts resting through a pair of cup springs on the second plate. The tensile force of the wire joint was controlled by the compression of calibrated cup springs. The cup springs made it possible to keep the load force of the joint almost unchanged under axial thermal deformation of the wires and the connecting sleeve during thermal testing.

The quality of the electrical connection was determined by the defectiveness coefficients of the electrical contact by electrical resistance –  $K_R$  and by overheating by nominal rated current –  $K_\theta$ :

$$K_R = \Delta U_C / \Delta U_P, \quad K_\theta = \Delta \theta_C / \Delta \theta_P,$$

where  $\Delta U_C$  and  $\Delta U_P$  are, respectively, the voltage drop at the joint and on the whole wire part of the same length, mV;  $\Delta \theta_C$  and  $\Delta \theta_P$  are, respectively, the temperature rise of the terminal and the connected wire outside the terminal above the ambient temperature when the same current flows through them, °C.

The current value for determining the defectiveness coefficients was set taking into account the permissible continuous current value for each brand of connecting wires, established by the regulatory and technical documentation [8]: 400, 500 and 600 A, and was maintained constant with an error of no more than 3 % during the test (controlled by a multimeter Masteh MY-62). The overheating temperature of the joint (middle of the connecting sleeve) and the wire (at a distance of 1 m from the sleeve) was measured using thermocouples and an APRA 109 digital multimeter (class 0.1). The voltage drop on the wire and in the joint was measured at each selected current value by a digital multimeter Masteh M890G (class 0.1). The defectiveness coefficient for resistance was determined as the arithmetic average of three values obtained at three current values.

Defectiveness coefficients of the joints were determined for the joints of the M-120 and ПБСМ-95 wires using copper sleeves; the A-185 wires joints using aluminum sleeves. For transitional joints of the wire M-120 and the wire A-185 aluminum and copper sleeves were used, respectively.

It has been established that the overheating temperature of the joints obtained is substantially lower than the overheating temperature of the wires themselves outside the joint. The resulting defectiveness coefficients of electrical contact changed from  $K_R = 0.56$  and  $K_\theta = 0.66$  for joints of the ПБСМ-95 wires to  $K_R = 0.74$  and  $K_\theta = 0.88$  for the transitional butt joint of the wires M120 and A185, which is lower the values established for the joints of the stranded wires of the contact network of electrified railways, made by the method of crimping [7].

To improve the quality of the connection of stranded wires produced by the pressure of pulsed magnetic field, a device [9] has been developed, which, in the process of magnetic-pulse pressing of terminals, pre-compresses the wires and creates tensile stresses in them. This allows, after assembling the joint, to create additional residual compressive stresses in the resulting joint, providing a high breaking force of the sleeve and minimal transient electrical resistance, as well as high density in the joint, minimizing oxidation of the contact surfaces.

**Conclusions.** As a result of investigations the following was found:

1. Magnetic-pulse pressing is accompanied by partial self-cleaning and grinding in the contacting surfaces of the elements of the electrical connection in the process of forming the joint. During high-speed collision and joint deformation of the bodies being joined, large shear stresses and contact pressures occur. Oxides and dirt are forced out into small local zones between the wires, wires and the sleeve, which leads to the contact of juvenile surfaces. With the mutual deformation and displacement of the surface volumes of the metals of the wires and the connecting element, a close physical contact is created, which ensures the minimum transient electrical resistance. This ensures high quality electrical contact in the joint.

2. At the magnetic-pulse assembly of electrical connections, due to the high speed of deformations and the action of large inertial forces, the deformations are localized in the load action zone. The wires at the places of contact with each other and with the sleeve get cut, and the wall of the sleeve has practically no thinning. Therefore, in contrast to the assembly of joints by hydraulic presses, with magnetic-pulse crimping there is practically no weakening of the wire cross section. In the case of magnetic-pulse assembly, the wires in the joint are compacted, the filling density of the cross section approaches 100 %, which ensures a high degree of tightness of the joint. This largely prevents oxidation of the contacting surfaces and an increase in the transient resistance of the electrical connection during operation.

3. As a result of processing the results of thermal and electrical tests, it was established that the defectiveness coefficients of the press joint of all types of wires for heating and electrical resistance are significantly lower than one, which ensures high operational reliability of the electrical connecting joints of the stranded wires of the contact network, electric transport and transmission lines obtained by magnetic-pulse pressing.

#### REFERENCES

1. Galkin A.S., Mitrofanov A.N., Mitrofanov S.A. *Matematicheskoe modelirovanie i informatsionnye tekhnologii v zadachakh diagnostiki kontaktnoi seti elektrifitsirovannykh zheleznnykh dorog* [Mathematical modeling and information technologies in diagnostics of the contact network of electrified railways]. Ekaterinburg, Ural State University of Railway Transport Publ., 2012. 226 p. (Rus).
2. Dmitriev V.V., Lifshits Iu.Ia., Rozin V.I. Magnetic-pulse processing of electrical engineering parts. *Forging and Stamping Production*, 1984, no.7, pp. 8-9. (Rus).
3. Kurlaev N.V., Gulidov A.I., Iudaev V.B. Numerical simulation of the process of assembly of the tips with electric clamps with the pressure of a pulsed magnetic field. *Forging and Stamping Production. Material Working by Pressure*, 2001, no.8, pp. 38-42. (Rus).
4. Kurlayev N., Gulidov A., Ryngach N., Mishukov A. Computer simulation of aircraft wires tips compression by pulse magnetic field. *5th Korea-Russia International Symposium on Science and Technology. Proceedings. KORUS 2001*, vol., pp. 36-39 (Cat. No.01EX478). doi: 10.1109/korus.2001.975047.
5. Belyj I.V., Fertik S.M., Khimenko L.T. *Spravochnik po magnitno-impulsnoy obrabotke metallov* [Directory of magnetic-pulse treatment of metals]. Kharkiv, Vishcha shkola Publ., 1977, 189 p. (Rus).

6. Fomin V.M., Gulidov A.I., Sapozhnikov G.A. *Vysokoskorostnoe vzaimodeistvie tel* [High-speed interaction of bodies]. Novosibirsk, Siberian Branch Russian Academy of Sciences Publ., 1999. 600 p. (Rus).

7. *GOST 12393-77. Armatura kontaktnoi seti dlia elektrifitsirovannykh zheleznykh dorog. Obshchie tekhnicheskie usloviia* [State Standard 12393-77. Armature of the contact network for electrified railways. General specifications]. Moscow, Standartinform Publ., 2004. 26 p. (Rus).

8. *Pravila ustroistva i tekhnicheskoi ekspluatatsii kontaktnoi seti elektrifitsirovannykh zheleznykh dorog (TsE-868)* [Rules of the device and technical operation of the contact network of electrified railways]. Department of Electrification and Electricity of the Ministry of Railways of the Russian Federation. Moscow, Transizdat Publ., 2002. 184 p. (Rus).

9. Samokhvalov V.N., Grigor'ev V.L., Samokhvalova Zh.V. *Ustroistvo dlia soedineniia mnogoprovolochnykh provodov* [Device for connecting stranded wires]. Patent Russian Federation, no. 53819, 2006. (Rus).

*Zh.V. Samokhvalova*<sup>1</sup>, *Candidate of Technical Science, Associate Professor;*

*V.N. Samokhvalov*<sup>2</sup>, *Doctor of Technical Science, Professor;*

<sup>1</sup> Samara State Transport University,  
2V, Svobody Str., Samara, 443066, Russia,  
phone +7 927 6568357,

e-mail: zhanna\_sam@mail.ru

<sup>2</sup> Samara National Research University,  
34, Moskovskoye shosse, Samara, 443086, Russia,  
phone +7 927 6544210,

e-mail: vn\_samokhvalov@mail.ru

*Received 20.09.2018*

*How to cite this article:*

Samokhvalova Zh.V., Samokhvalov V.N. Magnetic-pulse pressing of electrical connections for stranded wires. *Electrical engineering & electromechanics*, 2019, no.1, pp. 51-56. doi: 10.20998/2074-272X.2019.1.09.

O.V. Shutenko, A.A. Zagaynova, G.N. Serdyukova

## ANALYSIS OF OPERATING CONDITIONS AND MODES INFLUENCE ON TECHNICAL STATE OF MAIN INSULATION OF HIGH-VOLTAGE BUSHINGS OF DIFFERENT DESIGN

*The results of the analysis of the influence of operating conditions and design of high-voltage bushings on the values of dielectric loss tangent of high-voltage bushing basic insulation. For analysis a model of two-factor cross-sectional dispersion analysis, which allows to simultaneously evaluate the influence of two factors and evaluate the effect of their interaction is used. In the model used, it is assumed that the effects of changes in the levels of factors are non-additive, that is, the difference in mathematical expectations between any two levels of one factor is not the same for any levels of the other. Testing the hypothesis of the significance of the influence of factors and their interactions is performed using the Fisher criterion. This method was implemented in the form of the author's program «two-factor dispersion analysis». The results of periodic monitoring of the state of high-voltage bushings of 110, 220 and 330 kV with different types of insulation were used as initial data. Using the model of two-factor cross-sectional dispersion analysis, it was found that the aging intensity of the main insulation of bushings is influenced by both the operating conditions and the design features of the bushings. Maximum permissible values of diagnostic indicators of high-voltage bushings should be normalized taking into account such factors as nominal voltage, type of protection and type of insulation, load of bushings and the composition of consumers. Since, based on the analysis performed, it was established that these factors have a significant impact on the values of diagnostic indicators of insulation of bushings. According to the results of the analysis performed, it was established that such factors as the type of bushing and phase do not have a significant effect on the change in the values of diagnostic indicators of high-voltage bushings, and, therefore, they can be ignored when determining the maximum permissible values of the indicators. References 24, tables 7, figures 14.*

*Key words:* high-voltage bushing, insulation, two-factor cross-sectional dispersion analysis, insulation indicators, dielectric loss tangent.

*Метою статті є аналіз впливу умов, режимів експлуатації і конструкції високовольтних вводів на значення тангенса кута діелектричних втрат основної ізоляції конденсаторного типу високовольтних вводів. Для аналізу використовуються модель двохфакторного перехресного дисперсійного аналізу, яка дозволяє одночасно виконати оцінку впливу двох чинників і оцінити ефект їх взаємодії. У використовуваній моделі передбачається неадитивність ефектів зміни рівнів факторів, тобто різниця математичних очікувань між будь-якими двома рівнями одного фактора не однакова при будь-яких рівнях іншого. Перевірка гіпотези про значущість впливу факторів і їх взаємодії виконується за допомогою критерію Фішера. Результати. Даний метод був реалізований у вигляді авторської програми «двохфакторний дисперсійний аналіз». В якості вихідних даних були використані результати періодичного контролю стану високовольтних вводів напругою 110, 220 і 330 кВ з ізоляцією різного типу. Використовуючи модель двохфакторного перехресного дисперсійного аналізу, встановлено, що на інтенсивність старіння основної ізоляції вводів впливають як умови експлуатації, так і особливості конструктивного виконання вводів. Нові положення, в порівнянні з відомими рішеннями, полягають у тому, що гранично допустимі значення діагностичних ознак високовольтних вводів слід нормувати з урахуванням таких факторів, як номінальна напруга, тип захисту і тип ізоляції, завантаження вводів і склад споживачів. Отримані результати можуть бути алгоритмічно реалізовані у вигляді окремого модуля інформаційно-аналітичної системи (ІАС) для діагностики стану високовольтного маслонаповненого обладнання. Бібл. 24, табл. 7, рис. 14.*

*Ключові слова:* високовольтний ввід, ізоляція, двохфакторний перехресний дисперсійний аналіз, показники ізоляції, тангенс кута діелектричних втрат.

*Целью статьи является анализ влияния условий, режимов эксплуатации и конструкции высоковольтных вводов на значения тангенса угла диэлектрических потерь основной изоляции конденсаторного типа высоковольтных вводов. Для анализа используется модель двухфакторного перекрестного дисперсионного анализа, которая позволяет одновременно выполнить оценку влияния двух факторов и оценить эффект их взаимодействия. В используемой модели предполагается неаддитивность эффектов изменения уровней факторов, т.е. разность математических ожиданий между любыми двумя уровнями одного фактора не одинакова при любых уровнях другого. Проверка гипотезы о значимости влияния факторов и их взаимодействий выполняется с помощью критерия Фишера. Данный метод был реализован в виде авторской программы «двухфакторный дисперсионный анализ». В качестве исходных данных были использованы результаты периодического контроля состояния высоковольтных вводов напряжением 110, 220 и 330 кВ с изоляцией разного типа. Используя модель двухфакторного перекрестного дисперсионного анализа, установлено, что на интенсивность старения основной изоляции вводов оказывают влияние как условия эксплуатации, так и особенности конструктивного исполнения вводов. Новые положения, по сравнению с известными решениями, состоят в том, что предельно допустимые значения диагностических признаков высоковольтных вводов следует нормировать с учетом таких факторов, как номинальное напряжение, тип защиты и тип изоляции, нагрузка вводов и состав потребителей. Полученные результаты могут быть алгоритмически реализованы в виде отдельного модуля информационно-аналитической системы (ИАС) для диагностики состояния высоковольтного маслонаполненного оборудования. Библ. 24, табл. 7, рис. 14.*

*Ключевые слова:* высоковольтный ввод, изоляция, двухфакторный перекрестный дисперсионный анализ, показатели изоляции, тангенс угла диэлектрических потерь.

**Problem definition.** The decision on the possible state of high-voltage bushings, when conducting periodic

tests, is made by comparing the measured values of the

© O.V. Shutenko, A.A. Zagaynova, G.N. Serdyukova

insulation indicators with their maximum allowable values. It is obvious that the more adequate the maximum permissible values of bushing indicators will reflect the conditions of actual operation of bushings, the higher will be the reliability of decisions made with their use. Currently, according to [1], the maximum permissible values of the main insulation parameters of bushings (the values of the dielectric loss tangents of the main insulation and insulation of the measuring capacitor) are normalized only taking into account the nominal voltage and type of insulation. However, the study of the distribution laws of the insulation indicators of the bushings, performed in [2], showed that even for bushings of the same voltage class with the same type of insulation, there is a shift in the mathematical expectations of the distribution densities of the indicators. This is due to the influence of operational factors, the consideration of which is not regulated in [1]. The presence of such a shift indicates that the optimal maximum permissible values of indicators obtained for arrays of indicators with different parameters of the laws of distributions will differ significantly. And this means that when determining the maximum permissible values, it is necessary to take into account a larger number of factors than is regulated in [1]. In this regard, the analysis of factors influencing the values of diagnostic indicators of high-voltage bushings during long-term operation is an actual and practically important task.

#### Analysis of major achievements and literature.

Currently, open literature contains a significant number of publications devoted to improving the operational reliability of high-voltage bushings. For example, in [3-7] a detailed analysis of the main causes of damage and the most characteristic defects in high-voltage bushings was performed. It is shown that for bushings with different types of insulation there are different characteristic defects. According to international and national Standards [1, 8, 9], when conducting periodic tests of the state of insulation of high-voltage bushings, the values of the following indicators are monitored: dielectric loss angle tangent of main insulation ( $\text{tg}\delta_1$ ), main insulation capacitance ( $C_1$ ), dielectric loss angle tangent of measuring capacitor ( $\text{tg}\delta_2$ ), capacitance of measuring capacitor ( $C_2$ ), and the insulation resistance of the output to measure ( $R$ ). Examples of damage of high-voltage bushings with different types of insulation are given in [10, 11]. It is shown and justified that the most informative indicator for both paper-oil and RIP-insulated (*resin impregnated paper*) bushings is the dielectric loss tangent of the main insulation. In this case, the monitoring of this indicator should be carried out using continuous monitoring systems. A sufficient number of publications [12-14] are devoted to the analysis of the effect of the most characteristic defects of high-voltage bushings on the values of the tangent of the dielectric loss angle of the main insulation. At the same time, the issues of evaluating factors affecting the values of  $\text{tg}\delta_1$  of serviceable high-voltage bushings during long-term operation are not sufficiently analyzed. So in [15] the results of the dispersion analysis of operational factors on the values of bushing indicators are given. It has been established that

the type of bushing and the duration of operation have a significant impact on the values of the indicators. However, the above studies were performed on a limited amount of sample data and did not take into account the effects of loading the bushings. The latter circumstance was the basis for the performance of these studies.

**The goal of the paper** is analysis of the influence of conditions, modes of operation and design on the technical state of the main insulation of high-voltage bushings based on the results of preventive measurements of the dielectric loss tangent at frequency of 50 Hz.

**Research methods.** Currently, several models of dispersion analysis have been developed and are widely used for factor analysis [16, 17]. It should be noted that the choice of a particular model of analysis requires a sufficiently deep justification. For example, in [18], a single-factor model of dispersion analysis was used to form statistically homogeneous arrays of gas concentrations. This approach allows to perform a dispersion decomposition with an unequal number of measurements in cells, but it requires strict fixation of all factors, except for the variable factor, at strictly defined levels, which is not always possible when working with operational data. The use of models based on Latin squares [19] allows to simultaneously check the influence of several factors, but does not allow us to estimate the effects of interaction between them. In such conditions, the most optimal, according to the authors, is the use of a two-factor cross-sectional analysis model [15, 20, 21], which allows to simultaneously evaluate the influence of two factors and evaluate the effect of their interaction.

Taking into account the alleged non-additive effects of changing levels of factors (that is, the difference in mathematical expectations between any two levels of one factor is not the same for any levels of another), the model of the components of the dispersion can be represented as [22]:

$$y_{ijr} = \mu + \rho_i + \gamma_j + (\rho\gamma)_{ij} + \varepsilon_{ijr}, \quad (1)$$

where  $y_{ijr}$  is the value of the insulation indicator;  $\mu$  is the general average;  $\rho_i$  is the average deviation relative to  $\mu$  for the  $i$ -th level of the first factor;  $\gamma_j$  is the average deviation relative to  $\mu$  for the  $j$ -th level of the second factor;  $(\rho\gamma)_{ij}$  is the component that characterizes the interaction between factors;  $\varepsilon_{ijr}$  is the residual random variable;  $i$  is the level of the first factor;  $j$  is the level of the second factor; the order of occurrence of one of  $m_{ij}$  observations for combining the  $i$ -th level of the first with the  $j$ -th level of the second factor.

It is known [22] that the expression for the total sum of squares of deviations from the common average for model (1) is:

$$\begin{aligned} \sum_{i=1}^n \sum_{j=1}^k \sum_{r=1}^m (\bar{y}_{ij} - \bar{y})^2 &= k \cdot m \cdot \sum_{i=1}^n (\bar{y}_i - \bar{y})^2 + \\ &+ n \cdot m \cdot \sum_{j=1}^k (\bar{y}_j - \bar{y})^2 + m \cdot \sum_{i=1}^n \sum_{j=1}^k (\bar{y}_{ij} - \bar{y}_i - \bar{y}_j + \bar{y})^2 + (2) \\ &+ \sum_{i=1}^n \sum_{j=1}^k \sum_{r=1}^m (y_{ijr} - \bar{y}_{ij})^2; \end{aligned}$$

$$\text{or } Q_{tot} = Q_A + Q_B + Q_{AB} + Q_\varepsilon, \quad (3)$$

where  $Q_{tot} = \sum_{i=1}^n \sum_{j=1}^k \sum_{r=1}^m (\bar{y}_{ij} - \bar{y})^2$  is the total sum of squares of deviations from total average;

$Q_A = k \cdot m \cdot \sum_{i=1}^n (\bar{y}_i - \bar{y})^2$  is the sum of squares of deviations, which characterizes the scattering of the averages in rows relative to the total average;  $Q_B = n \cdot m \cdot \sum_{j=1}^k (\bar{y}_j - \bar{y})^2$  is the sum of squares of

deviations from the total average between the columns, which characterizes the scattering of the averages by the

columns;  $Q_{AB} = m \cdot \sum_{i=1}^n \sum_{j=1}^k (\bar{y}_{ij} - \bar{y}_i - \bar{y}_j + \bar{y})^2$  is the sum of squares of deviations characterizing the effect of

mutual influence;  $Q_\varepsilon = \sum_{i=1}^n \sum_{j=1}^k \sum_{r=1}^m (\bar{y}_{ijr} - \bar{y}_{ij})^2$  is the sum

of squares of deviations within the series, which characterizes the scattering of individual observations in a series relative to the average of the series, due to the influence of random variables only.

Checking the hypothesis about the significance of the influence of factors and their interactions was carried out using the Fisher criterion. For this, we first found the estimates of the mean squares.

General:

$$\bar{Q}_{tot}^2 = \frac{Q_{tot}}{n \cdot k \cdot m - 1} = \sigma_\varepsilon^2 + \sigma_A^2 + \sigma_B^2 + \sigma_{AB}^2; \quad (4)$$

between rows:

$$\bar{Q}_A^2 = \frac{Q_A}{n-1} = \sigma_\varepsilon^2 + k \cdot m \cdot \sigma_A^2 + m \cdot \sigma_{AB}^2; \quad (5)$$

between columns:

$$\bar{Q}_B^2 = \frac{Q_B}{k-1} = \sigma_\varepsilon^2 + n \cdot m \cdot \sigma_B^2 + m \cdot \sigma_{AB}^2; \quad (6)$$

interactions:

$$\bar{Q}_{AB}^2 = \frac{Q_{AB}}{(n-1) \cdot (k-1)} = \sigma_\varepsilon^2 + m \cdot \sigma_{AB}^2; \quad (7)$$

residual:

$$\bar{Q}_\varepsilon^2 = \frac{Q_\varepsilon}{n \cdot k \cdot (m-1)} = \sigma_\varepsilon^2. \quad (8)$$

The values of the  $F$ -criteria were calculated as the ratio of the respective mean squares to the residual mean square:

$$F_A = \frac{\bar{Q}_A^2}{\bar{Q}_\varepsilon^2}, \quad F_B = \frac{\bar{Q}_B^2}{\bar{Q}_\varepsilon^2}, \quad F_{AB} = \frac{\bar{Q}_{AB}^2}{\bar{Q}_\varepsilon^2}. \quad (9)$$

The hypothesis about the absence of the influence of a factor or interaction effect was not rejected if the calculated  $F$ -criterion value did not exceed the critical value, with the corresponding values of the number of

degrees of freedom and significance level  $\alpha = 0.05$ . This method was implemented in the form of the authors' program «DDA» (Two-Factor Dispersion Analysis), described in [23].

As initial data, the results of periodic monitoring of the state of high-voltage bushings of 110, 220 and 330 kV with different types of insulation, which are operated in Kharkiv, Poltava and Lugansk regions of Ukraine, were used. As a response, the values of the dielectric loss tangent of the main insulation of high-voltage bushings were analyzed.

**The results of numerical simulation.** Below are the results of checking the influence of various factors.

**Analysis of the significance of the differences of  $\text{tg}\delta_1$  values of high-voltage bushings, which are operated with different values of the load current.**

The operating temperature of the insulation is one of the main factors determining the intensity of its aging [24]. In [20] it was shown that the aging rate of transformer oils largely depends on the load on the transformers. In high-voltage bushings, the operating temperature is largely determined by both the operating current (load current) and the ambient temperature. For leveling the influence of ambient temperature and other factors, when assessing the impact of load of the bushings, we used the results of periodic tests for high-voltage bushings of 110 kV of sealed design with paper-oil insulation of the type ГБМТ-110/630 Y1, which were put into operation in the 80s years and operate in the Kharkiv region. The sample size was 144 values: 3 columns, the volumes of sample values in the cells is 6, the number of cells is 24. The first factor was considered to be transformer load ( $kz$ ), for which three levels of variation were allocated: up to 25 %, 25-50 % and over 50 %. As the second factor, the influence of the duration of operation was analyzed. The time interval from 0 (time of commissioning) to 21 years was considered. The test results, by the factor of operation duration (in rows), were divided into 7 levels, with a step of 3 years. The dynamics of change of  $\text{tg}\delta_1$  of the main insulation of high-voltage bushings with different values of the load factor  $kz$  during operation is shown in Fig. 1.

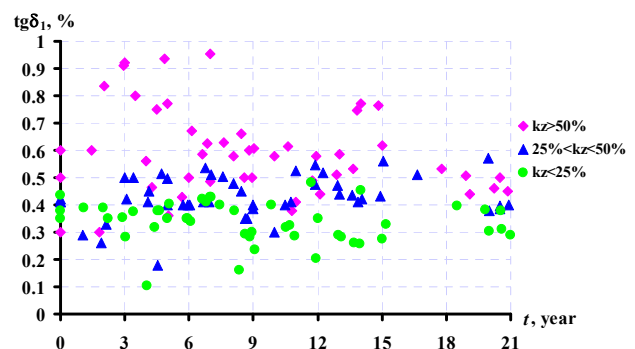


Fig. 1. Dynamics of change of  $\text{tg}\delta_1$  of the main insulation of high-voltage bushings with different values of the load factor  $kz$  during operation

The main hypothesis was the assumption that there are no significant effects of these factors. The distribution

of the average values of the tangent of the dielectric loss angle of the main insulation of high-voltage bushings, according to the levels of the influencing factors, is shown in Fig. 2. The results of the dispersion decomposition are given in Table 1. As can be seen from Table 1, the hypothesis of the absence of the influence of the operating time on the tangent of the dielectric loss angle of the main insulation of the bushings was rejected ( $F_A > F_{cr}$ ). This means that the values of  $\text{tg}\delta_1$  change over the duration of operation. The hypothesis about the absence of the influence of the load current on the values of the tangent of the dielectric loss angle of the insulation of the bushings was also rejected ( $F_B > F_{cr}$ ). This indicates the presence of significant differences in the values of  $\text{tg}\delta_1$  of serviceable high-voltage bushings, which are operated with different load values.

Quite interesting is the fact that according to the results of the analysis, the mutual influence of the duration of operation and load on the values of the tangent of the dielectric loss angle ( $F_{AB} > F_{cr}$ ) was established. This suggests that the effects of changing levels of factors are non-additive, i.e. the effect of a change in the level of influence of one factor leads to a change in the effect of the level of the impact of another. In other words, the aging process is cumulative, i.e. similar  $\text{tg}\delta_1$  values can be obtained with high loads over a relatively short period of operation, or with lower loads, but over a longer period of operation.

Table 1  
The results of checking the influence of load of bushings and duration of operation on the values of  $\text{tg}\delta_1$

Sums of dispersion decomposition	Sum of squares	Number of degrees of freedom		$F$ -criterion		
		$\nu$	$\nu$	$F$	calculated	critical
$Q_{\text{tot}}$	4.04	$\nu_{\text{tot}}$	143			
$Q_A$	0.20	$\nu_A$	7	$F_A$	3.090	2.408
$Q_B$	1.54	$\nu_B$	2	$F_B$	81.92	3.804
$Q_{AB}$	0.45	$\nu_{AB}$	14	$F_{AB}$	3.416	1.981
$Q_\varepsilon$	1.13	$\nu_\varepsilon$	120	—	—	—

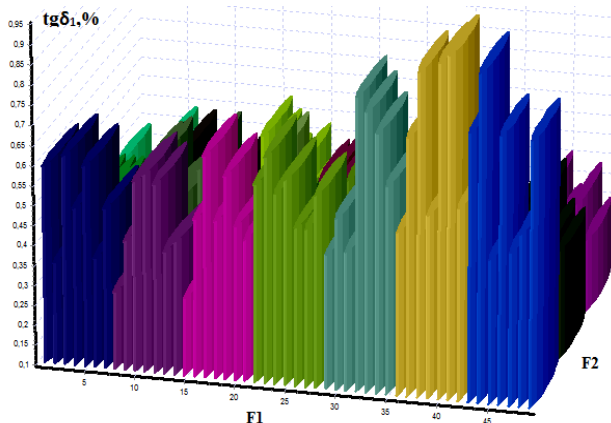


Fig. 2. The distribution of the average values of  $\text{tg}\delta_1$  of main insulation depending on the duration of operation (factor F1) and the load current (factor F2) of high-voltage bushings. The significant influence of the load factor was also confirmed for the bushings with voltage class of 220 and 330 kV with different types of insulation

**Analysis of the significance of the differences of  $\text{tg}\delta_1$  values in serviceable high-voltage bushings, with different types of insulation.** The normative document acting in Ukraine [1] regulates the values of diagnostic indicators depending on the type of insulation of bushings (oil-paper, oil barrier, paper-bakelite insulation of the bushing with mastic filling, solid insulation of the bushing with oil filling, etc.).

To check the expected impact of the bushing insulation type on the values of diagnostic indicators, a two-factor dispersion analysis of the tangent of the dielectric loss angle of the main insulation for paper-oil-insulated bushings of type ГМТА 110 kV and bushings of ГТТА type 110 kV (the frame is wired with cable crepe paper and impregnated with epoxy compound) was performed.

The analyzed bushings were commissioned in the mid-80s and operate in Kharkiv region. The average load of these bushings was 25-50 % of the rated current value. As in the previous case, the influence of the operating time was analyzed as the second factor, a time interval from 0 (commissioning time) to 24 years was considered. The test results, by the factor of operation duration (in rows), were divided into 6 levels, with a step of 4 years. The size of the analyzed sample was 156 values: 6 rows, 2 columns, 13 values per cell. The dynamics of  $\text{tg}\delta_1$  change during operation for bushings with different types of insulation is shown in Fig. 3.

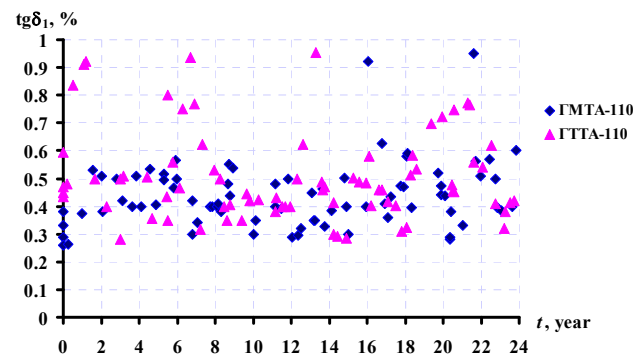


Fig. 3. Dynamics of change of  $\text{tg}\delta_1$  during operation for bushings with different types of insulation

The results of the dispersion decomposition are given in Table 2. The main hypothesis was the assumption that there are no significant effects of these factors. The distribution of the average values of the tangent of the dielectric loss angle of the main insulation of high-voltage bushings by the levels of the influencing factors is shown in Fig. 4. As can be seen from Table 2, the calculated value of the  $F_A$  criterion does not exceed the critical value; therefore, for the analyzed data, the change in  $\text{tg}\delta_1$  values during operation is not statistically significant. At the same time, there is a significant difference in the values of  $\text{tg}\delta_1$  in bushings with different types of insulation ( $F_B > F_{cr}$ ). At the same time, dispersion analysis did not reveal significant differences in the values of  $\text{tg}\delta_1$ , due to the mutual influence of the duration of operation and the type of insulation.

Table 2

The results of checking the influence of insulation type of bushings and duration of operation on the values of  $\text{tg}\delta_1$

Sums of dispersion decomposition		Number of degrees of freedom		F-criterion		
				F	calculated	critical
$Q_{\text{tot}}$	3.31	$\nu_{\text{tot}}$	155	—	—	—
$Q_A$	0.13	$\nu_A$	5	$F_A$	1.34	2.56
$Q_B$	0.17	$\nu_B$	1	$F_B$	8.97	5.02
$Q_{AB}$	0.16	$\nu_{AB}$	5	$F_{AB}$	1.65	2.56
$Q_\varepsilon$	2.84	$\nu_\varepsilon$	144	—	—	—

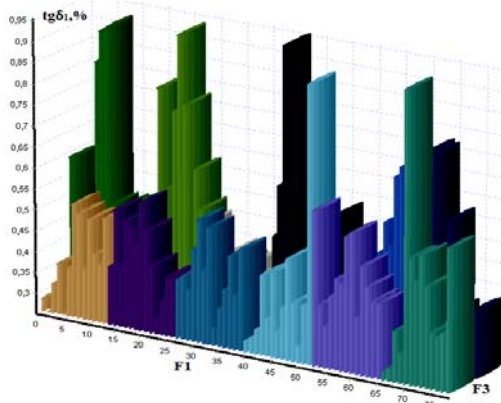


Fig. 4. The distribution of the average values of  $\text{tg}\delta_1$  of main insulation of bushings depending on the duration of operation (factor F1) and the type of insulation (factor F3)

**Analysis of the significance of differences of  $\text{tg}\delta_1$  values in serviceable high-voltage bushings of various types.** Since the analysis revealed a significant effect of the insulation type of high-voltage bushings on the values of  $\text{tg}\delta_1$ , it would be logical to check whether the type of bushings has a similar effect.

To test the hypothesis of the type of bushing influence, we analyzed the values of the tangent of dielectric loss angle for hermetic bushings with paper-oil insulation of two types: ГМТА and ГБМТУ.

As the second factor, the effect of the lifetime of the bushings was analyzed. As in the previous case, the values of  $\text{tg}\delta_1$  were analyzed in the operation interval up to 24 years, with a 4-year step.

Analyzed bushings are operated in Kharkiv region, and were put into operation in the 80s. The average load of high-voltage bushings exceeded 50%. The total sample size was 120 values: 6 rows, 2 columns, 10 values per cell.

Fig. 5 shows the dependence of  $\text{tg}\delta_1$  on the duration of operation for bushings of various types.

The main hypothesis was the assumption that there are no significant effects of these factors. The distribution of the average values of the tangent of the dielectric loss angle of the main insulation of high-voltage bushings by the levels of the influencing factors is shown in Fig. 6.

The results of the dispersion decomposition are given in Table 3.

As can be seen from Table 3, for the data analyzed, the change in  $\text{tg}\delta_1$  values over time is not statistically significant ( $F_A < F_{cr}$ ). There were also no significant differences in the values of  $\text{tg}\delta_1$  for high-voltage bushings

of various types ( $F_B < F_{cr}$ ). In addition, differences in the values of  $\text{tg}\delta_1$ , which are due to the mutual influence of the types of bushings and the duration of operation, are not statistically significant ( $F_{AB} < F_{cr}$ ).

It should be noted that similar results were obtained for bushings of the type ГТБТУ-110, ГТТБ-110 and ГТТА-110.

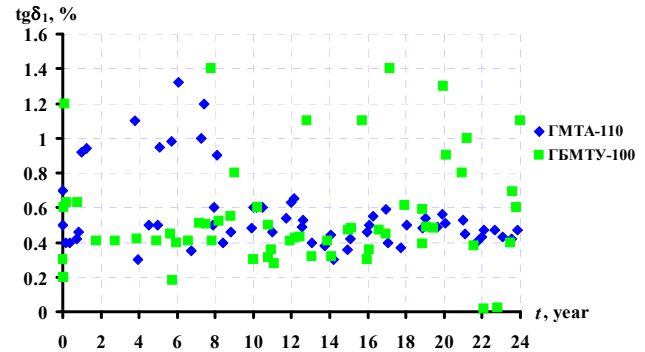


Fig. 5. Dynamics of change of  $\text{tg}\delta_1$  on the duration of operation for bushings of different types

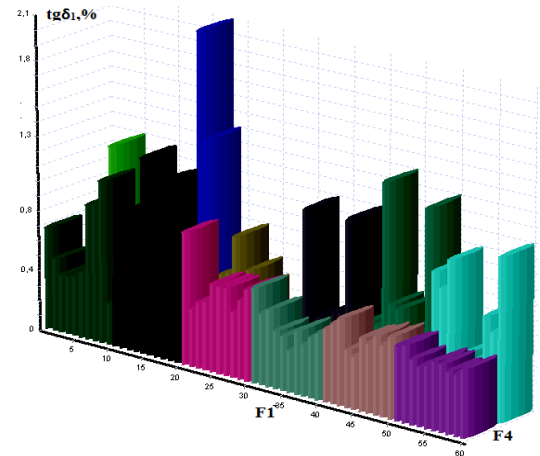


Fig. 6. The distribution of average values of  $\text{tg}\delta_1$  of main insulation depending on the duration of operation (factor F1) and type (factor F4) of high-voltage bushings

Table 3

The results of checking the influence of duration of operation and bushing type on values of  $\text{tg}\delta_1$

Sums of dispersion decomposition		Number of degrees of freedom		F-criterion		
				F	calculated	critical
$Q_{\text{tot}}$	10.89	$\nu_{\text{tot}}$	119	—	—	—
$Q_A$	0.76	$\nu_A$	5	$F_A$	1.715	2.69
$Q_B$	0.002	$\nu_B$	1	$F_B$	0.023	5.17
$Q_{AB}$	0.43	$\nu_{AB}$	5	$F_{AB}$	0.962	2.69
$Q_\varepsilon$	9.68	$\nu_\varepsilon$	108	—	—	—

**Analysis of the significance of differences of  $\text{tg}\delta_1$  values in serviceable high-voltage bushings with different types of bushing protection.** In addition to bushing load that determine the operating temperature of the insulation, the content of chemically aggressive media (moisture, atmospheric oxygen) has a significant effect on the intensity of the insulation aging processes. Obviously,

the degree of influence of chemically aggressive media on the aging intensity of the insulation will largely depend on the type of protection of the insulation of the bushings (hermetic or non-hermetic). To assess the impact of the type of protection, a dispersion analysis of the values of the tangent of the dielectric loss angle of the main insulation for the sealed-type bushings of the ГБМТ type and the non-hermetic bushings of the BMT type with rated voltage of 110 kV was carried out. These bushings were commissioned in the late 70s and operate in Kharkiv region. The average value of load currents on the analyzed period of time (up to 20 years) exceeded 50 % of the value of the rated current of the bushings. The sample size was 200 values: 10 rows, 2 columns, 10 measurements per cell. The dynamics of changes in the dielectric loss tangent of high-voltage bushings of non-hermetic and hermetic design during operation is shown in Fig. 7.

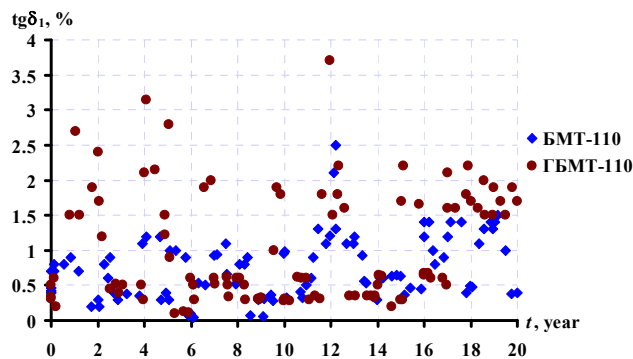


Fig. 7. Dynamics of changes in the dielectric loss tangent of high-voltage bushings of unsealed and hermetic designs during operation

The distribution of the average values of the tangent of the dielectric loss angle of the main insulation of high-voltage bushings by the levels of the influencing factors is shown in Fig. 8. The main hypothesis was the assumption that there are no significant effects of these factors. The results of the dispersion decomposition are given in Table 4. As can be seen from Table 4, for a given sample, the calculated value of the  $F_A$  criterion exceeds the critical value, and, therefore, changes in the  $\text{tg}\delta_1$  values over time are statistically significant. In addition, significant differences in the values of  $\text{tg}\delta_1$  for bushings of the hermetic and unpressurized design ( $F_B > F_{cr}$ ) were revealed. At the same time, unlike bushings with different values of load factor, for bushings with different types of protection there are no significant differences in the values of  $\text{tg}\delta_1$ , which are due to the mutual influence of the type of bushing protection and the duration of operation ( $F_{AB} < F_{cr}$ ).

**Analysis of the significance of the differences of  $\text{tg}\delta_1$  values in serviceable high-voltage bushings installed on different phases of transformers.** As a rule, electrical networks operate in a symmetric mode, i.e. the values of the load current in different phases should coincide and, therefore, the values of the diagnostic indicators in serviceable, normally operating bushings

should not differ significantly. At the same time, if a defect occurs in one of the bushings, the values of diagnostic indicators differ, which allows detecting a defect. This is the basis of the nonequilibrium-compensation method for continuous monitoring of the insulation state of the bushings [24].

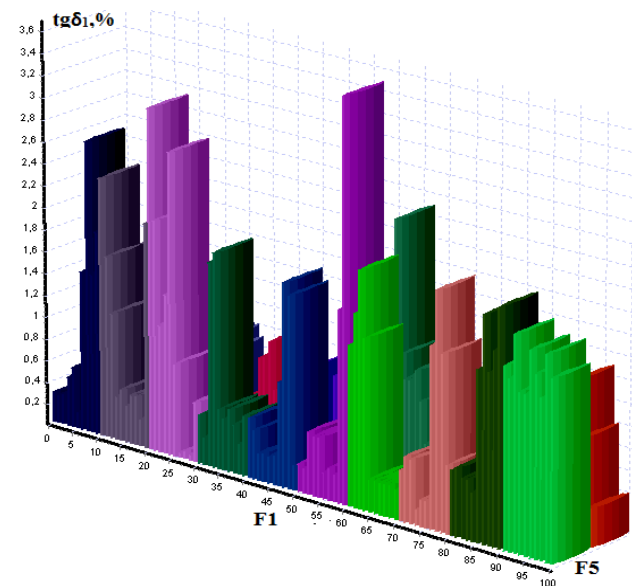


Fig. 8. The distribution of average values of  $\text{tg}\delta_1$  of basic insulation depending on the duration of operation (factor F1) and type of protection (factor F5) of high-voltage bushings

Table 4

The results of checking the influence of the duration of operation and the type of protection of bushings on the values of  $\text{tg}\delta_1$

Sums of dispersion decomposition		Number of degrees of freedom		$F$ -criterion		
				$F$	calculated	critical
$Q_{tot}$	86.3	$\nu_{tot}$	199			
$Q_A$	9.42	$\nu_A$	9	$F_A$	2.706	2.11
$Q_B$	4.16	$\nu_B$	1	$F_B$	10.77	5.02
$Q_{AB}$	3.19	$\nu_{AB}$	9	$F_{AB}$	0.917	2.11
$Q_c$	69.5	$\nu_c$	180	–	–	–

To check the hypothesis about the effect of the phase on the values of the indicators, the values of  $\text{tg}\delta_1$  of high-voltage bushings with voltage of 110 kV of the ГМТА type were analyzed. These bushings were commissioned in the early 90s. The sample size was 150 values: 10 rows, 3 columns, 5 measurements per cell. The division step by factor of the duration of operation was 2 years.

The dynamics of  $\text{tg}\delta_1$  change during the operation of high-voltage bushings of a hermetic design, installed on different phases of transformers, is shown in Fig. 9.

The distribution of the average values of the tangent of the dielectric loss angle of the main insulation of high-voltage bushings by the levels of the influencing factors is shown in Fig. 10.

The main hypothesis was the assumption that there are no significant effects of these factors.

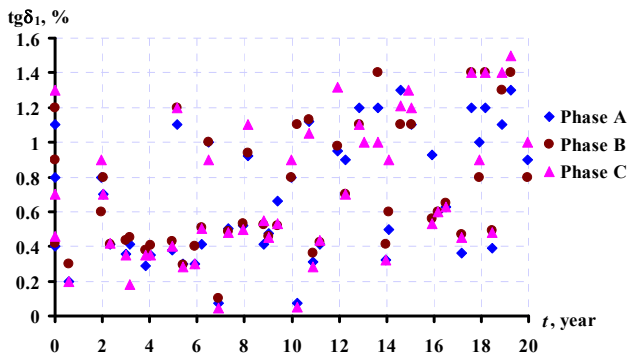


Fig. 9. Dynamics of change of  $\text{tg}\delta_1$  during the operation of high-voltage bushings of sealed design, installed on different transformer phases

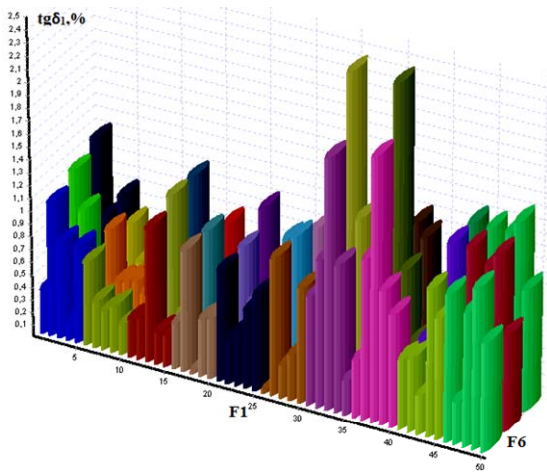


Fig. 10. The distribution of the average values of  $\text{tg}\delta_1$  of main insulation depending on the duration of operation (factor F1) and phase (factor F6) of high-voltage bushings

The results of the dispersion decomposition are given in Table 5. As can be seen from Table 5, the calculated value of the  $F_A$  criterion exceeds the critical value, and therefore, changes in the  $\text{tg}\delta_1$  values over time for a given sample are statistically significant. At the same time, there are no significant differences in the values of  $\text{tg}\delta_1$  for high-voltage bushings installed at different phases of transformers ( $F_B < F_{cr}$ ). There are also no significant differences in the values of  $\text{tg}\delta_1$ , due to the mutual influence of the bushing phase and the duration of operation ( $F_{AB} < F_{cr}$ ).

Table 5

The results of checking the influence of the duration of operation and the phase number of the bushings on the values of  $\text{tg}\delta_1$

Sums of dispersion decomposition		Number of degrees of freedom		$F$ -criterion		
				$F$	calculated	critical
$Q_{\text{tot}}$	29.6	$\nu_{\text{tot}}$	149			
$Q_A$	8.54	$\nu_A$	9	$F_A$	5.59	2.22
$Q_B$	0.14	$\nu_B$	2	$F_B$	0.43	3.68
$Q_{AB}$	0.63	$\nu_{AB}$	18	$F_{AB}$	0.20	1.87
$Q_\varepsilon$	20.3	$\nu_\varepsilon$	120	—	—	—

It should be noted that similar results were obtained for bushings of the type ГТБТУ-110, ГТТА-110, as well as for bushings of voltage class of 220 and 330 kV.

**Analysis of the significance of differences of  $\text{tg}\delta_1$  values in serviceable high-voltage bushings with different classes of rated voltage.** The normative document acting in Ukraine [1] provides the rationing of the values of diagnostic indicators depending on the rated voltage of the bushings, which implies the existence of significant differences in the values of the same indicator for the bushings of different voltage classes. To verify the presence of such differences, the dispersion analysis of  $\text{tg}\delta_1$  values was performed for bushings with paper-oil insulation of hermetic design with rated voltage of 110, 220 and 330 kV. These bushings were commissioned in the early 90s and operate with a load above 50 % of the nominal current value. The volume of sample values was 108 values: 3 columns, 6 rows, 6 measurements per cell. The dividing step by factor of the duration of operation (in rows) was 4 years in the observation interval of up to 24 years. The dynamics of changes in the dielectric loss tangent of bushings of a hermetic design of voltage class of 110, 220 and 330 kV during operation is shown in Fig. 11.

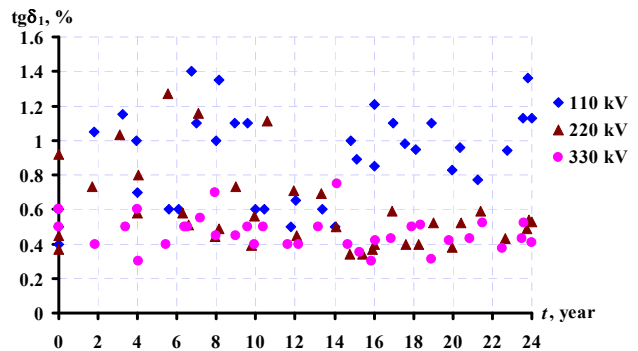


Fig. 11. Dynamics of changes in the dielectric loss tangent of bushings of a hermetic design of 110, 220 and 330 kV voltage classes during operation

The distribution of the average values of the tangent of the dielectric loss angle of the main insulation of high-voltage bushings, according to the levels of the influencing factors, is shown in Fig. 12.

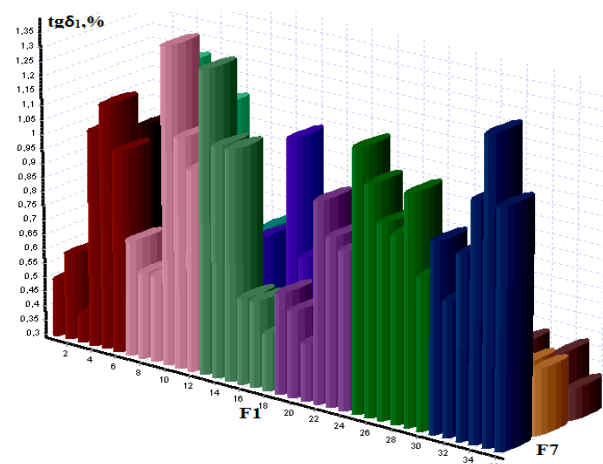


Fig. 12. The distribution of the average values of the tangent of dielectric loss of the main insulation of high-voltage bushings depending on the duration of operation (factor F1) and voltage class (factor F7) of high-voltage bushings

The main hypothesis was the assumption that there are no significant effects of these factors. The results of the dispersion decomposition are given in Table 6.

Table 6

The results of checking the influence of the duration of operation and the rated voltage of the bushings on the values of  $\text{tg}\delta_1$

Sums of dispersion decomposition		Number of degrees of freedom		$F$ -criterion		
				$F$	calculated	critical
$Q_{\text{tot}}$	8.48	$\nu_{\text{tot}}$	107			
$Q_A$	0.31	$\nu_A$	5	$F_A$	1.45	2.730
$Q_B$	3.52	$\nu_B$	2	$F_B$	41.0	3.865
$Q_{AB}$	0.78	$\nu_{AB}$	10	$F_{AB}$	1.83	2.213
$Q_e$	3.86	$\nu_e$	90	–	–	–

As can be seen from Table 6, the analysis performed revealed significant differences in the values of the tangent of dielectric loss of the main insulation of the bushings of different voltage classes ( $F_B > F_{cr}$ ).

But at the same time, a significant change over time of the  $\text{tg}\delta_1$  values for this sample was not established ( $F_A < F_{cr}$ ). There is also no significant difference in the values of  $\text{tg}\delta_1$ , which is due to the mutual influence of the rated voltage of the bushings and the duration of their operation ( $F_{AB} < F_{cr}$ ).

**Analysis of the significance of differences in  $\text{tg}\delta_1$  values in serviceable high-voltage bushings, which are operated in different regions of Ukraine.** In some works, for example, [18], results are presented indicating that there is a significant influence of the region in which the equipment is operated on the values of diagnostic indicators. Such influence may be due to both different climatic conditions, and different composition of the consumer and, as a result, differences in the density of daily load schedules.

To check the influence of the region of Ukraine on the change in the values of diagnostic indicators of high-voltage bushings, an analysis of the values of  $\text{tg}\delta_1$  was performed for 110 kV bushings of the hermetic design of type БМТ-110, which operate in Kharkiv, Lugansk and Poltava regions of Ukraine.

Taking into account that the bushings are approximately in the same climatic zone, the main factor influencing possible differences in the values of the dielectric loss tangent of the bushings will be the composition of consumers, and as a result, different density of daily load graphs. Analyzed bushings were put into operation in the late 70s and operate with a load above 50 % of the nominal value. The volume of sample values was 108 values: 3 columns, 6 rows, 6 measurements per cell. The dividing step by factor of the duration of operation (in rows) was 4 years in the observation interval of up to 24 years. The dynamics of changes in the dielectric loss tangent of high-voltage bushings from different regions of Ukraine in the process of operation is shown in Fig. 13.

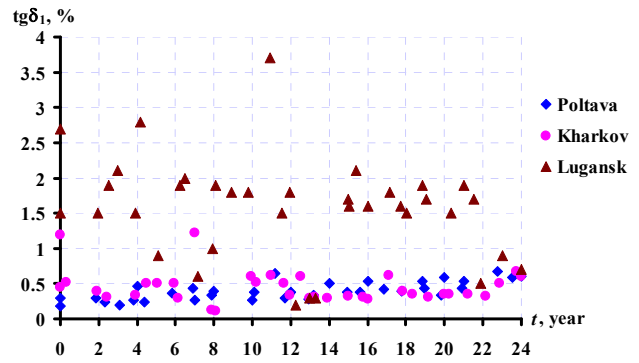


Fig. 13. Dynamics of changes in the dielectric loss tangent of high-voltage bushings from different regions of Ukraine during operation

The distribution of the average values of the tangent of the dielectric loss angle of the main insulation of high-voltage bushings by the levels of the influencing factors is shown in Fig. 14.

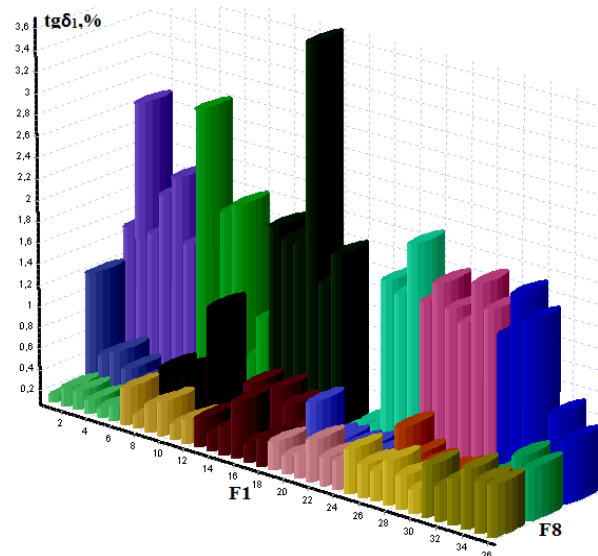


Fig. 14. The distribution of the average values of the tangent of dielectric loss of the main insulation depending on the duration of operation (factor F1) of high-voltage bushings and the region of Ukraine (factor F8)

The main hypothesis was the assumption that there are no significant effects of these factors. The results of the dispersion decomposition are given in Table 7. As can be seen from the Table 7, for this sample, a significant change in the  $\text{tg}\delta_1$  values during operation was not established ( $F_A < F_{cr}$ ). But at the same time, significant differences were revealed in the values of  $\text{tg}\delta_1$  for bushings that are operated in different regions of Ukraine ( $F_B > F_{cr}$ ). As in the previous cases, there are no significant differences in the values of  $\text{tg}\delta_1$ , due to the mutual influence of the region of Ukraine in which the bushings are operated, and the duration of their operation ( $F_{AB} < F_{cr}$ ). The conclusion about the significant effect of the density of the daily load schedule on the aging rate of the main insulation of the bushings was also confirmed for the bushings of the hermetic design of the type ГМТА -110.

Table 7

The results of checking the impact on the values of  $\text{tg}\delta_1$  of the duration of operation and the region of Ukraine

Sums of dispersion decomposition		Number of degrees of freedom		F-criterion		
				F	calculated	critical
$Q_{\text{tot}}$	51.90	$\nu_{\text{tot}}$	107			
$Q_A$	1.54	$\nu_A$	5	$F_A$	1.81	2.73
$Q_B$	31.39	$\nu_B$	2	$F_B$	92.5	3.86
$Q_{AB}$	15.26	$\nu_{AB}$	10	$F_{AB}$	2.18	2.21
$Q_e$	0.00	$\nu_e$	90	–	–	–

As a result of the analysis performed, it was found that the aging rate of the main insulation of the bushings is significantly affected by both the operating conditions (the load current value of the bushings and the consumer's composition) and the design features of the bushings: the rated voltage value, type of insulation and type of protection of the bushings. Some of these factors, namely the rated voltage and the type of insulation, are taken into account in the regulatory document in force in Ukraine [1] when rationing the maximum permissible values of the indicators. At the same time, such factors as the value of the load current, the composition of the consumer and the type of protection are not taken into account when rationing the maximum permissible values of the indicators.

The results obtained above do not allow to unambiguously assess the presence or absence of the influence of the operating time on the values of  $\text{tg}\delta_1$ . Of the seven examples given, the hypothesis of the absence of the influence of the duration of operation on the values of  $\text{tg}\delta_1$  was rejected only in three cases. It should be noted here that such discrepancies were revealed only for the factor of the duration of operation. For other factors when checking the hypothesis of the absence of their influence, the results obtained are identical for different samples. The revealed differences can be due both to the absence of influence of the duration of operation on the values of diagnostic indicators for serviceable bushings, and to the non-monotonic nature of the change in the values of  $\text{tg}\delta_1$  over time. The decision on the significance of the influence of the duration of operation on the values of diagnostic indicators of high-voltage bushings can be made after conducting additional studies, in particular, dispersion analysis of linear models of diagnostic indicators on the duration of operation.

### Conclusions.

1. Maximum permissible values of diagnostic indicators of high-voltage bushings should be normalized taking into account such factors as rated voltage, type of protection and type of insulation, load of bushings and the composition of consumers, since, based on the analysis performed, it was established that these factors have a significant effect on the values of diagnostic indicators.

2. According to the results of the analysis, it was established that such factors as the bushing type and phase do not have a significant effect on the change in the values of diagnostic indicators of high-voltage bushings, and, therefore, they can be ignored when determining the maximum permissible values of the indicators.

3. The obtained results of the analysis did not confirm the recommendations from literature sources regarding the influence of some factors on the values of diagnostic indicators of bushings.

4. As further research, it is advisable to evaluate the effect of the operation time of the bushings on the values of their diagnostic indicators using other models of dispersion analysis. Here, it is of scientific and practical interest to carry out a similar assessment, both for serviceable bushings, and bushings with developing defects.

### REFERENCES

- SOU-N EE 20.302: 2007. *Normy vyprovuvannja elektroobladnannja* [Norms of testing of electrical equipment]. Kyiv, Ministry of Fuel and Energy of Ukraine, 262 p. (Ukr).
- Shutenko O., Zagaynova A., Serdyukova G. Analysis of distribution laws of insulation indicators of high-voltage oil-filled bushings of hermetic and non-hermetic execution. *Technology audit and production reserves*, 2018, vol.4, no.1(42), pp. 30-39. doi: 10.15587/2312-8372.2018.140873.
- Feilat E.A. Analysis of the Root Causes of Transformer Bushing Failures. *International Journal of Computer, Electrical, Automation, Control and Information Engineering*, 2013, vol.7, no.6, pp. 791-796.
- Anglhuber M., Juan L. Contreras Velásquez. Dispersing the clouds – gain clear insight into your bushings using advanced diagnostics method. *Transformer Magazine. Special Edition: Bushing*, 2017, pp. 126-132.
- Septyani H.I., Arifianto I., Purnomoadi A.P. High voltage transformer bushing problems. *Proceedings of the 2011 International Conference on Electrical Engineering and Informatics*, Jul. 2011. doi: 10.1109/iceei.2011.6021566.
- Metwally I. Failures, Monitoring and New Trends of Power Transformers. *IEEE Potentials*, 2011, vol.30, no.3, pp. 36-43. doi: 10.1109/mpot.2011.940233.
- Rubanenko A.E., Gumenyuk A.I. *Vysokovoltni vvody. Konstruktsiia, ekspluatatsiia, diahnozyka i remont* [High-voltage bushings. Design, operation, diagnostics and repair]. Vinnitsa: VNTU Publ., 2011. 183 p. (Ukr).
- IEC – 60137, Edition 7.0 2017-06. International Electro-technical Commission Standard for Insulated bushings for alternating voltages above 1000 V.
- IEEE Std C57.19.01: Performance Characteristics and Dimensions for Outdoor Apparatus Bushings, 2000.
- Andrienko P.D., Sakhno A.A., Konogray S.P., Spitsa A.G., Skrupskaya L.S. Features of monitoring the technical condition of the main insulation of high-voltage bushings and current transformers. *Electrical engineering and power engineering*, 2014, no.1, pp. 43-48. (Rus). doi: 10.15588/1607-6761-2014-1-7.
- Anikeeva M.A., Arbuzov R.S., Zhivodernikov S.V., Lazareva E.A., Ovsyannikov A.G., Panov M.A. Diagnostic signs for rejection of high-voltage bushings with oil-paper insulation. *ELEKTRO. Electrical engineering, power industry, electrical industry*, 2009, no.1, pp. 22-25. (Rus).
- Lvov M.Yu. Colloid-dispersed processes in high-voltage sealed bushings of transformers. *Electric stations*, 2000, no.4, pp. 49-52. (Rus).
- Snetkova O.V. Experience of diagnostics of 110-500 kV oil-filled bushings in Mosenergo. *ELEKTRO. Electrical engineering, power industry, electrical industry*, 2004, no.2, pp. 39-42. (Rus).
- Osov V.N. Errors in measuring dielectric characteristics and assessing the state of high-voltage bushings. *Proceedings*

of the 10th annual conference «Methods and means of insulation control of high-voltage equipment». Perm: Dimrus Publ., 2013. (Rus).

15. Zahaynova O.A. Analysis of the influence of different factors on the aging of the insulation capacitor type high-voltage input. *Energy saving. Power engineering. Energy audit*, 2015, no.10(141), pp. 17-25. (Rus).

16. Scheffe G. *Dispersionnyi analiz* [Dispersion analysis]. Moscow, Nauka Publ., 1980. 512 p. (Rus).

17. Johnson N. *Statistika i planirovanie eksperimenta v tekhnike i nauke* [Statistics and Experiment Planning in Engineering and Science]. Moscow: Mir Publ., 1981. 520 p. (Rus).

18. Davidenko I.V. Investigation of indicators describing the operational state of oil-filled bushings, using mathematical statistics. *University news. North-Caucasian region. Technical sciences series*, 2006, no.15, pp. 31-33. (Rus).

19. Gmurman V.E. *Teoriia veroiatnostei i matematicheskaia statistika* [Theory of Probability and Mathematical Statistics]. Moscow, High school Publ., 1977. 479 p. (Rus).

20. Shutenko O.V. Evaluation of the influence of operating conditions on the intensity of aging of transformer oils. *Bulletin of NTU «KhPI»*, 2010, no.1. pp. 171-179. (Rus).

21. Shutenko O.V., Abramov V.B., Baklay D.N. Analysis of factors affecting the homogeneity of arrays of concentrations of gases dissolved in oil. *Energetic and electrification*, 2013, no.6, pp. 39-50. (Rus).

22. Davydenko A.P. *Organizatsiia i planirovanie nauchnykh issledovaniy, patentovedenie* [Organization and planning of scientific research, patent science]. Kharkiv, NTU «KhPI» Publ., 2004. 320 p. (Rus).

23. Shutenko O.V., Baklay D.N. *Planirovanie eksperimental'nykh issledovaniy v elektroenergetike. Metody obrabotki eksperimental'nykh dannykh* [Planning of experimental research in the electric power industry. Methods for processing experimental data]. Kharkiv, NTU «KhPI» Publ., 2013. 268 p. (Rus).

24. Svi P.M. *Kontrol' izoliatsii oborudovaniia vysokogo napriazheniia* [Insulation control of high voltage equipment]. Moscow, Energoatomizdat Publ., 1988. 128 p. (Rus).

Received 25.10.2018

O.V. Shutenko<sup>1</sup>, Candidate of Technical Science, Associate Professor,

A.A. Zagaynova<sup>1</sup>, Assistant Lecturer,

G.N. Serdyukova<sup>1</sup>, Candidate of Technical Science, Associate Professor,

<sup>1</sup> National Technical University «Kharkiv Polytechnic Institute», 2, Kyrpychova Str., Kharkiv, 61002, Ukraine,

e-mail: o.v.shutenko@gmail.com, zagaynova@gmail.com, serdukova.galina@gmail.com.

#### How to cite this article:

Shutenko O.V., Zagaynova A.A., Serdyukova G.N. Analysis of operating conditions and modes influence on technical state of main insulation of high-voltage bushings of different design. *Electrical engineering & electromechanics*, 2019, no.1, pp. 57-66. doi: 10.20998/2074-272X.2019.1.10.

D.G. Koliushko, S.S. Rudenko

## ANALYSIS OF METHODS FOR MONITORING OF EXISTING ENERGY OBJECTS GROUNDING DEVICES STATE AT THE PRESENT STAGE

*Purpose.* The purpose of the work is to analyze the modern methods of control and determine the most effective ones for monitoring the state of grounding of existing energy objects in operation. *Methodology.* The analysis of the methods was carried on the basis of comparison the experimental and calculation methods for determining the rated parameters of the grounding of existing energy objects. *Results.* Significant imperfections of measurements of the rated parameters of the grounding with different methods and devices was established. It has been shown that the electromagnetic diagnostics is the most complete, which allows to comprehensively assess the current state of the grounding and establish the resistance of the grounding, the voltage on it, the touch voltage and the resistance of the contact joints. The deficiencies of electromagnetic diagnostics are established at the present stage and further directions of its perfection are determined. *Originality.* For the first time the comparative analysis of existing methods for monitoring the state of the grounding and directions for improving electromagnetic diagnostics was made. *Practical value.* The obtained results allow to choose the optimum method for monitoring the state of the grounding. Elimination of the revealed drawbacks of the method of electromagnetic diagnostics will improve the accuracy of the determination of rated parameters. References 17, tables 1, figures 4.

*Key words:* grounding device, resistance of the grounding device, grounding device voltage, touch voltage, resistance of contact joints, electromagnetic diagnostics.

*Проведено аналіз і встановлено суттєві недоліки вимірювань нормованих параметрів заземлювальних пристроїв діючих энергооб'єктів при використанні різних методик та приладів. Показано, що електромагнітна діагностика стану заземлювального пристрою на теперішній час є найбільш повною, яка дозволяє комплексно оцінити поточний стан заземлювального пристрою та встановити значення опору заземлювального пристрою, напруги на ньому, напруги дотику та опору контактних з'єднань. Встановлені недоліки електромагнітної діагностики на сучасному етапі та визначені подальші напрямки її вдосконалення. Бібл. 17, табл. 1, рис. 4.*

*Ключові слова:* заземлювальний пристрій, опір заземлювального пристрою, напруга на заземлювальному пристрої, напруга дотику, опір контактних з'єднань, електромагнітна діагностика.

*Проведен анализ и установлены существенные недостатки измерения нормируемых параметров заземляющих устройств действующих энергообъектов при использовании различных методик и приборов. Показано, что электромагнитная диагностика состояния заземляющего устройства в настоящее время является наиболее полной и позволяет комплексно оценить текущее состояние заземляющего устройства и определить значение сопротивления заземляющего устройства, напряжения на нем, напряжение прикосновения и сопротивления контактных соединений. Установлены недостатки электромагнитной диагностики на современном этапе и определены дальнейшие направления ее совершенствования. Библ. 17, табл. 1, рис. 4.*

*Ключевые слова:* заземляющее устройство, сопротивление заземляющего устройства, напряжение на заземляющем устройстве, напряжение прикосновения, сопротивление контактных соединений, электромагнитная диагностика.

**Problem definition.** The lifetime of most of the existing power facilities in Ukraine is over 30 years. During this period both the electrical installation itself and the grounding device (GD) undergo significant changes, as a result of which its electrical normalized parameters (NPs) may exceed the permissible values, and the constructive execution does not meet the requirements of the design and normative documentation. There are a number of factors that significantly affect the state of the GD and its parameters:

- effect of corrosion on the elements of the GD (violation of the integrity of the grid and damage of grounding conductors on the boundary of the earth-air);
- incorrect restoration of the grounding of old and connection of new units of equipment to the existing GDs (serial connection of equipment, connection to metal parts that are not connected with GD);
- damage of the GD during excavation as a result of replacement or repair of equipment;
- increase of electrical power of installation with increasing values of short-circuit (SC) currents (exceeding the permissible values of the NP of the GD).

For the estimation of GD operational capacity, NPs

[1] are used, which are periodically monitored throughout the lifetime [2]. These include: resistance of the GD, the voltage on the GD, the touch voltage and the resistance of the contact joints. These values depend on the following factors: the structural performance of the GD, the electrophysical characteristics of the soil (resistivity and thickness of the layers) and the characteristics of the object (the value of SC current, time of protection, voltage class, etc.).

**The goal of the work** is analysis of existing methods of monitoring and determination of the most effective ones for assessing the state of the GD of existing power facilities during operation.

Let us consider the most common methods of determining the NP of the GD.

**1. Resistance of the grounding device and voltage on it.** At present, the value of the resistance of the GD is determined by a number of methods:

1) the introduction of high current (50-100 A). The specified method is divided into several types:

- synchronous [3], which uses the voltage source of the industrial frequency. The current and voltage in the

circuit are measured before and after the voltage source is switched on. Then the corresponding expressions determine the resistance of the GD;

- hit frequency [3], which uses an AC generator with frequency different from the industrial by 0.1-0.5 Hz. As a result of the phase shift between the input current and the current flowing through the GD during normal operation, there are maxima and minima of the measured current and voltage. Voltage and current are also measured before and after switching on the generator, and the resistance value is determined by the corresponding expressions;

- input of current whose frequency is different from the industrial frequency and its harmonics by several Hz;

- 2) input of low current (up to 3 A) [4]. In this case, generators with different from the industrial frequency are used;

- 3) calculation method [5-9].

Measurement according to the given methods is carried out by the method of an ammeter-voltmeter, while two circuits of arrangement of electrodes [2] are used –one and two-beam (see Fig. 1). A two-beam circuit may be appropriate for measuring in conditions where the area in the location of the power unit is limited. For both circuits, one and the same measurement procedure is used:

- 1) generator I is connected to the GD E and the current electrode C, which is set at a distance of  $3D$  for the one-beam and  $(1.5-2) D$  for the two-beam circuit, where  $D$  is the largest diagonal of the GD;

- 2) current value is determined by means of generator I and ammeter PA;

- 3) potential electrode P is clogged at a certain distance  $X$ , for example, 50 % of the distance to the current electrode (for a one-beam circuit on one straight line with a current electrode, for a two-beam one at an angle of  $40-45^\circ$ ), and the potential is measured;

- 4) further, moving the potential electrode away from the GD, the potential is measured through the selected distance (for example, after 5 m, 10 m, 15 m, etc.);

- 5) it is necessary to move the electrode P to such a distance  $X$  so that the value between the two adjacent dimensions does not differ by more than 10 %. This will mean that the point  $R_2$  of the curve [10] is found.

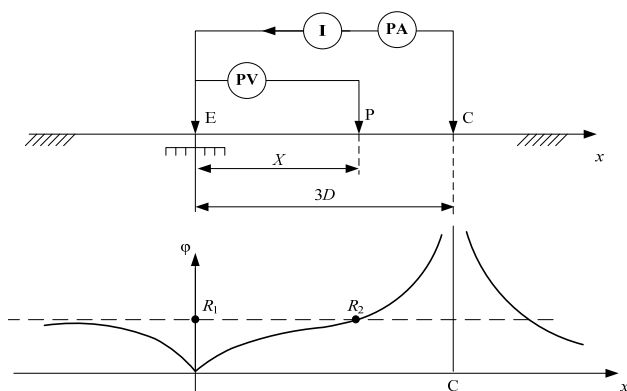


Fig. 1. Distribution of potential along the soil surface at carrying out measurements according to the one-beam circuit

The resistance of the GD in this case will be equal to the ratio of the potential at the point  $R_2$  to the generator

current. However, in practice, the most widespread, due to its simplicity, is the one-beam circuit by the «62 % method», when the potential electrode P is immediately set at a distance from the GD, which is 62 % of the removal of the current electrode C. This method ensures the greatest accuracy at the condition of homogeneity of the soil, but in other cases it is necessary to use the dependence of the length of the removal of the potential electrode on the length of the removal of the current one for the two-layer soil, which is given in [10].

The horizontal part on the dependence curve of the potential on the distance to the potential electrode appears at a sufficiently large increase in the distance to the current electrode. Depending on the structure of the soil, this condition is performed at a distance to the current electrode in (3-40) diagonals of the GD. It is clear that such a diversity of measuring circuits in many cases will be impossible.

In [11], the circuit of measuring the resistance of the GD with a three-electrode installation is considered. Here, despite the assertion about the possibility of measurements for any soil structure, only a homogeneous structure was considered during physical modelling, and measurements on active power facilities were not carried out. In [12], it has been shown that in soils with horizontal and vertical inhomogeneities there is the only possible option for the arrangement of an auxiliary potential electrode in a one-beam measuring circuit, at which the exact determination of the resistance of the GD is possible. The given algorithm for the experimental search of this variant for a soil with an unknown geoelectric structure is complicated in terms of practical implementation.

The voltage on the GD is the voltage that occurs when the current flows from grounding to the earth between the point of current input to the grounding and the zone of the zero potential [1]. The direction of the voltage on the GD influences the state of the cable production of the power unit, the microprocessor measuring equipment and control equipment, the relay protection panels, and also indirectly on the electrical safety (the value of the voltage on the GD together with the electrophysical characteristics of the soil are decisive for the value of the touch voltage). According to [1], for power objects operating in a network with grounded neutral, the voltage on the GD is regulated as follows: the excess of the value of 10 kV is allowed only on the GD, executed according to the touch voltage, and is not allowed on the GD executed according to requirements to resistance of the GD. In the case of a high potential beyond the boundary of the electrical installation and exceeding the value of 5 kV, it is necessary to apply means of insulation protection of communication and telemechanics cables that deviate from the electrical installation.

The easiest, but also the least accurate way to find the voltage on the GD is a direct recalculation, when measured according to the circuit in Fig. 1 the value of the resistance of the GD is multiplied by the real value of the SC current. The error in determining the voltage on the GD is due to inaccuracy in the measurement of the resistance of the GD and ignoring the nonlinear

dependence of the magnetic permeability of the grounding conductors on the value of the SC current. Due to the impossibility of carrying out measurements of the resistance of the GD and the voltage on the GD on a number of objects (industrial enterprises, in the conditions of urban development, etc.), the most universal and precise method of determination becomes calculations using special software complexes. A series of papers [5-9] is devoted to the simulation of electromagnetic processes that occur in the GD during the occurrence of emergency currents. In most cases, the mathematical model of the GD located in a two-layer soil is used, in particular, using the analogous model [8] the authors have calculated more than 1000 energy facilities of Ukraine of the voltage classes 35-750 kV, and the software complex used in [5] is one from the world's most popular commercial versions. Input parameters for it are the constructive execution of the GD (its circuit, the section of grounding conductors, the depth of location), the electrophysical characteristics of the soil, the neutral mode and the value of the SC current of the investigated object.

**2. Touch voltage.** The touch voltage is a parameter that characterizes the electrical safety of the service personnel of the power unit. It depends on the current flowing from the GD into the ground, the resistance of the GD, the design of the GD and the electrophysical characteristics of the soil. In contrast to the measurement of the resistance of the GD, in which the amplitude of the measuring current does not play a large role (it is given depending on the method used), the touch voltage is proportional to it, although this dependence is nonlinear.

There are two ways of experimentally measuring the touch voltage. The first one is directly under the SC current, that is, in real conditions. It is dangerous and can be justified only in rare cases in exceptional situations (when carrying out tests of the most responsible GDs), therefore, it is practically not used. The second one is at measuring current, which is many times smaller than the actual SC current, with subsequent reduction of the measured touch voltage proportionally to the real SC current [2].

The measuring circuit is practically the same as for measuring the resistance of the GD, but with the special performance of a potential electrode and bypassing the voltmeter with a resistor. Fig. 2 shows the circuit of measuring the touch voltage with the help of the complex «КД3-1Y» [2].

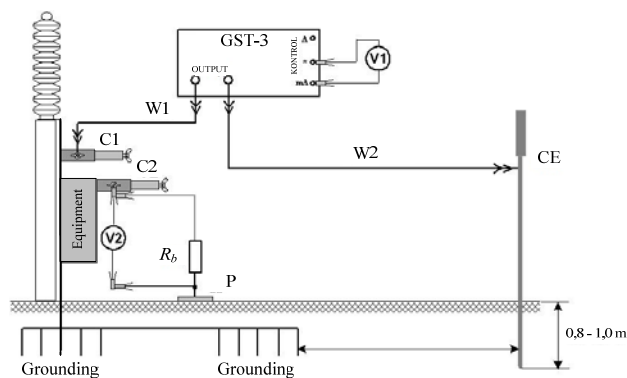


Fig. 2. Circuit for measuring the touch voltage

Potential electrode P must simulate two feet of a person. To do this, they use a special electrode-plate with a contact surface of  $25 \times 25 \text{ cm}^2$ . To create sufficient pressure on the ground, a load of at least 25 kg is installed on the plate. Voltmeter is shunted by a resistor with resistance  $R_b$ . The equivalent resistance of the parallel connected resistors must be equal to the resistance of the human body (as a rule, it is assumed to be  $1000 \Omega$ ). The horizontal distance from the contact point to the plate is assumed to be 0.8 m [1, 2] or 1 m [7].

The voltmeter, in parallel with the resistor with the clamp C2, is connected between the grounded equipment (in Fig. 2, this is a control box), on which the measurement is performed, and the potential electrode. The current electrode CE is located at the same distance, as in measuring the resistance of the GD. The GTS-3 generator from the «КД3-1Y» (or equivalent) is connected to the equipment and the CE with the help of the clamp C1 and wires W1 and W2, respectively. To simulate the most unfavorable seasonal conditions, the location of the potential electrode is moisturized. After that, the voltage is applied to the circuit and the voltage and current measurements are performed. The measured values of the touch voltage are reduced to the real SC current and the obtained result is compared with the acceptable normalized value. The disadvantages of this method are the impossibility of carrying out measurements under conditions of dense building and the methodological error of the method, which is connected with the ignoring of the dependence of the magnetic permeability of the grounding material on the current flowing through the elements of the GD, as well as the outflow of parts of the SC current in the grounded neutrals of transformers.

Thus, unlike the resistance of the GD, which can be determined both experimentally and by calculation, the voltage on the GD and the touch voltage at the real SC current can be found only by performing appropriate calculations using special computer programs.

**3. Resistance of contact joints.** One of the electrical NP of the GD is the resistance of the contact joint of the equipment with GD. In recent works, its significant influence on the voltage of the touch voltage was noted repeatedly [13-15]. The resistance of the contact joints is determined by the method of an ammeter-voltmeter at direct or alternating current using a micro-ohmmeter or double bridge [2]. The permissible value of the resistance of the contact joint is  $0.05 \Omega$  at commissioning and no more than  $0.1 \Omega$  during operation. The generally accepted measurement circuit for this NP, both in Ukraine [2] and abroad [7], is shown in Fig. 3.

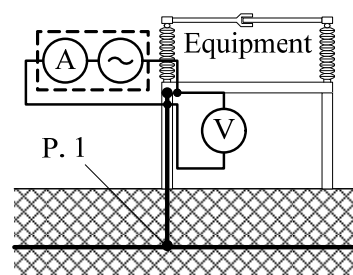


Fig. 3. Circuit for measuring the resistance of the contact joints

Thus, according to the measurement circuit, the resistance of the contact joint implies the transient resistance between the equipment and the grounding conductor. However, as the operation of the GD and the measurements of the NP of the GD show, the excess of the touch voltage can occur as a result of violation of the integrity of the grounding conductor at the boundary of the «ground-air», as well as in connection with the increase in the resistance of the contact joint at the point of welding the grounding conductor with the GD itself (see P. 1 in Fig. 3). Therefore, the consideration of the state of the grounding conductor and the quality of its connection, and, accordingly, of the equipment itself to the GD, is an important task. To control it, we can use the resistance of the connection, which is determined relative to other grounded equipment. However, this methodology does not exist at present in order to minimize the number of required measurements.

Summing up, we can state that the above methods have the following disadvantages:

- impossibility of measuring the touch voltage, the resistance of the GD and the voltage on the GD on a number of objects due to the lack of free from communications or facilities area for the placement of auxiliary current and potential electrodes;
- incorrect measurement of the NP of the GD due to the ignoring of the length of the removal of the current electrode for two-layer soil and the absence of such dependence for three- or more layer soils;
- incorrect measurement of the touch voltage and the voltage on the GD due to the ignoring of the dependence of the magnetic permeability of the grounding conductors on the current flowing through them, and the current outflow in the grounded neutrals;
- incomplete information about the grounding quality of the equipment based on measures the resistance of the contact joints;
- technical complexity and significant labor costs when measuring the touch voltage on each unit of the equipment of the power unit (the number of such units at the 330 kV substation can reach several hundreds, and the labor costs for measuring one point according to building codes [16] are 15 people·year).

In addition, for objects that have been in service for a long time, carrying out only measurements of the listed NPs does not allow to unambiguously assess the state of the GD: the design remains unidentified and the condition of underground grounding conductors is still unknown. Therefore, at the present stage, electromagnetic diagnostics (EMD) of the state of the GD is used for monitoring [2], which includes a complex experimental and calculation (on the basis of the real state of the GD and the results of additional experiments) determination of all NPs of the GD. The indicated method combines a number of methods: vertical electrical sounding of soil, induction method for determining the presence of grounding conductors, low current method, calculation method, etc.

**4. Method of electromagnetic diagnostics of the state of the grounding device.** The method of EMD of the GD [2] of active energy facilities as a whole is in line

with international Standards [7, 10] and involves three stages: the experimental, calculation and the stage of issuance of recommendations.

At the first stage, the following is performed:

- determination of the constructive implementation of the GD with the help of an induction method (location and depth of groundings), which is also needed for the construction of its mathematical model;
- measurement of the imaginary specific resistance to determine the electrophysical characteristics of the soil (specific resistance, thickness of the layers and their amounts) by the method of vertical electrical sounding;
- measurement of electrical parameters (base resistance, resistance of the GD, touch voltage, and voltage on the GD with respect to another grounded point) based on the ammeter-voltmeter method and known circuits, which are necessary to assess the adequacy of the mathematical model to the real GD.

The results of experimental studies, together with the characteristics of the energy object (voltage class, neutral mode of transformers, and the values of SC currents and protection time) are the input data for the second (calculation) EMD stage.

In carrying out calculations in the second stage, the mathematical model of non-equipotential GD, located in a three-layered conducting soil with plane-parallel separation boundaries developed by the authors [9] is used. In order to determine the input soil parameters, the means of interpretation of the vertical electrical sounding and ground equivalence curves are used. The simulation of processes in the GD is performed at real SC current, taking into account the nonlinear dependence of the magnetic permeability on its value, the skin effect and the real spread of emergency currents (including outflows in a grounded neutral), which allows determining the values of the NPs even for those objects that located in a concise building or on the territory of industrial enterprises. Existing software and mathematical models allow to take into account the two- and three-layer geoelectric structure of the soil and to cover more than 80 % of the energy objects of Ukraine.

In the third stage, the development of recommendations made by the requirements of normative documents for the constructive implementation of grounding conductors is carried out, as well as on the basis of comparison of the values of calculated and acceptable parameters the feasibility of introducing additional recommendations for the reconstruction of the grounding device is evaluated. After this, a recalculation is made taking into account the recommended additional groundings. Synthesis of these recommendations is a complicated technical task, since when it is solved, it is necessary to determine the optimal places for laying grounding conductors for saving labor and material costs, and at the same time, the most complete use of existing GD.

Thus, the EMD method for the state of the GD allows to carry out the most objective assessment of the current state of the GD and to develop ways to bring it in line with regulatory documents.

To defects of the EMD of state of the GD we should include errors in determining the constructive implementation of the GD and the influence of assumptions adopted in the construction of the mathematical model:

- error of determining the depth of the GD;
- variable section of groundings on different parts of the GD, which is difficult to consider;
- errors in the identification of horizontal groundings (acceptance of cables and underground communications as an artificial grounding);
- problems with finding the location of the installation of the vertical grounding and the lack of a method for determining its length;
- assumption of a flat-parallel multilayer soil structure, which in fact has slopes and local inclusions;
- insufficient depth of sounding of multilayer soils and lack of interpretive means.

**5. Devices for monitoring the state of the grounding device.** In Ukraine, the domestic complex for the diagnosis of the state of the GD «КДЗ-1У» [2] (see Fig. 4,*a*), the French devices C.A 6460 and C.A 6470N (see Fig. 4,*b*) are used, as well as domestic standard devices of the Soviet design: M-416 or Ф 4103-M1, which for the present time are used by insulation services and high-voltage laboratories at different power units.



Fig. 4. Devices for monitoring the state of the GD:  
*a* – «КДЗ-1У»; *b* – C.A 6470N

Table 1 presents a comparison of the functions of the most common devices for monitoring the state of the GDs of operating power facilities of Ukraine.

Table 1

Device name	GD state	Resistivity of the soil	GD resistance	Touch voltage	Contact joints resistance
«КДЗ-1У»	+	+	+	+	+
C.A 6470N	–	+	+	+	+
C.A 6460	–	+	+	+	+
Абрис-12/8	+	–	–	–	–
Ф 4103-M1	–	+	+	–	–
M-416	–	+	+	–	–
EP-331	–	–	–	–	+

The analysis of devices shows that only «КДЗ-1У» allows to carry out a full range of works for the EMD of the GD state. However, the disadvantage of the device is the lack of autonomous power and the small size of the permissible resistance of the measuring electrodes (which practically makes it impossible to conduct soil sounding with specific resistance of more than 350 Ω·m). The devices EP-331 and Абрис-12/8 are narrow-cut and allow only measuring the resistance of the contact joints and finding the trajectory of the grounding lines, respectively. Ф 4103-M1 and M-416 are technically outdated and also have a narrow spectrum of application. C.A 6460 in comparison with C.A 6470N has only one frequency of measurement and does not allow conducting sounding of soil for power units in the class of voltage 220 kV and above. In general, a detailed analysis of the characteristics and capabilities of instruments for soil sounding is made in [17].

Thus, the most wide-ranging possibilities for determining the NPs of the GDs have «КДЗ-1У» and C.A 6470N. Looking forward to improving the «КДЗ-1У» or developing a similar device without indicated shortcomings.

#### Conclusions.

1. An analysis of modern methods of monitoring the state of the GDs has been carried out and it has been established that, unlike the determination of the resistance of the GD, which can be done both experimentally and using calculations, the voltage on the GD and the touch voltage at the real current of ground fault should be found only by calculation using special computer codes.

2. It has been shown that the method of the EMD of the GD allows to carry out the most objective assessment of the current state of the GD and to develop recommendations for bringing it in line with the normative documents.

3. The disadvantages of the EMD of the GD that are associated with errors in determining its constructive execution and the influence of assumptions made when constructing a mathematical model are established.

4. The analysis of the devices used in the monitoring of the state of the GD is carried out. The perspective direction of improvement of the complex for diagnostics of grounding «КДЗ-1У» is determined.

#### REFERENCES

1. *Pravyla ulashtuvannja elektroustanovok* [Electrical Installation Regulations]. Kharkiv, Fort Publ., 2017. 760 p. (Ukr).
2. *Natsional'nyy standart Ukrainy. SOU 31.2-21677681-19:2009. Viprobuvannya ta kontrol' prystroyiv zazemlennya elektroustanovok. Tipova instruktsiya* [National Standard of Ukraine SOU 31.2-21677681-19:2009. Test and control devices, electrical grounding. Standard instruction]. Kyiv, Minenergovugillya Ukrainy Publ., 2010. 54 p. (Ukr).
3. Seljeseth H., Campling A., Feist K.H., Kuussaari M. Station Earthing. Safety and interference aspects. *Electra*, 1980, vol.71, pp. 47-69.
4. Boaventura W.C., Lopes I.J.S., Rocha P.S.A., Coutinho R.M., Castro F., Dart F.C. Testing and evaluating grounding systems of high voltage energized substations: alternative approaches. *IEEE Transactions on Power Delivery*, 1999, vol.14, no.3, pp. 923-927. doi: 10.1109/61.772335.

5. Tabatabaei N.M., Mortezaeei S.R. Design of grounding systems in substations by ETAP intelligent software. *International Journal on «Technical and Physical Problems of Engineering»*, 2010, iss.2, vol.2, no.1, pp. 45-49.
6. Kolechitsky Ye.S. Approximate estimates of the resistance of grounding devices. *Vestnik MEI*, 2006, no.4, pp. 56-62. (Rus).
7. *IEEE Std 80-2000 Guide for Safety in AC Substation Grounding*. New York, IEEE, 2000. 200 p. doi: **10.1109/ieeestd.2000.91902**.
8. Link I.Yu., Koliushko D.G., Koliushko G.M. A mathematical model is not an equipotential ground grids substation placed in a double layer. *Electronic modeling*, 2003, vol.25, no.2, pp. 99-111. (Rus).
9. Koliushko D.G., Rudenko S.S. Determination the electrical potential of a created grounding device in a three-layer ground. *Technical Electrodynamics*, 2018, no.4. pp. 19-24. (Rus). doi: **10.15407/techned2018.04.019**.
10. *IEEE Std 81-2012 Guide for Measuring Earth Resistivity, Ground Impedance, and Earth Surface Potentials of a Grounding System*. New York, IEEE, 2012. 86 p. doi: **10.1109/ieeestd.2012.6392181**.
11. Nizhevskiy I.V., Nizhevskiy V.I., Bondarenko V.E. The experimental validation of the grounding device resistance measurement method. *Electrical engineering & electromechanics*, 2016, no.6, pp. 60-64 (Rus). doi: **10.20998/2074-272X.2016.6.10**.
12. Tselebrovskiy Yu.V. The theory of measurement of resistance of earthing device. *Proceedings of TUSUR*, 2012, iss.1, part 1, pp. 196-198. (Rus).
13. Glebov O.Yu., Koliushko D.G., Link I.Yu. Determination of the touch voltage by the method of superposition of current components of a single-phase earth fault. *Bulletin of NTU «KhPI»*, 2005, no.49, pp. 85-88. (Rus).
14. Salam M.A., Rahman Q.M., Ang S.P., Wen F. Soil resistivity and ground resistance for dry and wet soil. *Journal of Modern Power Systems and Clean Energy*, 2015, vol.5, no.2, pp. 290-297. doi: **10.1007/s40565-015-0153-8**.
15. Fomenko O.V., Kostenko M.A., Novikova A.O. Influence of Communication Resistance on Damage of the Electronic Equipment in the Grounding Device. *Global Nuclear Safety*, 2014, no.3(12), pp. 44-48. (Rus).
16. *Resursnyye elementnye smetnye normy na puskonaladochnyye raboty. Sbornik 1. Elektrotekhnicheskie ustroystva. DBN D.2.6-1-2000* [Resource elemental estimates for commissioning. Collection 1. Electrotechnical devices. DBN D.2.6-1-2000]. Kyiv, Derzhbudivnytstvo Ukrainy Publ., 2001. 49 p. (Rus).
17. Rudenko S.S. Requirements for devices for vertical electrical sounding of soil at diagnostics of grounding devices. *Electrical engineering & electromechanics*, 2016, no.5, pp. 68-73. (Rus). doi: **10.20998/2074-272X.2016.5.12**.

Received 13.09.2018

*D.G. Koliushko*<sup>1</sup>, *Candidate of Technical Science, Senior Research Associate,*

*S.S. Rudenko*<sup>1</sup>, *Candidate of Technical Science, Research Associate,*

<sup>1</sup>National Technical University «Kharkiv Polytechnic Institute»,  
2, Kyrpychova Str., Kharkiv, 61002, Ukraine,  
e-mail: nio5\_molniya@ukr.net

How to cite this article:

Koliushko D.G., Rudenko S.S. Analysis of methods for monitoring of existing energy objects grounding devices state at the present stage. *Electrical engineering & electromechanics*, 2019, no.1, pp. 67-72. doi: **10.20998/2074-272X.2019.1.11**.

**Матеріали приймаються за адресою:**

**Кафедра "Електричні апарати", НТУ "ХПИ", вул. Кирпичова, 21, м. Харків, 61002, Україна**

**Електронні варіанти матеріалів по e-mail: [a.m.grechko@gmail.com](mailto:a.m.grechko@gmail.com)**

**Довідки за телефонами: +38 050 653 49 82 Клименко Борис Володимирович**

**+38 067 359 46 96 Гречко Олександр Михайлович**

**Передплатний індекс: 01216**